Creating a Functional Cardiac Patch From Decellularized Spinach Leaves

A Dissertation Submitted to the Faculty of WORCESTER POLYTECHNIC INSTITUTE
in partial fulfillment of the requirements for the Degree of
Doctorate of Philosophy in Biomedical Engineering

August 3rd, 2021

By:

Emily Rose Robbins

Approved by:

Glenn R. Gaudette, Ph.D.
Dissertation Advisor
Adjunct Professor
Department of Biomedical Engineering
Worcester Polytechnic Institute
&
John W. Kozarich '71 Chair and Professor
Department of Engineering
Boston College

George D. Pins, Ph.D.
Professor
Department of Biomedical Engineering
Worcester Polytechnic Institute

Marsha W. Rolle, Ph.D.
Professor
Department of Biomedical Engineering
Worcester Polytechnic Institute

Tanja Dominko, D.V.M., Ph.D.
Professor
Department of Biology and Biotechnology
Worcester Polytechnic Institute

Michael A. Laflamme, M.D, Ph.D.
Principal Investigator
Chair in Cardiac Regenerative Medicine
McEwen Stem Cell Institute

Acknowledgements

This dissertation work would not have been possible without the help and support from many people over the last five years. First, I would like to thank my advisor, Glenn Gaudette, Ph.D., for his research support and the number of opportunities that he has presented me with. Glenn has always been supportive during both successes and failures and encourages me to think outside of the box. In addition, he gave me opportunities to develop my skills by presenting my work at conferences, being a student mentor, and writing and reviewing grants and manuscripts. Furthermore, Glenn invited me to be the graduate assistant for both the KEEN and Value Creation Initiative programs at WPI, which has exposed me to the entrepreneurial and value creation mindsets. I will carry those mindsets with me for the rest of my career.

I would also like to recognize and thank my dissertation committee (George Pins, Ph.D., Marsha Rolle, Ph.D., Tanja Dominko, D.V.M., Ph.D., and Michael Laflamme, M.D., Ph.D.). Thank you for your time, guidance, and support. Your input has been invaluable and am I proud of this body of research.

Thank you to all members (past and present) of the Gaudette lab. Specifically, I would like to thank Katrina Hansen, Ph.D. and Joshua Gershlak, Ph.D., who trained me in lab techniques and developed my foundational knowledge to start my project. Additionally, I would like to thank Elizabeth English, M.S. (Pins lab) for her expertise in fibrin micropatterning. I would also like to thank my graduate student friends and colleagues at WPI. Your friendships have meant so much to me during my time at WPI.

None of this would have been possible without my family and friends. Specifically, my mom and dad (Susan and Dan Robbins), sister (Allison), and brother (James) who encouraged me to go back to graduate school and have been my biggest cheerleaders ever since. And thank you to my boyfriend, Eli Wiberg, who supports and inspires me through the highs and lows. I love you all and could not have done this without you.

Table of Contents

Table of Contents

Table of Figures

Table of Figures

Table of Tables

Abbreviations

3D	three-dimensional
ACE	angiotensin-converting-enzyme
AP	aprotinin
AV	atrioventricular
CM	cardiomyocyte
CV	cardiovascular
CVD	cardiovascular disease
ECM	extracellular matrix
EO	ethylene oxide
ES	embryonic stem
FBS	fetal bovine serum
FFT	fast fourier transform
GAG	glucosaminoglycan
HDM	high density mapping
hES-CM	human embryonic stem cell derived cardiomyocyte
hiPS	human induced pluripotent stem
hiPS-CM	human induced pluripotent stem cell derived cardiomyocyte
hMSC	human mesenchymal stem cell
IF	immunofluorescence
iPS	induced pluripotent stem
LV	left ventricle
MI	myocardial infarction
MRI	magnetic resonance imaging
PBS	phosphate-buffered saline
PDMS	polydimethylsiloxane
PFA	paraformaldehyde
Qdots	quantum dots
ROCK	rho-associated protein kinase
ROI	region of interest
SA	sinoatrial
TCP	tissue culture plastic

Abstract

Cardiovascular disease (CVD) is the leading cause of death worldwide. Myocardial infarction (MI), one type of CVD, affects over 800,000 Americans each year. MI is a regional disease that generally results from occlusion in a coronary artery leading to cell death, tissue ischemia, inflammation, and fibrotic scar formation. Cardiac scar formation stiffens the heart tissue, results in loss of electromechanical properties, reduced contractile function, and can lead to heart failure. Current treatments for MI and heart failure patients do not regenerate ischemic tissue function. A tissue engineered cardiac patch could be a solution to improve cardiac tissue function in the early months following MI. Decellularized spinach leaves are a promising scaffold for a tissue engineered cardiac patch due to their mature vascular system, biocompatibility, and comparable material properties to that of cardiac tissue. In addition, human induced pluripotent stem cell derived cardiomyocytes (hiPS-CMs) are an encouraging cell type to functionalize a cardiac patch scaffold. hiPS-CMs have been shown to be able to couple with host cardiomyocytes *in vivo* and improve cardiac function after MI. However, since hiPS-CMs perform functionally like immature cardiomyocytes, inducing maturation to adult cardiomyocyte behavior is a challenge.

This dissertation sought to develop a perfusable and functional tissue engineered cardiac patch using a decellularized spinach leaf that can be used to re-functionalize diseased heart tissue of MI patients. We first investigated the leaf's capability to perfuse cardioactive solutions through its vasculature to hiPS-CMs seeded on the leaf surface. Following perfusion, we found that hiPS-CM beat frequency of perfused leaves significantly increased, supporting our hypothesis. In addition, dye perfusion demonstrated that solutions perfused through the leaf vasculature enter the leaf tissue and cells on its surface. Next, we examined hiPS-CM adherence to and function on various decellularized spinach leaf substrate conditions. After 21 days, hiPS-CMs were found to adhere to protein coated and non-coated leaf scaffolds, with no statistically significant differences between hiPS-CMs' functional behavior on the coated and non-coated leaf surfaces. These results suggest that coating leaf scaffolds is not necessary to induce or improve cardiomyocyte adhesion and function. Finally, we examined methods to induce cell alignment on the decellularized leaf to mimic cardiac tissue and to mature cell function. We sought to align hiPS-CMs on decellularized spinach leaf scaffolds to promote directional contractile behavior

using two different methods: adherent fibrin microthreads and micropatterned fibrin hydrogel rows. Fibrin microthreads induced alignment of human mesenchymal stem cells (hMSCs) on leaves after 7 days; however, hiPS-CMs did not adhere to the leaf using the same techniques. Fibrin hydrogel successfully micropatterned on decellularized spinach leaves, and micropatterned rows provided the appropriate topographical cues for seeded hMSCs and hiPS-CMs to align. Micropatterned hiPS-CMs demonstrated increased contractile strain and synchronized contractile beating across the scaffolds. Overall, we exhibited that decellularized spinach leaves with hiPS-CMs are a viable option for a tissue engineered cardiac patch and aligned hiPS-CMs show enhanced function on the leaf, approaching behavior of cardiac tissue.

1. Overview

1.1 Introduction

Cardiovascular disease is the leading cause of death worldwide.[1] Each year, approximately 805,000 Americans have a new or recurrent myocardial infarction (MI).[2] MI is a regional disease that generally results from occlusion in a coronary artery, leading to cardiac cell death, tissue ischemia, inflammation, and fibrotic scar formation. Scar formation leads to myocardial stiffening and loss of electromechanical properties of the healthy myocardium, which results in overall reduced cardiac function.[3,4] Reduced contractile behavior and cardiac output function can eventually lead to heart failure.[5,6] Current treatments for MI and heart failure patients do not regenerate contractile function. The standard of care to recover cardiac function lost to MI is a heart transplant; however, the number of available donor organs does not meet the need of patients requiring a heart transplant.[4,7,8] In addition, heart transplants are primarily given to patients with advanced heart failure. Therefore, there is a clear need for an early treatment for patients who have suffered from a MI to improve cardiac function, alleviating the need for cardiac transplantation.

A tissue engineered cardiac patch could be a solution to improve cardiac tissue function in the early months following MI to reduce the chance of developing heart failure. Tissue engineering is the use of biomaterials, cells, and biological components for functional regeneration of diseased tissues.[9] Since cells are only able to survive up to 200 μm from a nutrient source due to oxygen diffusion limitations[10], a thick, therapeutic cardiac patch must have a vascular system within the scaffold to maintain cell viability. Decellularized spinach leaves are a promising scaffold for a cardiac patch since they have a mature vascular system, are primarily composed of cellulose, and have similar material properties to that of decellularized cardiac tissue.[11] Human induced pluripotent stem cell derived cardiomyocytes (hiPS-CMs) are an encouraging cell type to functionalize a cardiac patch scaffold. hiPS-CMs have also been shown to be able to couple with host cardiomyocytes *in vivo*[12] and improve cardiac function after MI.[13,14] However, since hiPS-CMs perform functionally like neonatal cardiomyocytes, maturation to demonstrate adult cardiomyocyte behavior is a challenge. Herein, we examine the decellularized spinach leaf's vasculature potential to deliver nutrients to seeded hiPS-CMs onto leaves through perfusion, characterize hiPS-CM function on the leaf surface, and induce hiPS-CM alignment on the decellularized leaf to mimic *in vivo* adult cardiac tissue anatomy and function.

1.2 Overall Goal and Hypothesis

We aim to develop a tissue engineered cardiac patch that may treat MI patients early to restore cardiac tissue function and avoid developing heart failure. The overall goal of this dissertation is to develop a perfusable and functional tissue engineered cardiac patch using a decellularized spinach leaf as the vascularized scaffold. We hypothesize that the decellularized spinach leaf's vasculature will be capable of affecting perfused cells and that aligning hiPS-CMs on decellularized leaf scaffolds will improve cardiac function. To test this hypothesis, this dissertation was divided into three specific aims. First, we aim to develop a leaf perfusion system and demonstrate that perfusion of leaf vasculature can affect cell behavior. Second, we aim to determine if protein coating is necessary to improve cardiac scaffold generation from decellularized leaves. Finally, we aim to develop an aligned cell seeded cardiac patch from decellularized leaves and stem cell derived cardiomyocytes. The expected outcome of this work is to understand the capability of the decellularized spinach leaf's vasculature to perfuse cells seeded on the leaf's surface, develop the appropriate seeding conditions required for cardiomyocyte adhesion on decellularized leaves, and develop a technique to induce cardiomyocyte alignment on decellularized spinach leaves and characterize cardiomyocytes' functional behavior.

1.3 Specific Aim 1: Determine if Fluid Perfusion Through Leaf Vasculature Affects Cell Function

Vasculature is required within a thick tissue engineered patch to supply cardiac cells with the nutrients required for survival. Therefore, we wanted to test the ability of the decellularized spinach leaf's vascular system to deliver cell media to cells seeded on the leaf. In this aim, we developed a leaf perfusion system to perfuse and affect change in hiPS-CMs seeded on decellularized spinach leaves. We hypothesized that leaf vascular perfusion will affect cell function on a decellularized leaf surface, comparable to static culture. We perfused the leaf vasculature with cell media containing cardioactive drugs to hiPS-CMs seeded on the leaf surface. Following perfusion, we measured hiPS-CM contractile strain and beat frequency using image-based strain measurements to detect changes in cell behavior on the leaf surface. Beat frequency of hiPS-CMs on leaves significantly increased with perfusion of 50 μM epinephrine,

supporting our hypothesis; however, contractile strain of perfusion and control conditions did not significantly increase. Furthermore, trypan blue dye perfusion showed that solution perfused through leaf vasculature enters the leaf tissue and cells on the leaf surface. The results of this aim suggest that leaf vascular perfused solutions travel to the leaf surface and can affect seeded cell function.

1.4 Specific Aim 2: Determine if Protein Coating is Necessary to Improve Cardiac Scaffold Generation from Decellularized Leaves

Early studies have demonstrated that coating decellularized spinach leaves with fibronectin is effective for cardiomyocyte adherence. However, allogeneic extracellular matrix (ECM) protein sourcing should be considered when planning on clinical translation. In this aim, hiPS-CMs were seeded on ECM coated and non-coated decellularized spinach leaves. We hypothesized that ECM coating is required for hiPS-CM adhesion and function on decellularized leaves. Cardiomyocyte behavior was analyzed using image-based strain measurements and immunofluorescence imaging. After 21 days, hiPS-CMs were found to adhere to coated and non-coated leaf scaffolds and there were no overall significant differences in hiPS-CMs' contractile behavior between ECM coated and non-coated leaf surfaces. Furthermore, there were no overall significant differences in cell number, elongation, or sarcomere lengths between coating conditions. The results of this aim suggest that coating leaf scaffolds with ECM protein is not necessary to improve cardiomyocyte adhesion, behavior, or contractility on decellularized leaf scaffolds.

1.5 Specific Aim 3: Develop Aligned Cell Seeded Cardiac Patch from Decellularized Leaves

Cardiac cell alignment is essential for mature cardiac function. We aligned hiPS-CMs on decellularized spinach leaf scaffolds to promote directional contractile behavior using physical cues on the scaffold. In this aim, we hypothesized that aligned hiPS-CMs cultured on decellularized spinach leaves would improve function.

1.5.1 Specific Aim 3A: Align Cardiomyocytes with Fibrin Microthreads on Leaf Scaffold

Previous research has demonstrated that hiPS-CMs adhere and align on extruded fibrin microthreads to form contractile cardiac fibers. In this aim, fibrin microthreads were used as a scaffold to align human mesenchymal stem cells (hMSCs) or contractile hiPS-CMs. Cell seeded microthreads were then cultured on decellularized spinach leaves in fibrinolytic culture conditions to transfer aligned cells from microthreads onto leaves. Cell behavior was measured using immunofluorescence imaging. Results demonstrated that hMSCs adhered and aligned on the leaf scaffold with microthread degradation. However, when hiPS-CMs were applied on microthreads, cells were displaced but did not transfer onto the leaf. This can likely be explained by the non-proliferative capability of hiPS-CMs, whereas hMSCs readily proliferate on substrates.

1.5.2 Specific Aim 3B: Manipulate Decellularized Leaf Topography to Align Cardiomyocytes

Cardiomyocytes adhere and conform to micropatterned protein conformations on given substrates. In this aim, we micropatterned decellularized spinach leaf scaffolds to provide topographical alignment cues for seeded hiPS-CMs, with the goal to improve hiPS-CM function. Cardiomyocyte cell behavior and contraction were analyzed with image-based strain measurements and immunofluorescence imaging. Micropatterned hMSCs and hiPS-CMs on leaves demonstrated significantly improved alignment compared to control conditions. Contractile strain of micropatterned hiPS-CMs was significantly higher than control conditions, exhibiting synchronized contractile beating across the micropatterned region. These results indicate that micropatterns can be induced in leaves, thereby increasing cell alignment on the substrate, to enhance hiPS-CM behavior and function.

1.6 **References**

1. Benjamin EJ, Muntner P, Alonso A, et al. Heart Disease and Stroke Statistics—2019 Update: A Report From the American Heart Association. Circulation. 2019;139(10):e56-e528. doi:10.1161/CIR.0000000000000659
2. Fryar CD, Chen TC, Li X. Prevalence of uncontrolled risk factors for cardiovascular disease: United States, 1999-2010. NCHS Data Brief. 2012;(103):1-8.
3. Rodness J, Mihic A, Miyagi Y, Wu J, Weisel RD, Li R-K. VEGF-loaded microsphere patch for local protein delivery to the ischemic heart. Acta Biomater. 2016;45:169-181. doi:10.1016/j.actbio.2016.09.009

4. Czirok A, Isai DG, Kosa E, et al. Optical-flow based non-invasive analysis of cardiomyocyte contractility. Sci Rep. 2017;7(1):10404. doi:10.1038/s41598-017-10094-7
5. Anzai T. Post-Infarction Inflammation and Left Ventricular Remodeling. Circ J. 2013;77(3):580-587. doi:10.1253/circj.CJ-13-0013
6. Holmes JW, Borg TK, Covell JW. Structure and Mechanics of Healing Myocardial Infarcts. Annu Rev Biomed Eng. 2005;7(1):223-253. doi:10.1146/annurev.bioeng.7.060804.100453
7. Yancy CW, Jessup M, Bozkurt B, et al. 2013 ACCF/AHA Guideline for the Management of Heart Failure. J Am Coll Cardiol. 2013;62(16):e147-e239. doi:10.1016/j.jacc.2013.05.019
8. Colvin M, Smith JM, Skeans MA, et al. OPTN/SRTR 2015 Annual Data Report: Heart. Am J Transplant. 2017;17:286-356. doi:10.1111/ajt.14128
9. Anderson JM, Rodriguez A, Chang DT. Foreign body reaction to biomaterials. Semin Immunol. 2008;20(2):86-100. doi:10.1016/j.smim.2007.11.004
10. Novosel EC, Kleinhans C, Kluger PJ. Vascularization is the key challenge in tissue engineering. Adv Drug Deliv Rev. 2011;63(4-5):300-311. doi:10.1016/j.addr.2011.03.004
11. Gershlak JR, Hernandez S, Fontana G, et al. Crossing kingdoms: Using decellularized plants as perfusable tissue engineering scaffolds. Biomaterials. 2017;125:13-22. doi:10.1016/j.biomaterials.2017.02.011
12. Eschenhagen T, Bolli R, Braun T, et al. Cardiomyocyte Regeneration. Circulation. 2017;136(7):680-686. doi:10.1161/CIRCULATIONAHA.117.029343
13. Wendel JS, Ye L, Tao R, et al. Functional Effects of a Tissue-Engineered Cardiac Patch From Human Induced Pluripotent Stem Cell-Derived Cardiomyocytes in a Rat Infarct Model. Stem Cells Transl Med. 2015;4(11):1324-1332. doi:10.5966/sctm.2015-0044
14. Masumoto H, Ikuno T, Takeda M, et al. Human iPS cell-engineered cardiac tissue sheets with cardiomyocytes and vascular cells for cardiac regeneration. Sci Rep. 2015;4(1):6716. doi:10.1038/srep06716

2. Background

2.1 The Cardiovascular System, Heart, and Cardiac Function

2.1.1 The Cardiovascular System

The human cardiovascular (CV) system is a closed loop network that transports oxygenated blood and nutrients through arteries throughout the human body, removes waste, and delivers deoxygenated blood though veins to the heart. The heart is a contractile, dynamic organ which collects deoxygenated blood, and pumps approximately 5 liters of oxygenated blood per minute to a body at rest.[1] The human heart is composed of 4 chambers: the right atrium, right ventricle, left atrium, and left ventricle. From the CV system, deoxygenated blood enters the heart's right atrium, and then travels into the right ventricle through the tricuspid valve. The right ventricle contracts and expels blood through the pulmonary valve into the pulmonary artery, where blood will be oxygenated in the lungs. Oxygenated blood from the lungs travels through the pulmonary vein into the left atrium. Blood fills from the atria into the left ventricle through the mitral valve. Then, oxygenated blood is ejected from the left ventricle into the aorta, through the aortic valve, to the rest of the body.

There are two phases in the heart in which blood is circulated: diastole and systole. In diastole, the ventricles fill with blood from the atria. In systole, blood is ejected from the ventricles. Ventricular contraction and blood ejection is controlled by a highly timed electrical signal that propagates from the atria.[2] Contraction is timed by action potentials originating in the sinoatrial (SA) node in the right atrium which travel to the atrioventricular (AV) node. The action potential signals continue through the bundle of His and into the ventricular muscle. Cardiac tissue directionally propagates action potentials through adjacent cardiomyocytes, thus contracting cells synchronously and pumping blood first out of the atria, followed then by the ventricle.

2.1.2 The Heart

The heart is composed of a variety of cell types including cardiomyocytes, cardiac fibroblasts, vascular cells, smooth muscle cells, and pacemaker cells. Pacemaker cells stimulate the action potentials in the SA and AV nodes to propagate the electrical signal and initiate myocyte contraction. Cardiomyocytes (CMs), or the heart's muscle cells, are responsible for muscle contraction. Atrial and ventricular CMs, named for the location in which they reside, contain the contractile units for the heart muscle. Other CMs include those involved in the cardiac

conduction system such as nodal myocytes. Atrial and ventricular CMs are adjacently connected end-to-end by intercalated disks to form linear and branched muscle fibers.[3] At intercalated disks, gap junctions facilitate action potential conduction and excitation from one cell to the next through the heart muscle.[4]

The cardiac extracellular matrix (ECM) network provides cardiac tissue mechanical support as well as signal transduction for cell communication and molecule regulation, in which disruption of ECM homeostasis can result in cardiac disfunction.[5] The structural network of the heart tissue is composed of several different ECM proteins, the majority of which are collagens (I, III, and IV), fibronectin, laminin, elastin, proteoglycans, and glucosaminoglycans (GAGs).[6] In the heart tissue, there are two main regions of cardiac ECM: the basement membrane and interstitial matrix. The basement membrane contains an ECM network that interacts with cells and promotes cell function signaling with integrins. The ECM in the interstitial matrix provides structural and mechanical support to the tissue.

Cardiac tissue is highly anisotropic.[7–9] The left ventricle (LV) of the heart has a complex wall structure in which fiber orientation rotates in direction in each of the three heart wall layers (epi-, myo-, and endocardial). Each layer has a different fiber orientation containing highly aligned cardiomyocytes (**Figure 2-1**) which are important for action potential propagation and effective contraction. For example, in healthy myocardium, cardiomyocytes are aligned within 13° of each other.[10] The complex wall structure allows the heart to twist circumferentially during contraction, causing opposite rotation of the base and apex around the long axis[11], and allows for efficient blood ejection.

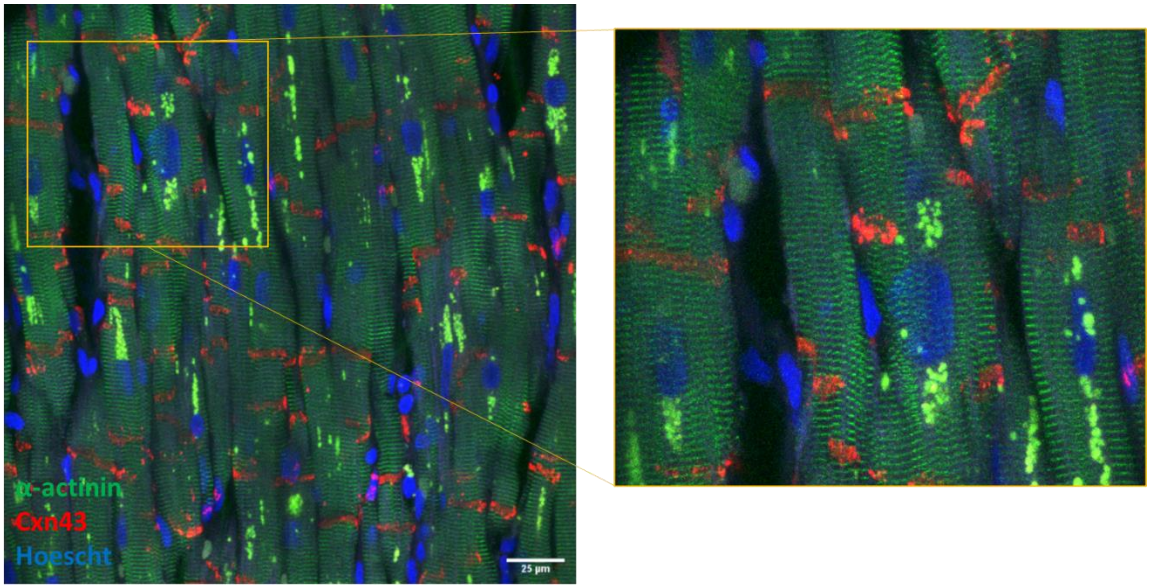

Figure 2-1: Cardiomyocyte alignment within human heart ventricular tissue. Human heart tissue was stained for sarcomeric α-actinin (green), connexin-43 (red), and Hoescht 33342 (blue). Muscle fibers and nuclei (blue) are highly aligned with muscle fibers illustrating rod-shaped structures. Sarcomeric α-actinin (green) bands illustrate mature contractile units within the cardiomyocytes. Connexin-43 (red) illustrates presence of gap junctions between cells, allowing for fast action potential propagation. Scale bar 25 µm.

2.1.3 Assessing Cardiac Function

Cardiac function and tissue health can be measured clinically by parameters such as morphology, blood ejection fraction, and tissue deformation using cardiovascular magnetic resonance imaging (MRI). Cardiac LV contraction, specifically, can be characterized by LV myocardial deformation and torsion *in vivo*.[12] Myocardial deformation is measured by calculated tissue strain of the heart wall as it contracts. MRI has become a standard evaluation technique to measure heart muscle morphology, motion, and deformation using various image acquisition and post-processing methods.[13] Use of these imaging techniques have determined healthy reference contractile parameters for adult human cardiac tissue that can be applied to patients. For instance, MRI information of healthy human hearts demonstrate average peak systolic longitudinal strain of 21.3 ± 4.8%, peak systolic circumferential strain of 26.1 ± 3.8%, and peak systolic radial strain of 39.8 ± 8.3%.[14] Other image-based techniques show cardiac contractile strain ranging from 15.9-22.1%.[15] In addition, the elastic moduli of healthy adult human myocardium during normal heart rhythm has been determined to range from 20-500 kPa.[16]

Outside of clinical measurements, measuring strain in contracting cardiomyocytes can be accomplished optically and non-invasively with a high-speed camera and video analysis.[17–20]

High density mapping (HDM), as previously described[20,21], can measure regional contractile strain to calculate small tissue deformation based on an initial reference state and is not affected by rigid body motion or rotation.[22] This technology has been applied to *in vivo*[23,24] and *in vitro*[21,25] conditions to effectively calculate contractile parameters of cardiac tissue and cardiomyocytes.

2.2 **Cardiovascular Disease**

2.2.1 Coronary Heart Disease and Myocardial Infarction

Cardiovascular disease (CVD) is the leading cause of death worldwide.[26] Coronary heart disease, one form of CVD and the leading cause of death in the United States (43.2%)[26], can be induced by cardiac events such as a myocardial infarction (MI). Approximately 805,000 Americans have a new or recurrent MI each year.[27] MI most frequently occurs due to plaque build-up in the coronary artery (**Figure 2-2**), followed by rupture of the atherosclerotic plaque and formation of an occlusive thrombus. The formation of the thrombus results in an interruption of blood flow to the myocardial layer of the LV. Lack of blood flow to the myocardium induces an inflammatory response causing cardiomyocyte cell death and tissue ischemia.[28] In addition, rapid breakdown and damage to ECM organization occurs after infarct.[29]

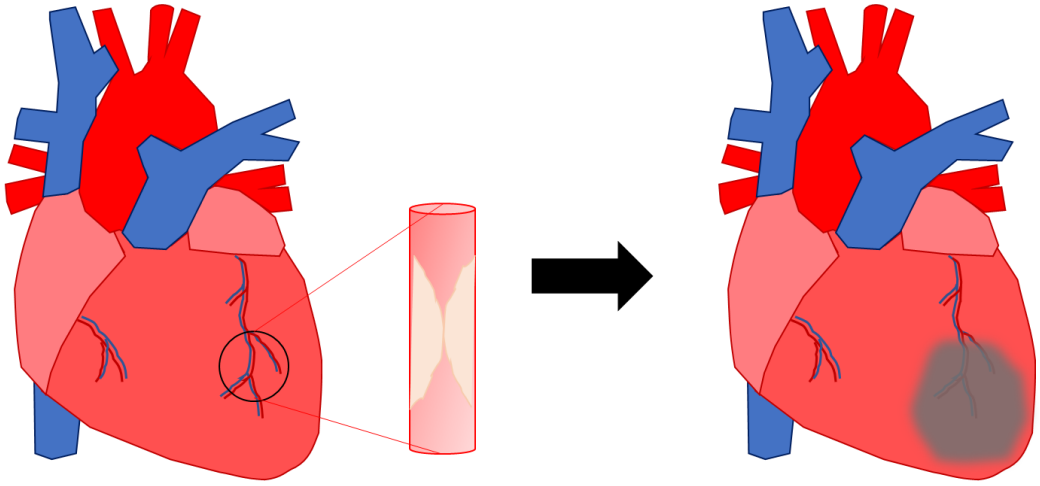

Figure 2-2: Myocardial infarction in the left ventricle due to plaque build-up in the coronary artery. Blockage of the coronary artery reduces blood flow to the left ventricle myocardium. Subsequent rupture of the blockage and occlusive thrombus formation in the vessel results in cardiac cell death, tissue ischemia, and scar tissue formation downstream.

MI-induced coronary heart disease is generally a regional disease, resulting in decreased contraction in part of the heart. This is because in the weeks after MI, endothelial cells and fibroblasts migrate to the injured region to form granulation tissue, resulting in a thick fibrous scar.[9,30] Scar formation leads to tissue stiffening and loss of electromechanical properties of healthy functional myocardium, all resulting in reduced cardiac function.[28] Specifically, patients exhibit decreased LV twist due to fibrous stiffening of the tissue, which leads to impairment in blood ejection fraction. If a significant amount of tissue is infarcted, overall cardiac function decreases. Furthermore, ventricular remodeling due to MI can result in infarct expansion[29], ventricular hypertrophy, and progressive ventricular dilation, which weakens the myocardium. This tissue remodeling, inflammation, and lack of vascularization in the immediate ischemic tissue region can lead to heart failure.[31]

2.2.2 Current Clinical Methods to Treat MI and CVD

There are limited functional treatments after MI to prevent heart failure since cardiac tissue is unable to regenerate after injury. Currently, pharmacological agents, such as angiotensin-converting-enzyme (ACE) inhibitors or beta blockers, are used early after MI to reduce the inflammatory response found in MI patients.[32] These therapeutic drugs can reduce mortality, but they do not repair the injured cardiac tissue nor return tissue function to baseline levels. Procedures such as placement of vascular stents[33] and coronary bypass[34] are early stage interventions used to reduce patient mortality after MI by restoring blood flow to cardiac tissue. However, these procedures do not restore contractile function to ischemic tissue nor decrease the risk of heart failure mortality.[35] Once patients have been diagnosed with heart failure, treatment strategies can include implantation of ventricular assist devices which aim to restore normal blood flow through the body by pumping blood through a pumping chamber into the aorta.[36] For patients with advanced heart failure, a heart transplant is often the only solution to restore contractile function; however, the number of available donor organs does not meet the need of patients requiring a transplant.[19,32,37] There is no early treatment for MI patients that restores contractile function of ischemic cardiac tissue to avoid patients developing heart failure.

2.3 **Tissue Engineered Cardiac Patch**

2.3.1 Cardiac Tissue Engineering

A tissue engineered implantable cardiac patch could be a treatment approach to improve cardiac tissue function of scarred ischemic tissue in the early months following MI. Tissue engineering is the use of biomaterials, cells, and biological components for functional regeneration of diseased tissues.[38] Current FDA cleared tissue engineered solutions exist on the market for skin or wound[39–41] applications and orthopedic[42] implantation. These solutions have made progress in the field, however no tissue engineered solutions are available for cardiac regeneration after MI.

Previous work attempting direct cell transplantation for cardiac regeneration has shown levels of success in enhancing cardiac function[43,44]; however, there is risk of poor cell retention in the injected regions and low survival.[9,45] By utilizing a three-dimensional (3D) biomaterial scaffold functionalized with cells, we may be able to replace diseased infarcted tissue, provide support for transplanted cells, and customize the size and shape of the graft for implantation. This could prevent cell migration and increase localized cell survival.

A 3D biomaterial scaffold can be used to provide appropriate structural support, biological, and mechanical cues to promote tissue regeneration *in vivo*.[46] Biomaterial scaffolds can be tailored by material choice or engineered conditions to promote specific cell behavior. The scaffold can also initially provide the structural integrity and biomechanical profile for the engineered cardiac tissue.[47] Furthermore, a cardiac tissue scaffold must integrate with the host tissue when implanted and should replicate essential characteristics of healthy myocardium. Healthy myocardium tissue has three key features of importance: high density of myocytes, efficient oxygen exchange between cells and blood, and synchronous contractions due to cell signal propagation.[9] To achieve these features, an engineered cardiac tissue must have an inherent vascular system, have similar mechanical properties as the myocardium to withstand contractile behavior, and have highly aligned cardiomyocytes that synchronously contract.

2.3.2 Cardiac Patch Scaffold Design Considerations

Engineered cardiac tissues could be a solution to restore contractile function to the infarcted region of the heart. A 3D implantable tissue engineered cardiac patch could improve function of the infarcted heart, providing an early treatment for MI patients and prevent the need for heart transplantation. However, cardiac tissue patch scaffold design considerations are important due

to the heart's dynamic environment. Therefore, the tissue engineered patch scaffold must have an inherent vascular system, be biocompatible, and have similar material properties as the human myocardium to recapitulate functional behavior.

2.3.2.1 Vasculature

A major limitation affecting current tissue engineered solutions is the lack of adequate vasculature. As tissue thickness increases, vasculature is needed to properly provide oxygen and nutrients to all parts of the tissue. Vasculature is required because mammalian cells are only able to survive a maximum of 200 μm from a nutrient source due to limitations of oxygen diffusion[48–50], which requires small sized vessels in a high density. Ideally, vasculature should be integrated in the scaffold, branched, and perfusable to maintain tissue function. A lack of a vasculature within the scaffold limits the tissue thickness, reducing clinical efficacy and preventing scale-up for use in humans. Therefore, a tissue engineered patch should have a functional vascular system within the biomaterial scaffold to support thick tissue scale-up as a therapeutic device. Previous research have engineered vascularized cardiac patches using cell co-culture[51–56]; however, neovascularization and angiogenesis is delayed after *in vivo* implantation.[50,56–58] Few engineered tissue constructs have demonstrated immediate functional vascular flow *in vitro* and *in vivo*, in which perfusion is capable during *in vitro* culture or red blood cells are found within conduits soon after implantation *in vivo*.

2.3.2.2 Biocompatibility

A biocompatible scaffold is one that is able to perform with an appropriate host response in a specific application.[16] The host response following implantation of a biomaterial undergoes a sequence of inflammatory and wound healing response events. This includes injury, blood-material interactions, provisional matrix formation, acute inflammation, chronic inflammation, granulation tissue development, foreign body reaction, and fibrosis/fibrous capsule development.[38,59] When a biocompatible scaffold is implanted *in vivo*, there should be a limited foreign body response due to the intervention. A therapeutic cardiac patch scaffold should not initiate a significant host response *in vivo* to maintain the tissue patch's viability and contractile function.

2.3.2.3 Material Properties

Implanted cardiac patch retention is important to consider because the heart is a dynamic organ. A therapeutic cardiac patch must have mechanical properties like healthy LV myocardium to not impede cardiac function. Specifically, the scaffold's stiffness and contractile strain should be within that of myocardium. Healthy adult human myocardium has an elastic modulus ranging from 20-500 kPa.[16] Upon implantation, the patch would immediately be subject to contractile loading conditions. During normal heart rhythm, the contractile strain of healthy adult human myocardium ranges from 15.9-22.1%.[15] Because of the cyclic mechanical stretch induced on cardiomyocytes by rhythmic heart beating[60], the mechanical properties of the tissue engineered patch should match that of the myocardium with regards to modulus and contractile strain to avoid localized stresses on the heart or patch during *in vivo* contraction.[61]

2.3.3 Cardiac Patch Scaffold Technologies

2.3.3.1 Hydrogel Scaffolds

Hydrogels as cardiac tissue engineered scaffolds are commonly composed of materials such as fibrin, collagen I, synthetic polymers, or cardiac-derived matrix proteins.[62] Cardiomyocytes (CMs) cultured in hydrogel patches have shown positive effects on infarct scar thickness reduction after *in vivo* implantation.[63,64] However, concerns of slow microvascularization formation and weak mechanical properties hinder these products from clinical application. Microvasculature formation in hydrogels can be induced using cell co-culture from vascular cells. Fibrin hydrogels co-cultured with vascular cells and cardiomyocytes have shown the ability to form microvessels within the hydrogel.[48,64] However, microvessels did not migrate towards cardiomyocytes *in vitro* or *in vivo* after two weeks.[64] Additional time and modified culture conditions would be required to form mature vascular networks for scaffold-wide perfusion using this platform. This demonstrates the time inefficiency required to form functional vasculature within scaffolds using co-culture techniques.

Another concern in using hydrogels as cardiac patch scaffolds is their relatively weak material properties compared to human heart tissue. Where fibrin hydrogels have a stiffness near 0.25 kPa[65], the adult human heart myocardium's stiffness ranges from 20-500 kPa during contraction.[16] To better match cardiac tissue material properties, mechanical stimulation and physical reinforcement of hydrogels have been investigated. Mechanically loading fibrin and collagen I hydrogels improves their mechanical properties.[62,66] In addition, fibrin hydrogels

integrated with layers of fibrin microthreads significantly increases its elastic moduli[65], approaching that of human myocardium. However, significant challenges remain since the maximum human myocardium contractile stiffness is approximately five times greater than that of reinforced fibrin hydrogels.

2.3.3.2 Decellularized Tissue Scaffolds

Decellularized tissues are promising tissue engineered scaffolds since they retained the native structure and vasculature of the derived tissue.[7,67–70] Specifically, decellularized mammalian cardiac tissue retains the complex material properties and structure of the heart and native vasculature[7,67,69–72], and the tissue can be repopulated with cells.[7,67,73–75] Decellularized tissue's native vasculature can be utilized as a nutrient source for seeded cells and assist in integration with host vessels *in vivo*.[70] Acellular tissue matrices have also been shown to support the ingrowth of cells and tissues *in vivo* without inducing a gross immune response.[46] However, decellularized tissues are limited since animal sacrifice is required. In this, decellularization can be prohibitively expensive since a limited supply of mammalian tissues are able to be harvested for use.[7,67–70]

2.3.3.3 Synthetic Material Scaffolds

Synthetic materials have been utilized as an option for a cardiac patch scaffold. Synthetic polymers can be reproducibly manufactured with a wide range of mechanical properties to produce scaffolds with specific properties.[46] Although synthetic materials are highly tunable, significant effort is required to create functionalized scaffolds with vascular systems for clinical therapy. In addition, since synthetic materials are not native to humans, biocompatibility is a concern.

Utilizing synthetic materials for a patch design provides the ability to engineer finely tuned vascular systems within scaffolds using rapid casting techniques. One example of this scaffold system is the Angiochip, an elastomer material that contains a perfusable, porous vascular network for cell and nutrient mobility.[54,76] Although the miniaturized system is composed of an crosslinked elastomer, the design also relied on natural materials such as gelatin and Matrigel® for mammalian cell adhesion and function. The complexity, time, and cost required to design and produce the system, in addition to the multiple materials required for function, limits its use as a

clinical therapy. For this reason, it is unlikely such a synthetic device would be clinically applicable for an implanted tissue engineered cardiac patch.

2.3.3.4 Bioprinted Scaffolds

Bioprinting is another strategy to form vascularized engineered tissue scaffolds[51–56,77], and the availability of commercial biological printers such as the Allevi 1 (Allevi, Inc) has made bioprinting technology more accessible. Bioprinters extrude bioinks, composed of viscous biomaterials, in their intended design to form layered 3D scaffolds. Cells can be extruded with a bioink or added post-extrusion to functionalize the scaffold.[55] However, weeks of culture has been required to achieve confluent cell layers.[55] Bioprinting is a promising technology to design engineered tissues; however, culturing vascular cells for vessel formation is currently inefficient. At this time, more time and resources are required to achieve sustainable vascular system designs for a functional cardiac patch. Thus, there remains a need to select a cardiac patch scaffold that has an inherent vasculature, is biocompatible, and has comparable material properties as the myocardium.

2.3.4 Decellularized Spinach Leaf as Cardiac Patch Scaffold

A tissue engineered cardiac patch has the potential to replace the function of ischemic cardiac tissue after MI. However, the engineered patch requires a vascular network for thick tissue viability due to oxygen diffusion limitations.[50] Inspired by nature, we found leaves have many desirable properties for a cardiac tissue engineering scaffold. Decellularized spinach leaves, specifically, have been considered for a cardiac tissue engineered scaffold. Spinach leaves are decellularized using a simple, detergent-based perfusion process to remove the plant nucleic material from the leaf (**Figure 2-3**).[69]

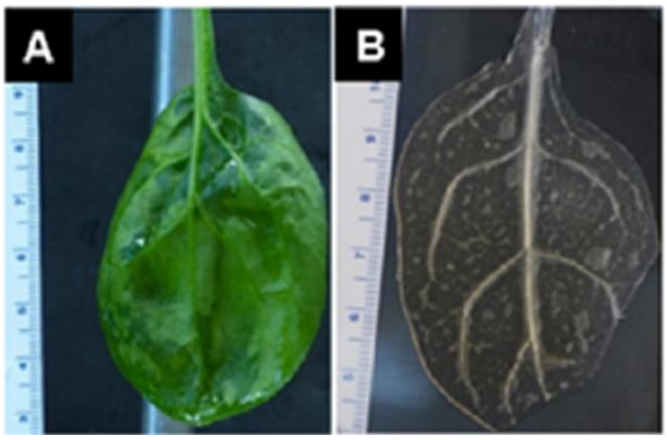

Figure 2-3: Perfusion based decellularization of spinach leaves. Perfusion decellularization of spinach leaves removes plant cells and maintains vasculature. (A) Cannulated spinach leaf prior to decellularization. (B) Decellularized spinach leaf retains patent vasculature. Figure modified from Gershlak et al.[69]

After perfusion based decellularization, the leaf vasculature remains intact and is capable of perfusion[69], and the leaf's branching network is similar to that of the human cardiovascular system.[84] Furthermore, since the leaf stem is flexible and cylindrical, it could potentially be attached to blood vessels for *in vivo* scaffold perfusion.[85]

In addition, leaves are primarily composed of organized microfibrillar cellulose that supports a matrix of hemicellulose and pectin or lignin.[69,86,87] Cellulose is a biocompatible material used in tissue engineering research and in FDA-approved surgical hemostatic wound dressings.[88–91] Decellularized plant based scaffolds, such as apple derived material, have previously demonstrated low inflammatory response, promote cell invasion and extracellular matrix deposition, and act as a pro-angiogenic environment after implantation *in vivo*.[88] Preliminary studies of decellularized spinach leaf biocompatibility are promising as decellularized spinach provoked minimal immune response after four week subcutaneous implantation in adult female Sprague-Dawley rats.[92]

Also, material properties of decellularized spinach leaves are appropriate for cardiac tissue. The maximum tangent modulus of decellularized leaves (0.3 MPa)[69] is within the range of healthy human decellularized cardiac tissue (0.371 ± 0.151 MPa at apex and 0.451 ± 0.258 MPa at septum).[7] Additionally, spinach leaves have symmetric geometry and vasculature, are of the same size scale as the human ventricular wall (approximately 30 mm – 60 mm in adult humans)[93], are pliable, and easily accessible. Overall, the decellularized spinach leaf's

vasculature, material properties, and shape make it an excellent candidate for a tissue engineered cardiac patch scaffold.

2.3.5 Cells For Cardiac Patch

Seeded cells on a tissue engineered scaffold will provide functional behavior to the cardiac patch to replicate properties of heart tissue. Several cell types have been examined for cardiac application including bone marrow stem cells, xenograft primary cells, and cardiomyocytes derived from pluripotent stem cells.

2.3.5.1 Bone Marrow Stem Cells

Bone marrow stem cells such as human mesenchymal stem cells (hMSCs) are derived from the bone marrow and can differentiate into several cell lineages such as bone, fat, and cartilage. Bone marrow stem cells have been found to excrete paracrine factors such as vascular endothelial growth factor, fibroblast growth factor 2, and hepatocyte growth factor which promote angiogenesis, neovascularization, and cell survival, and increase regional blood flow in ischemic animal hearts.[94,95] Also, transplantation of MSCs in ischemic heart models has been found to attenuate fibrotic factors including matrix metalloproteinases-2 and -9 [96], which are responsible for extracellular left ventricular remodeling during heart failure.[97] Therefore, transplanted MSCs may have the potential of reducing ischemic remodeling after cardiac injury. With this, hMSCs have been studied to determine if they can also be differentiated into cardiac muscle cells for contractile regeneration.

Although MSCs transplantation has been shown to improve blood flow and reduce cell death after ischemia, there is conflicting evidence whether MSCs can differentiate into cardiomyocytes (CMs) to restore contractile function of the ischemic heart muscle. Research conducted to determine if MSCs can differentiate into cardiac lineage has been done with varying degrees of success. For example, when hMSCs were implanted in immunodeficient mouse models, cells expressed cardiac-specific markers comparable to that of host CMs.[98] However, upon hMSC injection in ischemic nude rats, no cardiomyocyte differentiation was observed.[99] Further studies have confirmed that MSCs do not undergo cardiomyogenic differentiation after transplantation into normal or injured mouse hearts, and direct injection does not result in *de novo* cardiomyogenic events or tissue regeneration.[100] Instead, the low number of observed bone marrow derived cardiomyocytes may be due to cell fusion of bone marrow cells with host

cardiomyocytes.[101] Despite no direct cardiomyocyte differentiation, MSCs may still provide a therapy in their use as a paracrine factor mediator for tissue health. In fact, tissue engineered patches containing both hMSCs cocultured with functional cardiomyocytes have shown promise to enhance cardiac repair.[102]

2.3.5.2 Primary Isolated Cardiomyocytes

To better functionalize ischemic heart tissue, we should utilize healthy cardiomyocytes (CMs) for a cardiac tissue engineered patch so that the heart muscle can repopulate. However, patient donor CMs are not a viable option for clinical application due to the diseased cardiac tissue and health concerns of the patient. In addition, due to the limited proliferation of adult cardiomyocytes, many cells would be required for cell seeding of tissue constructs, adding to the complexity of using primary CMs. Therefore, preliminary investigations have turned to isolated primary CMs from xenografts, most commonly from neonatal rats, as a cell source.

Cardiomyocytes isolated from neonatal rat hearts have been applied as a cell model for cardiomyocytes in cardiac engineered tissue models.[103,104] For these applications, neonatal rat CMs are well defined and effective to model cell mechanisms of action on substrates under defined *in vitro* conditions. These primary cells can also be used as a control to evaluate the functional attributes of progenitor derived cardiac cells in engineered tissues.[105] For short term *in vitro* models, isolated neonatal CMs may be viable controls to test hypotheses and compare to progenitor cells.

Although using primary neonatal rat CMs is considered cost-effective, the cell isolation process requires animal sacrifice, is time consuming, and primary CMs in long-term culture can lose their contractile phenotype within weeks.[106] In addition, clinical use of xenograft CMs is not feasible. Cell implantation would result in rejection and biocompatibility concerns for human patients. Furthermore, discrepancies in cardiac functional outputs such as contractile strain, force production, and beat frequency in xenografts compared to humans are a concern.[45,107] Therefore, moving forward, cardiac tissue engineered solutions and models should use proliferative human cells of non-cardiac donor origin to start.

2.3.5.3 Pluripotent Stem Cells

Due to adult cardiomyocytes' non-proliferative nature, the most promising cell source of human cardiomyocytes for an engineered cardiac patch is pluripotent stem cells differentiated into

cardiomyocytes. The two major sources of pluripotent stem cells are embryonic stem (ES) cells and induced pluripotent stem (iPS) cells. Human embryonic stem cell derived CMs (hES-CMs) are derived from human embryonic cell lines and differentiated into CMs using a differentiation protocol. Human induced pluripotent stem (hiPS) cells are formed by genetically reprogramming adult somatic cells to exhibit characteristics of embryonic stem cells, without the ethical concerns of embryonic stem cells.[108,109] There are three major protocol strategies to induce CM differentiation in pluripotent stem cells: (1) inductive coculture for endoderm conditioning[110], (2) embryoid body formation with spontaneous differentiation[111–113] or with growth factors[114,115], or (3) monolayer culture using growth factors[45] or small molecules.[116,117] It has been demonstrated that hiPS cell derived cardiomyocytes (hiPS-CMs) have greater than 80% purity *in vitro.*[114,118–120]

The addition of pluripotent stem cell derived cardiomyocytes to ischemic cardiac tissue has demonstrated effective improvement in cardiac tissue health. Cardiac remuscularization and graft maturation have been observed after *in vivo* bolus injection of hES-CMs into infarcted ventricles of both small and large animal models; however, porcine and non-human primate large animal models can develop ventricular arrhythmias a few days after hES-CM transplantation.[43,44,121] It is hypothesized that arrythmias occur due to the presence of pacemaker cells in the hES-CM population. With an electrically quiescent pure ventricular cell population, the incidence of arrhythmias would likely be less.[44]

As with hES-CMs, hiPS-CMs also functionalize and integrate well with host cardiac tissue after implantation. When transplanted *in vivo*, hiPS-CMs contract and electrically couple with host cardiomyocytes.[118] Also, hiPS-CMs improve tissue function through the attenuation of ventricle remodeling after transplantation in post-MI small animal models.[58,122] Likewise, engineered tissues containing hiPS-CMs demonstrate improved function and remuscularization following *in vivo* implantation on scarred cardiac tissue.[63,81] Moving forward, tissue engineered cardiac patches ought to be developed with hiPS-CMs as their cell source due to the potential for autologous and allogeneic donor specificity, lack of ethical concerns, and ability to re-functionalize diseased cardiac tissue.

2.3.6 Cardiac Patch Contractile Function

An effective tissue engineered cardiac patch will provide contractile function to a diseased myocardial region following a MI. To regenerate regional function, an engineered therapeutic cardiac patch must match the properties present in healthy cardiac tissue during contraction. Hence, a clinically applicable engineered cardiac patch should have contractile strain similar to that of *in vivo* conditions.[15] It has been determined that hiPS-CMs functionally mature on aligned substrates compared to non-aligned substrates, developing characteristics of adult CMs.[123,124] Cardiac patch contractility could be improved by aligning hiPS-CMs, as demonstrated on other biomaterial substrates.[25] In addition, cardiac cell alignment dictates healthy cardiac tissue's electromechanical function. Cardiomyocytes on a tissue patch should mimic human myocardium morphology for healthy contraction and electrical propagation. Organized cell implantation on the cardiac patch is critical in order to avoid cardiac arrhythmias *in vivo*, which could lead to death of a patient.[74,125] An engineered cardiac patch that recapitulates cardiac tissue's highly aligned structure could integrate with the native tissue and mitigate improper electromechanical behavior. Therefore, an engineered cardiac patch should aim for this alignment to achieve healthy contractile behavior.

2.3.7 Cardiac Patch Functional Considerations

Developing a clinical tissue engineered cardiac patch to regain cardiac tissue function has been of great interest for many years. In addition to recapitulating vasculature, biocompatibility, and mechanical behavior of the tissue as properties of the scaffold, the new cell population and its behavior on the scaffold must be considered as design benchmarks. A cardiac tissue patch's electromechanical function is dependent upon cell behavior in the scaffold. Therefore, considerations for population cell number, mechanical contractile performance, and synchronized electrophysiology should be considered.

To regain contractile function, infarcted cardiac tissue must be repopulated with new cells. There are approximately 3.2 billion cardiomyocytes (CMs) in the healthy adult human heart.[121] Furthermore, the mean inner left ventricular dimension is 4.5 ± 0.5 cm.[122] Induced myocardial infarcts in porcine models can range from 10-20% of the total area of the left ventricle (LV), based on MRI measurements.[44] Also, clinical infarcts range from 0% to 68% of the LV, with an average size of 17±17% .[123] Therefore, to repopulate the lost cardiomyocytes after infarct, a

cardiac patch should aim to have a surface area of at least 1 cm^2 and contain at least 10% of the total cell population, or 320 million CMs. Bolus injections of 1 billion CMs into porcine MI heart models have demonstrated remuscularization and increased regional and global LV contractile function after infarct[44]; however, a large number of these cells can be lost following injection. CMs in a cardiac patch scaffold should allow for localized therapy in the diseased region. Initial study of engineered cardiac tissues upon implantation in large animal models have demonstrated successful integration with a patch containing 450 million CMs per 35 cm^2 (12.9 million CMs per cm^2) in the porcine heart, with previous successful remuscularization observed in small cryoinjured animal models.[117] Also, small animal model epicardial engraftment has been demonstrated with as few as 500,000 CMs in a 0.49 cm^2 patch (approximately 1 million CMs per cm^2)[62], with patch implants also improving fractional shortening and LV ejection fraction after infarction.[63] Upon *in vivo* implantation on scarred cardiac tissue, engineered tissues with 10% or less of the heart's total cell volume have demonstrated remuscularization of cardiac tissue and functional improvements after infarction.

Contractile performance of the cardiac patch *in vitro* needs to translate to *in vivo* function upon implantation. Contractile strain of healthy adult human myocardium ranges from 15.9-22.1%.[15] Cells on a cardiac patch should aim to achieve contractile results within this range; however, these strain values are difficult to achieve with immature CMs. Stem cell derived CMs are immature in their morphological and functional characteristics compared to adult CMs[124]; but, they are one of the most promising sources of CMs for cardiac tissue patches. Promoting functional maturation of stem cell derived CMs is an area of interest in the field of cardiac tissue engineering. For example, contractile strain within range of *in vivo* cardiac tissue has been demonstrated with hiPS-CMs cultured on fibrin microthread scaffolds after 21 days.[25] To maximize the benefit of cardiac patches, CMs on scaffolds should be mature, so as to represent adult tissue behavior.

In addition, synchronized functional performance of CMs is also essential. One measure of synchronized CM behavior is conduction velocity, or the velocity in which depolarization occurs through cardiac tissue. Conduction velocities in *in vivo* healthy adult human ventricular tissue range from 50 cm/sec to 65 cm/sec.[124] Engineered, aligned cardiac tissues have demonstrated *in vitro* conduction velocities ranging from 24 cm/sec [25] to 41 cm/sec [117], approaching the range of

mature human cardiac tissue. Conduction velocity can be affected by several factors including cell excitability, intercellular coupling, and size, shape and orientation of the CMs.[25,125] Indeed, when stem cell derived CMs are not provided with orientation cues upon *in vivo* injection into the infarcted ventricle, they remuscularize infarcted tissue, but arrhythmias may occur.[43,44]

As conduction propagates through individual cardiomyocytes, the cell depolarizes leading to cell contraction. In this, conduction leads to contraction of the tissue. We have previously demonstrated that we can measure conduction velocity by rate of calcium dye propagation across hiPS-CMs.[25] Based on CM excitation-contraction coupling, we correlated the conduction dynamics with contractile strain dynamics, showing a direct temporal relationship.[21] From this relationship, CM contraction velocity is a surrogate measurement for conduction velocity. Contraction velocity can be measured by the time to initiate contraction and distance between measurements. Contraction dynamics, such as velocity, have been previously used as an indicator of synchronized functional performance.[19]

Overall, successful design parameters for a cardiac patch include:

- Appropriate patch size: >1 cm^2
- Population cell number: >320 million cells
- Mature contractile strain dynamics
- Synchronized cardiomyocyte performance

A decellularized spinach leaf scaffold with CMs may be an appropriate substrate to meet these design parameters. We will evaluate our patch performance based upon these parameters. These design benchmarks provide a mechanism of measuring patch effectiveness and readiness for clinical applications.

2.4 **References**

1. Levick J. An Introduction to Cardiovascular Physiology. 2nd ed. Reed Educational and Professional Publishing, Ltd; 1995.
2. Severs NJ. The cardiac muscle cell. BioEssays. 2000;22(2):188-199. doi:10.1002/(SICI)1521-1878(200002)22:2<188::AID-BIES10>3.0.CO;2-T
3. Severs NJ. Gap junction remodeling in heart failure. J Card Fail. 2002;8(6):S293-S299. doi:10.1054/jcaf.2002.129255

4. Pinnell J, Turner S, Howell S. Cardiac muscle physiology. Contin Educ Anaesth Crit Care Pain. 2007;7(3):85-88. doi:10.1093/bjaceaccp/mkm013
5. Valiente-Alandi I, Schafer AE, Blaxall BC. Extracellular matrix-mediated cellular communication in the heart. J Mol Cell Cardiol. 2016;91:228-237. doi:10.1016/j.yjmcc.2016.01.011
6. Silva AC, Pereira C, Fonseca ACRG, Pinto-do-Ó P, Nascimento DS. Bearing My Heart: The Role of Extracellular Matrix on Cardiac Development, Homeostasis, and Injury Response. Front Cell Dev Biol. 2021;8:1-21. doi:10.3389/fcell.2020.621644
7. Guyette JP, Charest JM, Mills RW, et al. Bioengineering Human Myocardium on Native Extracellular Matrix. Circ Res. 2016;118(1):56-72. doi:10.1161/CIRCRESAHA.115.306874
8. Pijnappels DA, Schalij MJ, Atsma DE, de Vries AAF. Cardiac Anisotropy, Regeneration, and Rhythm. Circ Res. 2014;115(4):e6-e7. doi:10.1161/CIRCRESAHA.115.304644
9. Vunjak-Novakovic G, Tandon N, Godier A, et al. Challenges in Cardiac Tissue Engineering. Tissue Eng Part B Rev. 2010;16(2):169-187. doi:10.1089/ten.teb.2009.0352
10. Wei-Ning Lee, Pernot M, Couade M, et al. Mapping Myocardial Fiber Orientation Using Echocardiography-Based Shear Wave Imaging. IEEE Trans Med Imaging. 2012;31(3):554-562. doi:10.1109/TMI.2011.2172690
11. Stöhr EJ, Shave RE, Baggish AL, Weiner RB. Left ventricular twist mechanics in the context of normal physiology and cardiovascular disease: a review of studies using speckle tracking echocardiography. Am J Physiol Circ Physiol. 2016;311(3):H633-H644. doi:10.1152/ajpheart.00104.2016
12. Arts T, Reneman RS. Measurement of deformation of canine epicardium in vivo during cardiac cycle. Am J Physiol - Hear Circ Physiol. 1980;239(8):H432-7. http://www.ncbi.nlm.nih.gov/pubmed/7435589
13. Scatteia A, Baritussio A, Bucciarelli-Ducci C. Strain imaging using cardiac magnetic resonance. Heart Fail Rev. 2017;22(4):465-476. doi:10.1007/s10741-017-9621-8
14. Taylor RJ, Moody WE, Umar F, et al. Myocardial strain measurement with feature-tracking cardiovascular magnetic resonance: normal values. Eur Hear J – Cardiovasc Imaging. 2015;16(8):871-881. doi:10.1093/ehjci/jev006
15. Yingchoncharoen T, Agarwal S, Popović ZB, Marwick TH. Normal Ranges of Left Ventricular Strain: A Meta-Analysis. J Am Soc Echocardiogr. 2013;26(2):185-191. doi:10.1016/j.echo.2012.10.008
16. Reis LA, Chiu LLY, Feric N, Fu L, Radisic M. Biomaterials in myocardial tissue engineering. J Tissue Eng Regen Med. 2016;10(1):11-28. doi:10.1002/term.1944
17. Gaudette GR, Todaro J, Azeloglu EU, Krukenkamp IB, Chiang F-P. Determination of regional stroke work with high spatial resolution in the isolated beating rabbit heart. Cardiovasc Eng An Int J. 2002;2(4):129-137.
18. Kamgoué A, Ohayon J, Usson Y, Riou L, Tracqui P. Quantification of cardiomyocyte contraction based on image correlation analysis. Cytom Part A. 2009;75A(4):298-308. doi:10.1002/cyto.a.20700
19. Czirok A, Isai DG, Kosa E, et al. Optical-flow based non-invasive analysis of cardiomyocyte contractility. Sci Rep. 2017;7(1):10404. doi:10.1038/s41598-017-10094-7
20. Kelly DJ, Azeloglu EU, Kochupura P V., Sharma GS, Gaudette GR. Accuracy and reproducibility of a subpixel extended phase correlation method to determine micron level displacements in the heart. Med Eng Phys. 2007;29(1):154-162. doi:10.1016/j.medengphy.2006.01.001

21. Hansen KJ, Favreau JT, Gershlak JR, Laflamme MA, Albrecht DR, Gaudette GR. Optical Method to Quantify Mechanical Contraction and Calcium Transients of Human Pluripotent Stem Cell-Derived Cardiomyocytes. Tissue Eng Part C Methods. 2017;23(8):445-454. doi:10.1089/ten.tec.2017.0190
22. Formaggia L, Quarteroni A, Veneziani A. Cardiovascular Mathematics. 1st ed. (Quarteroni A, Hou T, Le Bris C, Patera AT, Zuazua E, eds.). Springer-Verlag Italia; 2009.
23. Tao Z-W, Favreau JT, Guyette JP, et al. Delivering stem cells to the healthy heart on biological sutures: effects on regional mechanical function.pdf. J Tissue Eng Regen Med. 2017;11(1):220-230.
24. Kochupura P V, Azeloglu EU, Kelly DJ, et al. Tissue-Engineered Myocardial Patch Derived From Extracellular Matrix Provides Regional Mechanical Function. Circulation. 2005;112(S1):144–I-149. doi:10.1161/CIRCULATIONAHA.104.524355
25. Hansen KJ, Laflamme MA, Gaudette GR. Development of a Contractile Cardiac Fiber From Pluripotent Stem Cell Derived Cardiomyocytes. Front Cardiovasc Med. 2018;5(52):1-11. doi:10.3389/fcvm.2018.00052
26. Benjamin EJ, Muntner P, Alonso A, et al. Heart Disease and Stroke Statistics—2019 Update: A Report From the American Heart Association. Circulation. 2019;139(10):e56-e528. doi:10.1161/CIR.0000000000000659
27. Fryar CD, Chen TC, Li X. Prevalence of uncontrolled risk factors for cardiovascular disease: United States, 1999-2010. NCHS Data Brief. 2012;(103):1-8.
28. Rodness J, Mihic A, Miyagi Y, Wu J, Weisel RD, Li R-K. VEGF-loaded microsphere patch for local protein delivery to the ischemic heart. Acta Biomater. 2016;45:169-181. doi:10.1016/j.actbio.2016.09.009
29. Holmes JW, Borg TK, Covell JW. Structure and Mechanics of Healing Myocardial Infarcts. Annu Rev Biomed Eng. 2005;7(1):223-253. doi:10.1146/annurev.bioeng.7.060804.100453
30. Sun Y. Infarct scar: a dynamic tissue. Cardiovasc Res. 2000;46(2):250-256. doi:10.1016/S0008-6363(00)00032-8
31. Anzai T. Post-Infarction Inflammation and Left Ventricular Remodeling. Circ J. 2013;77(3):580-587. doi:10.1253/circj.CJ-13-0013
32. Yancy CW, Jessup M, Bozkurt B, et al. 2013 ACCF/AHA Guideline for the Management of Heart Failure. J Am Coll Cardiol. 2013;62(16):e147-e239. doi:10.1016/j.jacc.2013.05.019
33. Grines CL, Cox DA, Stone GW, et al. Coronary Angioplasty with or without Stent Implantation for Acute Myocardial Infarction. N Engl J Med. 1999;341(26):1949-1956. doi:10.1056/NEJM199912233412601
34. Petrie MC, Jhund PS, She L, et al. Ten-Year Outcomes After Coronary Artery Bypass Grafting According to Age in Patients With Heart Failure and Left Ventricular Systolic Dysfunction. Circulation. 2016;134(18):1314-1324. doi:10.1161/CIRCULATIONAHA.116.024800
35. Maron DJ, Hochman JS, Reynolds HR, et al. Initial Invasive or Conservative Strategy for Stable Coronary Disease. N Engl J Med. 2020;382(15):1395-1407. doi:10.1056/NEJMoa1915922
36. Rose EA, Gelijns AC, Moskowitz AJ, et al. Long-Term Use of a Left Ventricular Assist Device for End-Stage Heart Failure. N Engl J Med. 2001;345(20):1435-1443. doi:10.1056/NEJMoa012175

37. Colvin M, Smith JM, Skeans MA, et al. OPTN/SRTR 2015 Annual Data Report: Heart. Am J Transplant. 2017;17:286-356. doi:10.1111/ajt.14128
38. Anderson JM, Rodriguez A, Chang DT. Foreign body reaction to biomaterials. Semin Immunol. 2008;20(2):86-100. doi:10.1016/j.smim.2007.11.004
39. Griffiths M, Ojeh N, Livingstone R, Price R, Navsaria H. Survival of Apligraf in Acute Human Wounds. Tissue Eng. 2004;10(7):1180-1195. doi:10.1089/1076327041887835
40. Schmidt C. FDA approves first cell therapy for wrinkle-free visage. Nat Biotechnol. 2011;29(8):674-675. doi:10.1038/nbt0811-674
41. Schmidt C. Gintuit cell therapy approval signals shift at US regulator. Nat Biotechnol. 2012;30(6):479-479. doi:10.1038/nbt0612-479
42. Fischer A. FDA approves first autologous cellularized scaffold for the repair of cartilage defects of the knee. US Food & Drug Administration. Published 2016. https://www.fda.gov/news-events/press-announcements/fda-approves-first-autologous-cellularized-scaffold-repair-cartilage-defects-knee
43. Liu Y-W, Chen B, Yang X, et al. Human embryonic stem cell–derived cardiomyocytes restore function in infarcted hearts of non-human primates. Nat Biotechnol. 2018;36(7):597-605. doi:10.1038/nbt.4162
44. Romagnuolo R, Masoudpour H, Porta-Sánchez A, et al. Human Embryonic Stem Cell-Derived Cardiomyocytes Regenerate the Infarcted Pig Heart but Induce Ventricular Tachyarrhythmias. Stem Cell Reports. 2019;12(5):967-981. doi:10.1016/j.stemcr.2019.04.005
45. Laflamme MA, Chen KY, Naumova A V., et al. Cardiomyocytes derived from human embryonic stem cells in pro-survival factors enhance function of infarcted rat hearts. Nat Biotechnol. 2007;25(9):1015-1024. doi:10.1038/nbt1327
46. Atala A, Kasper FK, Mikos AG. Engineering Complex Tissues. Sci Transl Med. 2012;4(160):160rv12-160rv12. doi:10.1126/scitranslmed.3004890
47. LEOR J, COHEN S. Myocardial Tissue Engineering: Creating a Muscle Patch for a Wounded Heart. Ann N Y Acad Sci. 2004;1015(1):312-319. doi:10.1196/annals.1302.026
48. Riemenschneider SB, Mattia DJ, Wendel JS, et al. Inosculation and perfusion of pre-vascularized tissue patches containing aligned human microvessels after myocardial infarction. Biomaterials. 2016;97:51-61. doi:10.1016/j.biomaterials.2016.04.031
49. Mao AS, Mooney DJ. Regenerative medicine: Current therapies and future directions. Proc Natl Acad Sci. 2015;112(47):14452-14459. doi:10.1073/pnas.1508520112
50. Novosel EC, Kleinhans C, Kluger PJ. Vascularization is the key challenge in tissue engineering. Adv Drug Deliv Rev. 2011;63(4-5):300-311. doi:10.1016/j.addr.2011.03.004
51. Lesman A, Habib M, Caspi O, et al. Transplantation of a Tissue-Engineered Human Vascularized Cardiac Muscle. Tissue Eng Part A. 2010;16(1):115-125. doi:10.1089/ten.tea.2009.0130
52. Stevens KR, Kreutziger KL, Dupras SK, et al. Physiological function and transplantation of scaffold-free and vascularized human cardiac muscle tissue. Proc Natl Acad Sci. 2009;106(39):16568-16573. doi:10.1073/pnas.0908381106
53. Sakaguchi K, Shimizu T, Horaguchi S, et al. In Vitro Engineering of Vascularized Tissue Surrogates. Sci Rep. 2013;3(1):1316. doi:10.1038/srep01316
54. Zhang B, Montgomery M, Chamberlain MD, et al. Biodegradable scaffold with built-in vasculature for organ-on-a-chip engineering and direct surgical anastomosis. Nat Mater. 2016;15(6):669-678. doi:10.1038/nmat4570

55. Zhang YS, Arneri A, Bersini S, et al. Bioprinting 3D microfibrous scaffolds for engineering endothelialized myocardium and heart-on-a-chip. Biomaterials. 2016;110:45-59. doi:10.1016/j.biomaterials.2016.09.003
56. Kreutziger KL, Muskheli V, Johnson P, Braun K, Wight TN, Murry CE. Developing Vasculature and Stroma in Engineered Human Myocardium. Tissue Eng Part A. 2011;17(9-10):1219-1228. doi:10.1089/ten.tea.2010.0557
57. Coulombe KLK, Murry CE. Vascular perfusion of implanted human engineered cardiac tissue. In: 2014 40th Annual Northeast Bioengineering Conference (NEBEC). Vol April. IEEE; 2014:1-2. doi:10.1109/NEBEC.2014.6972763
58. Masumoto H, Ikuno T, Takeda M, et al. Human iPS cell-engineered cardiac tissue sheets with cardiomyocytes and vascular cells for cardiac regeneration. Sci Rep. 2015;4(1):6716. doi:10.1038/srep06716
59. Anderson JM. Biological Responses to Materials. Annu Rev Mater Res. 2001;31(1):81-110. doi:10.1146/annurev.matsci.31.1.81
60. Yang X, Pabon L, Murry CE. Engineering Adolescence. Circ Res. 2014;114(3):511-523. doi:10.1161/CIRCRESAHA.114.300558
61. Ozawa T, Mickle DAG, Weisel RD, Koyama N, Ozawa S, Li R-K. Optimal Biomaterial for Creation of Autologous Cardiac Grafts. Circulation. 2002;106(12_suppl_1):176-182. doi:10.1161/01.cir.0000032901.55215.cc
62. Shadrin IY, Allen BW, Qian Y, et al. Cardiopatch platform enables maturation and scale-up of human pluripotent stem cell-derived engineered heart tissues. Nat Commun. 2017;8(1):1825. doi:10.1038/s41467-017-01946-x
63. Wendel JS, Ye L, Tao R, et al. Functional Effects of a Tissue-Engineered Cardiac Patch From Human Induced Pluripotent Stem Cell-Derived Cardiomyocytes in a Rat Infarct Model. Stem Cells Transl Med. 2015;4(11):1324-1332. doi:10.5966/sctm.2015-0044
64. Schaefer JA, Guzman PA, Riemenschneider SB, Kamp TJ, Tranquillo RT. A cardiac patch from aligned microvessel and cardiomyocyte patches. J Tissue Eng Regen Med. 2018;12(2):546-556. doi:10.1002/term.2568
65. Chrobak MO, Hansen KJ, Gershlak JR, et al. Design of a Fibrin Microthread-Based Composite Layer for Use in a Cardiac Patch. ACS Biomater Sci Eng. 2017;3(7):1394-1403. doi:10.1021/acsbiomaterials.6b00547
66. Tulloch NL, Muskheli V, Razumova M V., et al. Growth of Engineered Human Myocardium With Mechanical Loading and Vascular Coculture. Circ Res. 2011;109(1):47-59. doi:10.1161/CIRCRESAHA.110.237206
67. Ott HC, Matthiesen TS, Goh S-K, et al. Perfusion-decellularized matrix: using nature's platform to engineer a bioartificial heart. Nat Med. 2008;14(2):213-221. doi:10.1038/nm1684
68. Song JJ, Ott HC. Organ engineering based on decellularized matrix scaffolds. Trends Mol Med. 2011;17(8):424-432. doi:10.1016/j.molmed.2011.03.005
69. Gershlak JR, Hernandez S, Fontana G, et al. Crossing kingdoms: Using decellularized plants as perfusable tissue engineering scaffolds. Biomaterials. 2017;125:13-22. doi:10.1016/j.biomaterials.2017.02.011
70. Shevach M, Soffer-Tsur N, Fleischer S, Shapira A, Dvir T. Fabrication of omentum-based matrix for engineering vascularized cardiac tissues. Biofabrication. 2014;6(2):024101. doi:10.1088/1758-5082/6/2/024101
71. Guyette JP, Gilpin SE, Charest JM, Tapias LF, Ren X, Ott HC. Perfusion decellularization of whole organs. Nat Protoc. 2014;9(6):1451-1468. doi:10.1038/nprot.2014.097

72. Matsuda K, Falkenberg KJ, Woods AA, Choi YS, Morrison WA, Dilley RJ. Adipose-Derived Stem Cells Promote Angiogenesis and Tissue Formation for In Vivo Tissue Engineering. Tissue Eng Part A. 2013;19(11-12):1327-1335. doi:10.1089/ten.tea.2012.0391
73. Williams C, Quinn KP, Georgakoudi I, Black LD. Young developmental age cardiac extracellular matrix promotes the expansion of neonatal cardiomyocytes in vitro. Acta Biomater. 2014;10(1):194-204. doi:10.1016/j.actbio.2013.08.037
74. Parsa H, Ronaldson K, Vunjak-Novakovic G. Bioengineering methods for myocardial regeneration. Adv Drug Deliv Rev. 2016;96:195-202. doi:10.1016/j.addr.2015.06.012
75. Schwan J, Kwaczala AT, Ryan TJ, et al. Anisotropic engineered heart tissue made from laser-cut decellularized myocardium. Sci Rep. 2016;6(1):32068. doi:10.1038/srep32068
76. Zhang B, Lai BFL, Xie R, Davenport Huyer L, Montgomery M, Radisic M. Microfabrication of AngioChip, a biodegradable polymer scaffold with microfluidic vasculature. Nat Protoc. 2018;13(8):1793-1813. doi:10.1038/s41596-018-0015-8
77. Kolesky DB, Homan KA, Skylar-Scott MA, Lewis JA. Three-dimensional bioprinting of thick vascularized tissues. Proc Natl Acad Sci. 2016;113(12):3179-3184. doi:10.1073/pnas.1521342113
78. McCulloh KA, Sperry JS, Adler FR. Water transport in plants obeys Murray's law. Nature. 2003;421(6926):939-942. doi:10.1038/nature01444
79. NIKLAS KJ. A mechanical perspective on foliage leaf form and function. New Phytol. 1999;143(1):19-31. doi:10.1046/j.1469-8137.1999.00441.x
80. Fontana G, Gershlak J, Adamski M, et al. Biofunctionalized Plants as Diverse Biomaterials for Human Cell Culture. Adv Healthc Mater. 2017;6(8):1601225. doi:10.1002/adhm.201601225
81. Gibson LJ. The hierarchical structure and mechanics of plant materials. J R Soc Interface. 2012;9(76):2749-2766. doi:10.1098/rsif.2012.0341
82. Modulevsky DJ, Cuerrier CM, Pelling AE. Biocompatibility of Subcutaneously Implanted Plant-Derived Cellulose Biomaterials. Zhao F, ed. PLoS One. 2016;11(6):e0157894. doi:10.1371/journal.pone.0157894
83. Entcheva E, Bien H, Yin L, Chung C-Y, Farrell M, Kostov Y. Functional cardiac cell constructs on cellulose-based scaffolding. Biomaterials. 2004;25(26):5753-5762. doi:10.1016/j.biomaterials.2004.01.024
84. Helenius G, Bäckdahl H, Bodin A, Nannmark U, Gatenholm P, Risberg B. In vivo biocompatibility of bacterial cellulose. J Biomed Mater Res Part A. 2006;76A(2):431-438. doi:10.1002/jbm.a.30570
85. Hart J, Silcock D, Gunnigle S, Cullen B, Light ND, Watt PW. The role of oxidised regenerated cellulose/collagen in wound repair: effects in vitro on fibroblast biology and in vivo in a model of compromised healing. Int J Biochem Cell Biol. 2002;34(12):1557-1570. doi:10.1016/S1357-2725(02)00062-6
86. Gershlak JR. Decellularized Spinach Leaves and Electrically Conducting Biofibers: Approaches to Overcome the Major Challenges in the Clinical Translation of a Tissue Engineered Cardiac Patch. Published online 2018. https://digital.wpi.edu/concern/etds/n009w252j
87. Basavarajaiah S, Wilson M, Naghavi R, Whyte G, Turner M, Sharma S. Physiological upper limits of left ventricular dimensions in highly trained junior tennis players. Br J Sports Med. 2007;41(11):784-788. doi:10.1136/bjsm.2006.033993

88. Kamihata H, Matsubara H, Nishiue T, et al. Implantation of Bone Marrow Mononuclear Cells Into Ischemic Myocardium Enhances Collateral Perfusion and Regional Function via Side Supply of Angioblasts, Angiogenic Ligands, and Cytokines. Circulation. 2001;104(9):1046-1052. doi:10.1161/hc3501.093817
89. Uemura R, Xu M, Ahmad N, Ashraf M. Bone Marrow Stem Cells Prevent Left Ventricular Remodeling of Ischemic Heart Through Paracrine Signaling. Circ Res. 2006;98(11):1414-1421. doi:10.1161/01.RES.0000225952.61196.39
90. Nagaya N, Kangawa K, Itoh T, et al. Transplantation of Mesenchymal Stem Cells Improves Cardiac Function in a Rat Model of Dilated Cardiomyopathy. Circulation. 2005;112(8):1128-1135. doi:10.1161/CIRCULATIONAHA.104.500447
91. Thomas C V., Coker ML, Zellner JL, Handy JR, Crumbley AJ, Spinale FG. Increased Matrix Metalloproteinase Activity and Selective Upregulation in LV Myocardium From Patients With End-Stage Dilated Cardiomyopathy. Circulation. 1998;97(17):1708-1715. doi:10.1161/01.CIR.97.17.1708
92. Toma C, Pittenger MF, Cahill KS, Byrne BJ, Kessler PD. Human Mesenchymal Stem Cells Differentiate to a Cardiomyocyte Phenotype in the Adult Murine Heart. Circulation. 2002;105(1):93-98. doi:10.1161/hc0102.101442
93. Grinnemo K, Månsson-Broberg A, Leblanc K, et al. Human mesenchymal stem cells do not differentiate into cardiomyocytes in a cardiac ischemic xenomodel. Ann Med. 2006;38(2):144-153. doi:10.1080/07853890500422982
94. Murry CE, Soonpaa MH, Reinecke H, et al. Haematopoietic stem cells do not transdifferentiate into cardiac myocytes in myocardial infarcts. Nature. 2004;428(6983):664-668. doi:10.1038/nature02446
95. Nygren JM, Jovinge S, Breitbach M, et al. Bone marrow–derived hematopoietic cells generate cardiomyocytes at a low frequency through cell fusion, but not transdifferentiation. Nat Med. 2004;10(5):494-501. doi:10.1038/nm1040
96. Park S-J, Kim RY, Park B-W, et al. Dual stem cell therapy synergistically improves cardiac function and vascular regeneration following myocardial infarction. Nat Commun. 2019;10(1):3123. doi:10.1038/s41467-019-11091-2
97. Zimmermann WH, Fink C, Kralisch D, Remmers U, Weil J, Eschenhagen T. Three-Dimensional Engineered Heart Tissue from Neonatal Rat Cardiac Myocytes. Biotechnol Bioeng. 2000;68(1):106-114.
98. Alford PW, Feinberg AW, Sheehy SP, Parker KK. Biohybrid thin films for measuring contractility in engineered cardiovascular muscle. Biomaterials. 2010;31(13):3613-3621. doi:10.1016/j.biomaterials.2010.01.079
99. Feinberg AW, Ripplinger CM, van der Meer P, et al. Functional Differences in Engineered Myocardium from Embryonic Stem Cell-Derived versus Neonatal Cardiomyocytes. Stem Cell Reports. 2013;1(5):387-396. doi:10.1016/j.stemcr.2013.10.004
100. Banyasz T, Lozinskiy I, Payne CE, et al. Transformation of adult rat cardiac myocytes in primary culture. Exp Physiol. 2008;93(3):370-382. doi:10.1113/expphysiol.2007.040659
101. Milani-Nejad N, Janssen PM. Small and large animal models in cardiac contraction research: Advantages and disadvantages. Pharmacol Ther. 2014;141(3):235-249. doi:10.1016/j.pharmthera.2013.10.007
102. Takahashi K, Yamanaka S. Induction of Pluripotent Stem Cells from Mouse Embryonic and Adult Fibroblast Cultures by Defined Factors. Cell. 2006;126(4):663-676. doi:10.1016/j.cell.2006.07.024

103. Yu J, Vodyanik M a, Smuga-Otto K, et al. Induced Pluripotent Stem Cell Lines Derived from Human Somatic Cells. Science (80-). 2007;318(5858):1917-1920. doi:10.1126/science.1151526
104. Mummery C, Ward-van Oostwaard D, Doevendans P, et al. Differentiation of Human Embryonic Stem Cells to Cardiomyocytes. Circulation. 2003;107(21):2733-2740. doi:10.1161/01.CIR.0000068356.38592.68
105. Kehat I, Kenyagin-Karsenti D, Snir M, et al. Human embryonic stem cells can differentiate into myocytes with structural and functional properties of cardiomyocytes. J Clin Invest. 2001;108(3):407-414. doi:10.1172/JCI200112131
106. Zhang J, Wilson GF, Soerens AG, et al. Functional cardiomyocytes derived from human induced pluripotent stem cells. Circ Res. 2009;104(4). doi:10.1161/CIRCRESAHA.108.192237
107. Itskovitz-Eldor J, Schuldiner M, Karsenti D, et al. Differentiation of Human Embryonic Stem Cells into Embryoid Bodies Comprising the Three Embryonic Germ Layers. Mol Med. 2000;6(2):88-95. doi:10.1007/BF03401776
108. Kattman SJ, Witty AD, Gagliardi M, et al. Stage-Specific Optimization of Activin/Nodal and BMP Signaling Promotes Cardiac Differentiation of Mouse and Human Pluripotent Stem Cell Lines. Cell Stem Cell. 2011;8(2):228-240. doi:10.1016/j.stem.2010.12.008
109. Yang L, Soonpaa MH, Adler ED, et al. Human cardiovascular progenitor cells develop from a KDR+ embryonic-stem-cell-derived population. Nature. 2008;453(7194):524-528. doi:10.1038/nature06894
110. Lian X, Hsiao C, Wilson G, et al. Robust cardiomyocyte differentiation from human pluripotent stem cells via temporal modulation of canonical Wnt signaling. Proc Natl Acad Sci. 2012;109(27):E1848-E1857. doi:10.1073/pnas.1200250109
111. Burridge PW, Matsa E, Shukla P, et al. Chemically defined generation of human cardiomyocytes. Nat Methods. 2014;11(8):855-860. doi:10.1038/nmeth.2999
112. Eschenhagen T, Bolli R, Braun T, et al. Cardiomyocyte Regeneration. Circulation. 2017;136(7):680-686. doi:10.1161/CIRCULATIONAHA.117.029343
113. Zhu W-Z, Van Biber B, Laflamme MA. Methods for the Derivation and Use of Cardiomyocytes from Human Pluripotent Stem Cells. In: Schwartz PH, Wesselschmidt RL, eds. Methods Mol Biol. Vol 767. Methods in Molecular Biology. Humana Press; 2011:419-431. doi:10.1007/978-1-61779-201-4_31
114. Burridge PW, Keller G, Gold JD, Wu JC. Production of De Novo Cardiomyocytes: Human Pluripotent Stem Cell Differentiation and Direct Reprogramming. Cell Stem Cell. 2012;10(1):16-28. doi:10.1016/j.stem.2011.12.013
115. Chong JJH, Yang X, Don CW, et al. Human embryonic-stem-cell-derived cardiomyocytes regenerate non-human primate hearts. Nature. 2014;510(7504):273-277. doi:10.1038/nature13233
116. Guan X, Xu W, Zhang H, et al. Correction to: Transplantation of human induced pluripotent stem cell-derived cardiomyocytes improves myocardial function and reverses ventricular remodeling in infarcted rat hearts. Stem Cell Res Ther. 2020;11(1):201. doi:10.1186/s13287-020-01673-z
117. Querdel E, Reinsch M, Castro L, et al. Human Engineered Heart Tissue Patches Remuscularize the Injured Heart in a Dose-Dependent Manner. Circulation. 2021;143(20):1991-2006. doi:10.1161/CIRCULATIONAHA.120.047904

118. Karbassi E, Fenix A, Marchiano S, et al. Cardiomyocyte maturation: advances in knowledge and implications for regenerative medicine. Nat Rev Cardiol. 2020;17(6):341-359. doi:10.1038/s41569-019-0331-x
119. Ribeiro AJS, Ang Y-S, Fu J-D, et al. Contractility of single cardiomyocytes differentiated from pluripotent stem cells depends on physiological shape and substrate stiffness. Proc Natl Acad Sci. 2015;112(41):12705-12710. doi:10.1073/pnas.1508073112
120. Fenoglio J, Albala A, Silva FG, Friedman PL, Wit AL. Structural Basis of Ventricular Arrhythmias in Human Myocardial Infarction: A Hypothesis. Hum Pathol. 1976;7(5):547-563.
121. Tirziu D, Giordano FJ, Simons M. Cell Communications in the Heart. Circulation. 2010;122(9):928-937. doi:10.1161/CIRCULATIONAHA.108.847731
122. Popp RL, Wolfe SB, Hirata T, Feigenbaum H. Estimation of right and left ventricular size by ultrasound. Am J Cardiol. 1969;24(4):523-530. doi:10.1016/0002-9149(69)90495-0
123. Miller TD, Christian TF, Hopfenspirger MR, Hodge DO, Gersh BJ, Gibbons RJ. Infarct Size After Acute Myocardial Infarction Measured by Quantitative Tomographic 99m Tc Sestamibi Imaging Predicts Subsequent Mortality. Circulation. 1995;92(3):334-341. doi:10.1161/01.CIR.92.3.334
124. Yang X, Pabon L, Murry CE. Engineering Adolescence: Maturation of Human Pluripotent Stem Cell-derived Cardiomyocytes. Circ Res. 2014;114(3):511-523. doi:10.1161/CIRCRESAHA.114.300558.Engineering
125. Taggart P, Sutton PM, Opthof T, et al. Inhomogeneous transmural conduction during early ischaemia in patients with coronary artery disease. J Mol Cell Cardiol. 2000;32(4):621-630. doi:10.1006/jmcc.2000.1105
126. De Boer TP, Van Rijen HVM, Van Der Heyden MAG, De Bakker JMT, Van Veen TAB. Adrenergic regulation of conduction velocity in cultures of immature cardiomyocytes. Netherlands Hear J. 2008;16(3):106-109. doi:10.1007/BF03086127

3. Specific Aim 1: Determine if Fluid Perfusion Through Leaf Vasculature Affects Cell Function

3.1 Introduction

The major limitation of current thick tissue engineered solutions is the lack of vasculature to perfuse cells. As tissue thickness increases, vasculature is needed to properly provide oxygen and nutrients to all parts of the tissue. This is particularly concerning when engineering heart muscle. The left ventricular wall thickness ranges on average from 2.3 millimeters at the apex to 10.3 millimeters at the base.[1] A tissue engineered solution to re-functionalize diseased heart tissue must be able to withstand the heart's contractile behavior, as well as provide nutrients to the entire tissue. Thick engineered cardiac tissue for implantation requires a vasculature to provide nutrients and remove waste to retain tissue viability because cells are only able to survive a maximum of 200 μm from a nutrient source due to limitations of oxygen diffusion.[2,3] Vasculature within a thick-walled tissue engineered patch would supply cardiac cells with the nutrients required for survival. In addition, the vasculature of engineered tissues should be integrated, branched and perfusable to maintain tissue function. Currently, lack of vasculature limits the thickness of current scaffolds, reducing clinical efficacy and limiting use in humans. Few engineered constructs demonstrate immediate functional vascular flow through engineered tissues *in vitro* and *in vivo*, and instead demonstrate delayed integration and neovascularization after *in vivo* implantation.[4–7]

Inspired by nature, we found leaves have many desirable properties for cardiac tissue engineering. Leaves have a native patent vasculature with branching similar to that of the human cardiovascular system.[8] The leaf's vasculature is composed of branching vessels, with water and nutrient transport occurring through the petiole, xylem, phloem, and stomata. The petiole is composed of a lumen and vascular bundles surrounding the lumen. The petiole lumen is hollow and can be perfused. The vascular bundles contain xylem and phloem, which are tube-like structures that conduct nutrient, water, and oxygen transport for leaves when growing.[9] Water flow through the xylem occurs by transport through the vascular bundles which feed into second and third order veins. Water exits the veins into the plant tissue or additional branching veins into the mesophyll.[10] Stomata are 30 to 80 μm long epidermal pores on the surface of the leaf that control the diffusion of CO_2 and water vapor in and out of the leaf in nature.[11] During leaf perfusion, the stomata may play a role in how solutions exit through the leaf tissue to the surface.

Unlike microvasculature, the spinach leaf's vascular system has large vessels branching into smaller ones. The decellularized spinach leaf petiole has been seeded with human umbilical vein endothelial cells, mimicking the inner lining of mammalian blood vessels.[12] However, it was recently observed that full endothelialization with cells in decellularized spinach leaves may not be feasible due to the anatomical limitations of cross sections of the leaf vasculature past the petiole.[9] Despite this, perfusion of media and small molecules through the leaf vasculature remains feasible for use in tissue engineering. To verify this, small molecules in solution should be perfused through the spinach leaf vasculature's and demonstrate the appropriate effect on mammalian cells cultured on the leaf surface.

To demonstrate the leaf vasculature's capacity to perfuse cells seeded on the leaf surface, we designed a flow system that supports nutrient perfusion of the patent decellularized spinach leaf vasculature. With the perfusion system, we set to perfuse a cardiomyocyte seeded decellularized spinach leaf with cardioactive drug media. Two clinically relevant cardioactive drugs were selected: epinephrine (adrenaline) and verapamil. Epinephrine is an alpha- and beta-adrenergic receptor agonist which promotes binding to adrenergic receptors. Epinephrine was chosen due to its strong effect on hiPS-CM beat frequency compared to other adrenergic receptor agonists like isoproterenol.[13] Verapamil is a non-torsadogenic drug that inhibits calcium channels and sarcomere shortening[14], and has been found to decrease cardiomyocyte contractile beat frequency and contractility.[15] Both epinephrine and verapamil rapidly affect hiPS-CM contractile beat frequency and contractility *in vitro*.[13,15,16] We pursued the use of these drugs to demonstrate functional changes in hiPS-CM behavior following leaf perfusion due to their rapid effect on hiPS-CMs demonstrated in culture. Measuring contractile strain and beat frequency functional parameters will allow us to determine if the cardioactive drug reaches the cells on the leaf surface flowing through the leaf vasculature.

3.2 **Materials and Methods**

3.2.1 Spinach Decellularization and Scaffold Preparation

Spinach leaves were cannulated with 27 gauge needles, decellularized, and lyophilized as previously described[12] and outlined in Appendix A. Lyophilized leaves were stored at room temperature until used. Whole, cannulated leaves were rehydrated on a shaker plate with 10 mM

Tris buffer pH 9.0 solution for 30 minutes, rinsed with deionized (DI) water for 1 hour, and sterilized with 70% ethanol for 1 hour. Leaves in 70% ethanol were transferred into a biosafety cabinet and rinsed three times in sterile 1X PBS. Sterile 10 mm diameter Pyrex cloning wells (Corning Inc., Corning, NY) were positioned in two to four locations on the leaf surface, approximately one inch from the initiation of the vascular branching, and equidistant from the leaf's primary vein (left and right). RPMI-B27 cell media (RPMI 1640, 2% B-27™, 1% L-glutamine, and 1% Penicillin/Streptomycin) was pipetted into the cloning wells and incubated at 37°C overnight prior to cell seeding.

3.2.2 hiPS-CM Differentiation, Isolation, and Seeding on Leaves

hiPS-CMs were differentiated into cardiomyocytes with induction of activin-A and bone morphogenetic protein-4 in the lab of Dr. Michael Laflamme at McEwen Stem Cell Institute (Appendix B).[17,18] Cells were cryopreserved, with cell preparations contained >75% cardiomyocytes.[18–20] hiPS-CMs were shipped overnight to Worcester Polytechnic Institute and stored in cryogenic conditions. When they were ready to be used, they were thawed. hiPS-CMs were thawed and seeded in RPMI-B27 media with 10% fetal bovine serum (FBS) (Gibco) and 1% Rho-associated protein kinase (ROCK) inhibitor (Y-27632 dihydrochloride, Sigma Aldrich) to reduce cell apoptosis (Appendix B).

After media incubation overnight, RPMI-B27 was aspirated from the decellularized leaves. 200,000 hiPS-CMs were seeded in the sterile 10 mm diameter cloning wells (255,000 cells/cm^2) and were incubated for 18-24 hours at 37°C (N=2, n=6). Cells were seeded in cloning wells on left and right sides of the leaf main stem. We assumed there were no behavior differences between left and right sides of a single leaf in their perfusion properties. As positive controls, 90,909 hiPS-CMs/cm^2 were seeded in triplicate on collagen IV (human placenta, 10 μg/mL, Sigma Aldrich) coated tissue culture plastic (TCP) (N=2, n=6). Cells were cultured in RPMI-B27 media on leaves and controls at 37°C for a minimum of 3 days, or until contraction is observed. RPMI-B27 cell media was replenished every day.

3.2.3 hiPS-CM Contractile Strain and Beat Frequency

Cardiac left ventricular contraction is defined by tissue deformation and strain in the left ventricle *in vivo*.[21] Measuring hiPS-CMs contractile strain and frequency can be accomplished optically and non-invasively under a microscope with a high-speed camera.[22–25] We used high

density mapping (HDM), as previously described[25,26], to measure hiPS-CM contractile strain and contractile frequency on decellularized spinach leaves. Live hiPS-CM contraction videos were visualized with an inverted microscope (DMIL, Leica Microsystems, Buffalo Grove, IL) and recorded at 60 frames per second with a high-speed camera (HiSpec 4, Fastec Imaging Corp, San Diego, CA). HDM analysis of hiPS-CM contraction was performed using code written in MATLAB (MathWorks, Natick, MA), previously explained in detail[26] (Appendix C). HDM uses a defined region of interest (ROI) and segments it into smaller subimages (32x32 pixels). Each subimage is transformed into the discrete Fourier domain using the light intensity. The subimage intensity is compared to that of the following frame using phase correlation to determine deformation. An inverse Fourier transform is then applied to find the peak displacement value between the two frames.[25] This process continues across the ROI with an overlap of 16 pixels. Green-Lagrange strain is calculated with reference to the first video frame. Green-Lagrange strain allows us to calculate small tissue deformation based on an initial reference state and is not affected by rigid body motion or rotation.[27]

Maximum contractile strain is reported as the peak strain value from initiation of contraction.[26] Contractile beat frequency is calculated using Fast Fourier transform and power analysis of contractile strain measurements over several beats in MATLAB. This allows us to calculate the frequency between strain contraction peaks, or the beat frequency. The associated frequency plot in which peaks occur are the most frequent peak intervals in Hz or beats per second. At the appropriate frequency peak, frequency in beats per minute is calculated by multiplying the corresponding frequency by 60 seconds/minute.

3.2.4 Cardioactive Drug Dosing Study on TCP

We first conducted a preliminary experiment to determine the appropriate drug dose to use for perfusion. Previous studies have shown that hiPS-CM contractile strain and beat frequency change in response to a variety of cardioactive drug dosages.[13] Collagen IV (human placenta, 10 μg/mL, Sigma Aldrich) coated tissue culture plastic (TCP) were seeded with 90,909 hiPS-CMs/cm^2 and cultured in RPMI-B27 media for 3 to 7 days before drug dosing (N=2, n=5 control, n=6 per cardioactive drug concentration). Stock solutions of 50 mg/mL epinephrine (Sigma-Aldrich) and 50 mg/mL verapamil (Sigma-Aldrich) were prepared by dissolving in DI water or methanol, respectively. Drug potency of cardioactive drugs can be measured by the

concentration in which they induce a 50% change in cell effect. For cardiomyocytes, effect can be measured by cell sarcomere shortening[14], an indication of contractile behavior, with an increase (EC_{50}) or decrease (IC_{50}) in shortening. Epinephrine's EC_{50} in adult human cardiomyocytes is 0.03 μM *in vitro*.[28] Verapamil's IC_{50} adult human cardiomyocytes is 0.04 μM *in vitro*.[14] Previous research has demonstrated substantial change in contractile behavior with higher concentrations of cardioactive drugs when applied to hiPS-CMs[13] compared to that of adult cardiomyocytes. Therefore, we dosed hiPS-CMs with higher concentrations values than the respective EC_{50} or IC_{50} values to observe significant changes in hiPS-CM function. Furthermore, 3D engineered heart tissues have exhibited a ten-fold increase in Verapamil IC_{50} value compared to cells in monolayer culture.[15] To test the effect of cardioactive drug concentrations on hiPS-CMs, epinephrine (5, 10, 50 μM) and verapamil (0.1, 1, 10 μM) concentrations were prepared with stock solution diluted in warm RPMI-B27. Control media solutions contained RPMI-B27 with the largest added volume of DI water or methanol, respectively. Drug dosing was performed with static media incubation in the TCP wells.

Individual TCP wells were marked with ink stamps to mark cell cluster locations. hiPS-CM contractile strain and beat frequency were collected with HDM analysis prior to and after 5 minutes of exposure to cardioactive drugs. Video data from one cell cluster region within a well sample was analyzed. Immediately after data collection, samples were fixed in 4% paraformaldehyde (PFA), rinsed three times in 1X PBS, and stored in 1X PBS at 4°C.

3.2.5 Leaf Perfusion System

The leaf perfusion system was designed to fit on an inverted microscope (DMIL, Leica Microsystems, Buffalo Grove, IL) to accommodate high speed imaging contractile measurements during perfusion. The perfusion system was comprised of a platform, tubing, media reservoir, and pump (**Figure 3-1**). The cannulated leaf was placed on a platform composed of a modified 150 mm Petri dish and perfused through a 27-gauge needle. Perfusion was performed using luer lock-connected 1/16" ID Tygon® PVC tubing, attached to a sterile 3 mL syringe and syringe pump (Harvard Apparatus© PHD 2000 Syringe Pump, model 70-2001) to apply a constant flow rate for leaf perfusion. Warm cardioactive media was pushed through the tubing prior to initiation of the pump to purge air and remove bubbles. The syringe contained

warm media for leaf perfusion. Waste solution exiting the leaf during perfusion was manually drawn up with a micropipette and disposed of as waste.

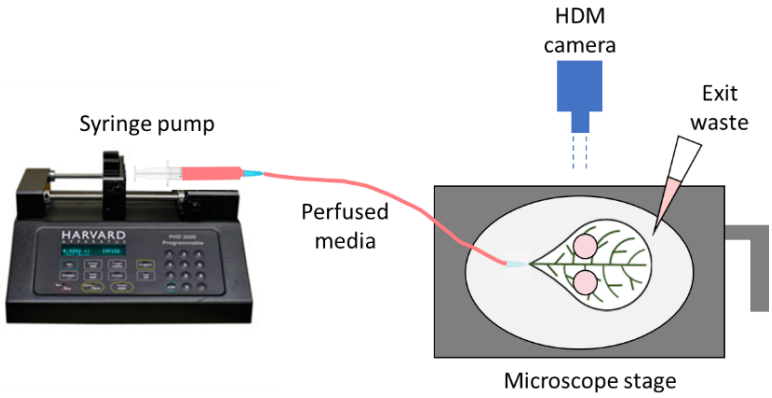

Figure 3-1: Leaf perfusion system for live hiPS-CM imaging. The leaf perfusion system utilizes a syringe pump and tubing in which to perfuse media through leaf vasculature to seeded hiPS-CMs on the leaf's surface. Leaf perfusion occurs on a microscope stage with high density mapping (HDM) live imaging. Exit waste is manually drawn up around the leaf.

3.2.6 Cardioactive Drug Perfusion of hiPS-CM Seeded Leaves

Media perfusion flow rate on the syringe pump was set based on previous data and physiological cardiac tissue blood flow. Based on previous experiments, an average confluent layer of human induced pluripotent stem cell derived cardiomyocytes (hiPS-CMs) on decellularized spinach leaves holds 1557 cells/mm^2 (n=4). The average surface area of a whole spinach leaf is approximately 2000 mm^2 (n=5). Therefore, a confluent layer of hiPS-CMs on a spinach leaf would hold 3.114 million cells. The average blood flow rate through the left ventricular myocardium is 1 mL/min/gram [29], and assuming an average human heart weight (300 grams) and number of cardiomyocytes (3.2 billion cells), each healthy cardiomyocyte receives blood at approximately 9.375x10^{-8} mL/min. Therefore, to maintain this rate, a confluent layer of cells on the decellularized spinach leaf would require at least 0.292 mL/min, or 292 µL/min, of nutrients. To perfuse cardioactive media through the leaf effectively, we set the perfusion syringe pump to a rate of 500 µL/min.

Prior to leaf drug perfusion, warm RPMI-B27 media was incubated on cell surface in the cloning wells for 5 minutes at room temperature ambient conditions. Positive controls included hiPS-CMs on collagen IV coated TCP. During this period in RPMI-B27 static culture, HDM data collection was performed for the pre-drug condition. Static RPMI-B27 was removed from the leaves and TCP after 5 minutes. Perfusion of warm 50 µM epinephrine dosed RPMI-B27 was

perfused through the decellularized spinach leaf's vasculature with the syringe pump for 5 minutes (N=2, n=6). Positive controls on collagen IV coated TCP were induced with warm 50 μM epinephrine dosed RPMI-B27 with direct static incubation (N=2, n=6). HDM data was collected after 5 minutes of exposure to cardioactive drugs to detect changes in hiPS-CM contractile strain and beat frequency. An additional single leaf perfusion experiment for drug washout was initiated with fresh, warm RPMI-B27 for 5 minutes to determine if washout occurred (N=1, n=4). Immediately after data collection, samples were fixed in 4% PFA, rinsed three times with 1X PBS, and stored in 1X PBS at 4°C.

3.2.7 Perfusion of Trypan Blue Through Leaf Vasculature

Trypan blue dye (Thermo Fisher, 0.4%) was perfused through a fixed hiPS-CM seeded decellularized leaf to detect dye perfusion through leaf vasculature to cells. Trypan blue is routinely used as a cell stain to assess cell viability using the dye exclusion test. The dye exclusion test is the concept that viable cells do not take up dyes, but non-viable cells are permeable and take up dye. The hiPS-CMs on the decellularized leaf were not contractile prior to fixation and did not appear viable on the leaf upon observation under microscopy. Non-contractile hiPS-CMs on a leaf (n=1) were imaged under bright light at 4X objective prior to dye perfusion on an Eclipse 3600 microscope (Nikon, Tokyo, Japan). The attached camera was a SPOT Insight 5.1Mps CMOS Color Camera (SPOT Imaging™, Sterling Heights, MI) with Sony Pregius™ sCMOS sensor. White balance was performed prior to imaging. The hiPS-CM seeded leaf was perfused with 0.5 mL of trypan blue dye and imaged in the same cell region to detect dye migration through the vasculature and to cells. Presence of trypan blue dye was detected by quantifying image color intensity in ImageJ (NIH) using measured RGB colorimetry. Collected images were 8 bit and each RGB channel ranged from 0-255 color scale, where 0 corresponds to black and 255 corresponds to white per color channel. RGB values were collected at the following regions with three measurements each: cell cluster, vasculature, and leaf tissue. Intensity per location was calculated by $I = \frac{1}{3}(R + G + B)$, where R, G, and B are channel color values. Calculating intensity decouples intensity from the color information.[30,31] The intensity of each pixel location had a value between 0 and 255. The percent change in intensity after trypan blue perfusion at each location was calculated by: $I = \frac{I_0 - I_t}{I_0} * 100$, where I_0 is the intensity value

before perfusion and I_t is intensity after perfusion at a paired location. The average change in intensity was calculated per location on the leaf.

3.2.8 Statistical Analysis

All data are reported as mean ± standard deviation. To detect meaningful changes in beat frequency and contractile strain after drug addition in the cardioactive drug dosing study, we performed paired t-tests for pre- versus post-drug conditions ($p<0.05$). Strain and beat frequency analyses at various drug concentrations and control media were analyzed with a one-way ANOVA with post-hoc Tukey t-test ($p<0.05$).

For leaf perfusion studies, data were collected from two biological replicates (N=2) and six separate well samples (n=6) seeded on collagen IV coated TCP or perfused leaves. Paired t-tests ($p<0.05$) were completed for hiPS-CM contractile strain and beat frequency before and after epinephrine addition on substrates. Unpaired t-tests ($p<0.05$) were performed to compare differences in average strain and beat frequency after epinephrine on TCP and leaf perfusion samples. All statistical analyses were performed in GraphPad Prism 9 (GraphPad Software, San Diego, CA).

3.3 **Results**

3.3.1 10 μM and 50 μM Epinephrine Increase hiPS-CM Beat Frequency on TCP

In all epinephrine dosing conditions, there were no significant changes in hiPS-CM contractile strain between pre- and post-drug addition on collagen IV coated TCP (**Figure 3-2A**). Also, there were no differences in hiPS-CM strain between control media and epinephrine dosed media (**Figure 3-2B**). From this information, we determined that hiPS-CM contractile strain on collagen IV coated TCP is not significantly affected by 5, 10, or 50 μM epinephrine in RPMI-B27 media after 5 minutes of incubation at room temperature.

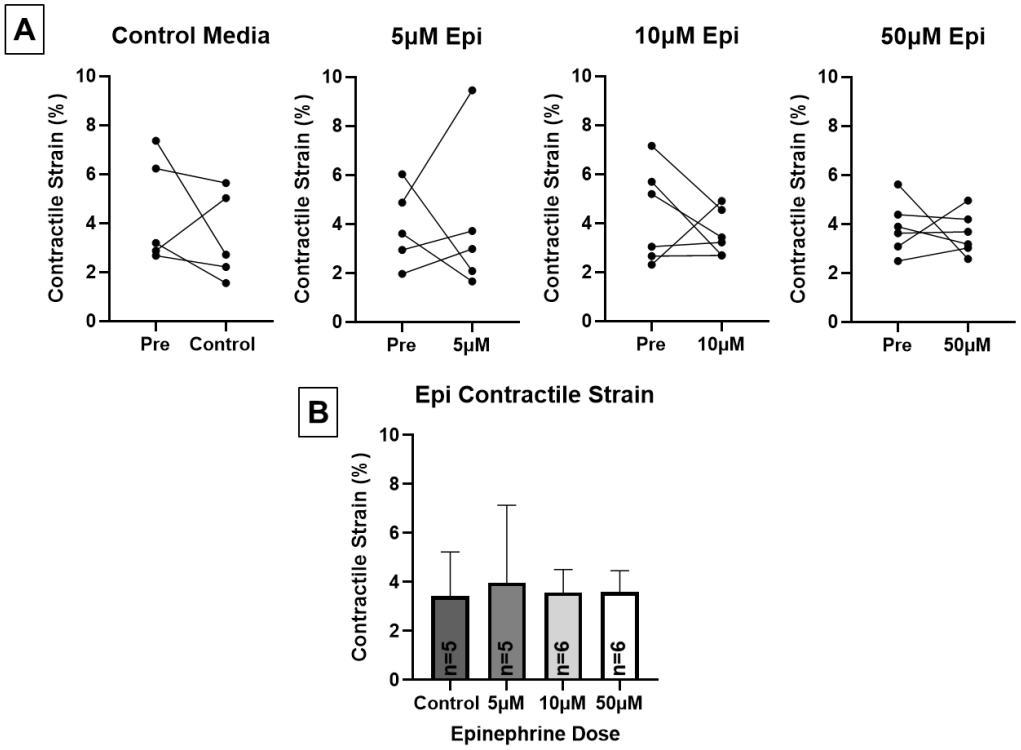

Figure 3-2: hiPS-CM contractile strain after exposure to various concentrations of epinephrine on TCP. (A) HDM analysis demonstrated no significant differences in contractile strain in hiPS-CMs before and after addition of 5, 10, or 50 μM epinephrine media. (B) No significant differences found in contractile strain between control and epinephrine dosed hiPS-CMs on collagen IV TCP. Sample sizes n for each condition are noted within the data.

However, we observed significant increases in hiPS-CM beat frequency on collagen IV coated TCP with the addition of 10 μM ($p<0.01$), and 50 μM ($p<0.001$) epinephrine in RPMI-B27 media (**Figure 3-3A**). In addition, both 10 μM ($p<0.05$) and 50 μM ($p<0.01$) epinephrine addition effectively changed beat frequency compared to control media conditions (**Figure 3-3B**). For leaf perfusion conditions, we proceeded to use 50 μM epinephrine concentration for perfusion to ensure that any increases in beat frequency were substantial and different from controls.

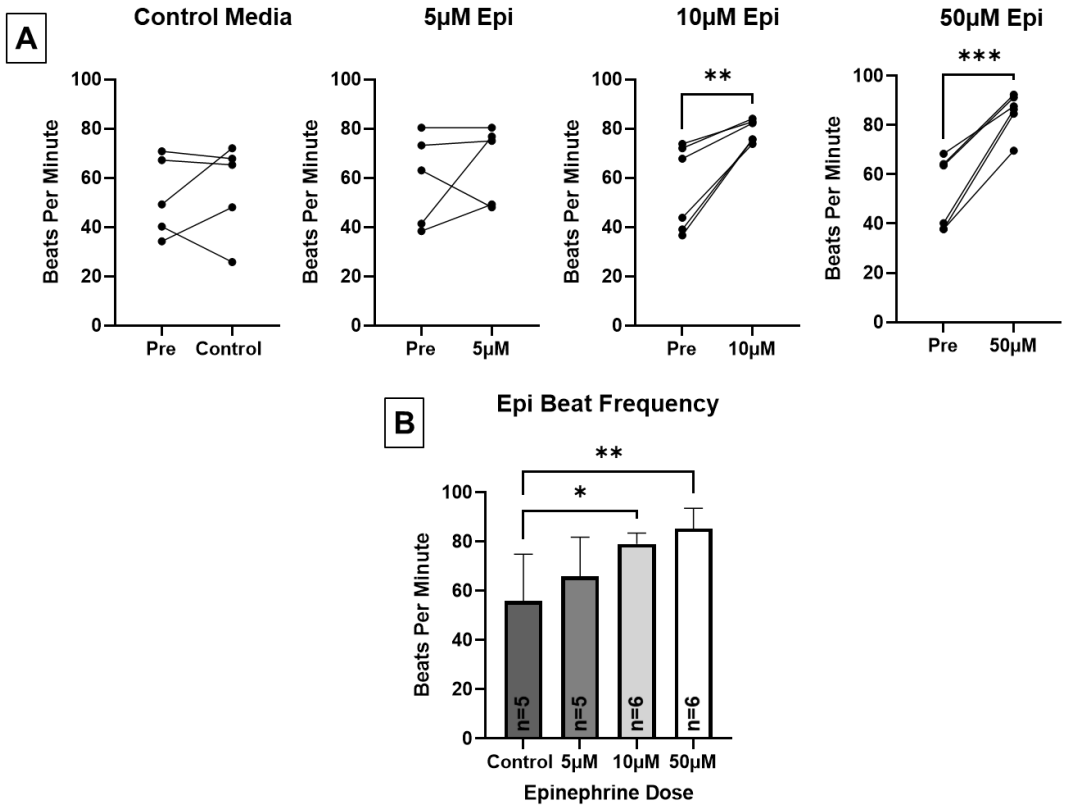

Figure 3-3: hiPS-CM beat frequency after exposure to various concentrations of epinephrine on TCP. (A) HDM analysis demonstrated significant increases in contractile beat frequency in hiPS-CMs on TCP after addition of 10 μM ($p<0.01$), and 50 μM ($p<0.001$) epinephrine media. No significant differences in beat frequency were observed after control media or 5 μM epinephrine addition. (B) Significant differences found in contractile strain between control and 10 μM ($p<0.05$) and 50 μM ($p<0.01$) epinephrine dosed hiPS-CMs on collagen IV TCP. Sample sizes n for each condition are noted within the data.

3.3.2 hiPS-CM Contraction Not Observed After Addition of Verapamil

Contraction was observed in all collagen IV coated TCP wells prior to addition of verapamil in RPMI-B27. Application of all concentrations of verapamil including the lowest concentration (0.1 μM) resulted in cessation of hiPS-CM contraction in all wells. In addition, after RPMI-B27 media washout and incubation for 30 minutes, cell samples did not resume contracting. For this reason, we focused only on epinephrine as a cardioactive drug for perfusion.

3.3.3 Epinephrine Does Not Significantly Affect hiPS-CM Contractile Strain

Static culture addition of 50 μM epinephrine in RPMI-B27 media to collagen IV coated TCP demonstrated no statistically significant changes in hiPS-CM contractile strain (**Figure 3-4A**) (N=2, n=6). Following addition of 50 μM epinephrine through leaf perfusion, we also saw no significant changes in contractile strain in the perfusion group (**Figure 3-4B**) (N=2, n=6). These

results are consistent with contractile strain results in Section 3.3.1. In addition, there were no significant differences between hiPS-CM contractile strain between static culture and leaf perfusion before or after epinephrine addition (**Figure 3-4C, 3-4D**).

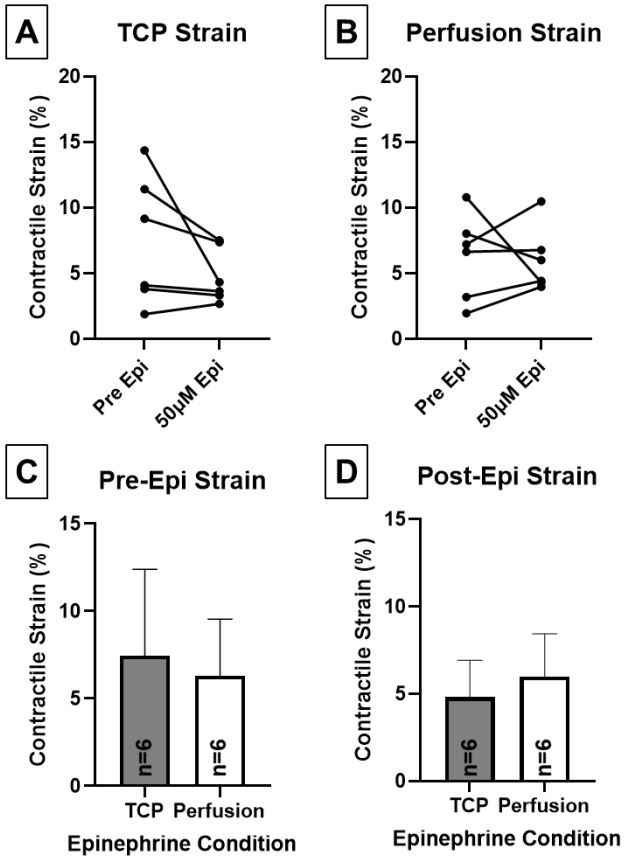

Figure 3-4: hiPS-CM contractile strain before and after epinephrine addition to TCP and perfused leaves. (A) No significant changes in contractile strain were observed in hiPS-CMs on TCP after static culture addition of 50 μM epinephrine. (B) No significant changes in hiPS-CM contractile strain on the leaf surface were observed after epinephrine media leaf vascular perfusion. (C, D) Average contractile strain before (C) and after (D) epinephrine addition showed no significant differences between the TCP and leaf perfused conditions. Sample sizes n for each condition are noted within the data.

3.3.4 Epinephrine Perfusion Significantly Affects hiPS-CM Beat Frequency

Delivery of 50 μM epinephrine media significantly increased hiPS-CM beat frequency in both static collagen IV coated TCP (**Figure 3-5A**) and leaf perfusion conditions (N=2, n=6) ($p<0.05$) (**Figure 3-5B**). This demonstrates that epinephrine in cell media affected cells through leaf perfusion after 5 minutes at room temperature. There were no differences in hiPS-CM beat frequency prior to epinephrine addition between TCP and leaf substrates ($p=0.08$) (**Figure 3-5C**), although beat frequency is slightly lower in hiPS-CMs on leaves prior to epinephrine

perfusion. However, epinephrine-induced hiPS-CM beat frequency was significantly higher in TCP conditions than leaf perfusion ($p<0.05$) (**Figure 3-5D**).

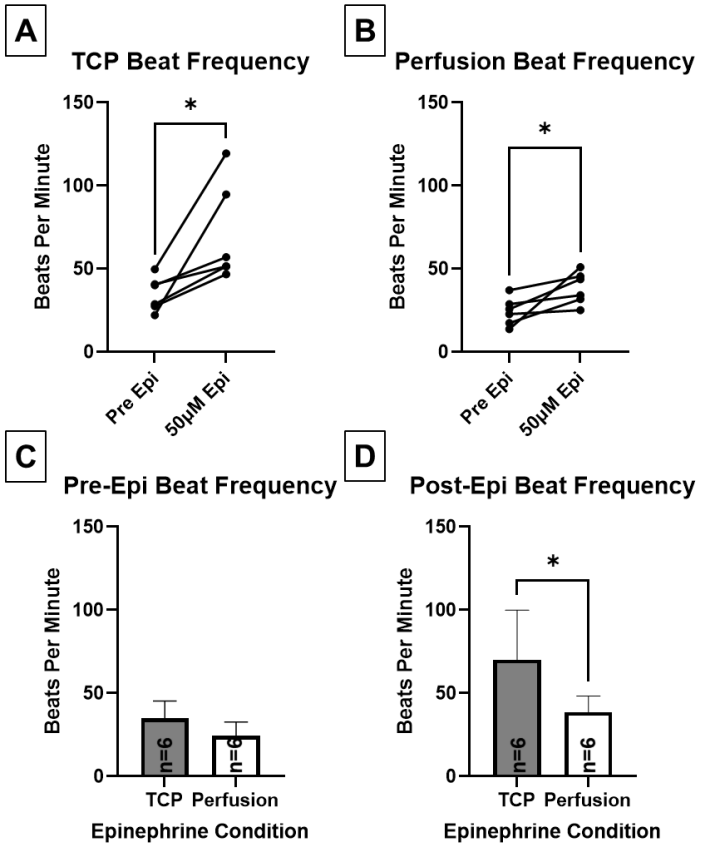

Figure 3-5: hiPS-CM beat frequency before and after epinephrine addition to TCP and perfused leaves. (A) Static culture addition of 50 μM epinephrine significantly increased contractile beat frequency in hiPS-CMs on TCP ($p<0.05$). (B) Perfused epinephrine leaves demonstrated significantly increased hiPS-CM beat frequency on the leaf surface compared to before perfusion ($p<0.05$). (C) Beat frequency prior to epinephrine addition shows no differences between TCP and leaf frequency. (D) After epinephrine addition, there were significant differences between TCP and leaf perfused conditions ($p<0.05$), with slower frequency on hiPS-CMs on perfused leaves than on TCP. Sample sizes n for each condition are noted within the data.

3.3.5 Perfusion Washout Does Not Lower Beat Frequency After Epinephrine Perfusion

Following 50 μM epinephrine perfusion, fresh warm RPMI-B27 media was perfused through a leaf for 5 minutes to wash out epinephrine media (N=1, n=4). Washout perfusion did not demonstrate a decrease in contractile strain (**Figure 3-6A**) nor beat frequency (**Figure 3-6B**). In fact, some samples continued to demonstrate a further increase in beat frequency.

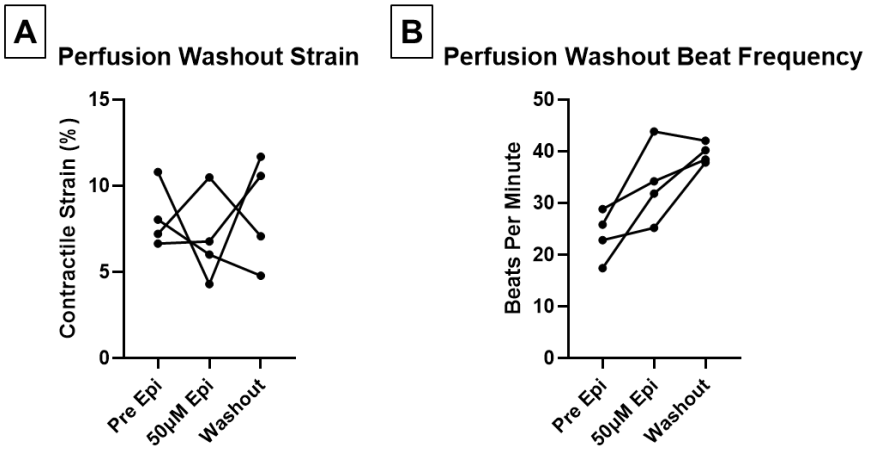

Figure 3-6: Effect of leaf perfusion media washout on hiPS-CM contractile strain and beat frequency following epinephrine perfusion. (A) RPMI-B27 media washout did not demonstrate meaningful change in contractile strain. (B) Media washout perfusion did not affect hiPS-CM beat frequency. Washout was performed for a single biological replicate (N=1, n=4).

3.3.6 Trypan Blue Leaf Perfusion Travels to Seeded hiPS-CMs

To the naked eye, decellularized spinach leaf vasculature is stained blue following trypan blue dye perfusion, including where the hiPS-CMs were seeded (circled in red) (**Figure 3-7A**). Trypan blue also stained the leaf tissue and cells, showing that the perfused dye traveled through the vasculature and exited into the leaf tissue (**Figure 3-7B**, **3-7C**). Microscopy images comparing before and after trypan blue perfusion illustrate dark blue hiPS-CMs after dye perfusion, indicating that the trypan blue traveled to the cell and permeated the cell membrane. However, it is difficult to distinguish the dye in the leaf vasculature. Upon quantification of color using image intensity measurements, we observed that pixel intensity (where 0 corresponds to no light, and 255 is white light) of the cell cluster, leaf vasculature and leaf tissue decreases on average by 42%, 60%, and 11%, respectively, after trypan blue perfusion. There was no change in white space color. As trypan blue is a dark blue dye and the decellularized spinach leaf is initially transparent, it is logical that the dye decreases light intensity after dye perfusion. Although we cannot draw conclusions from one hiPS-CM leaf sample, these data suggest that perfusion of trypan blue traveled through the leaf vasculature to the leaf tissue and cells.

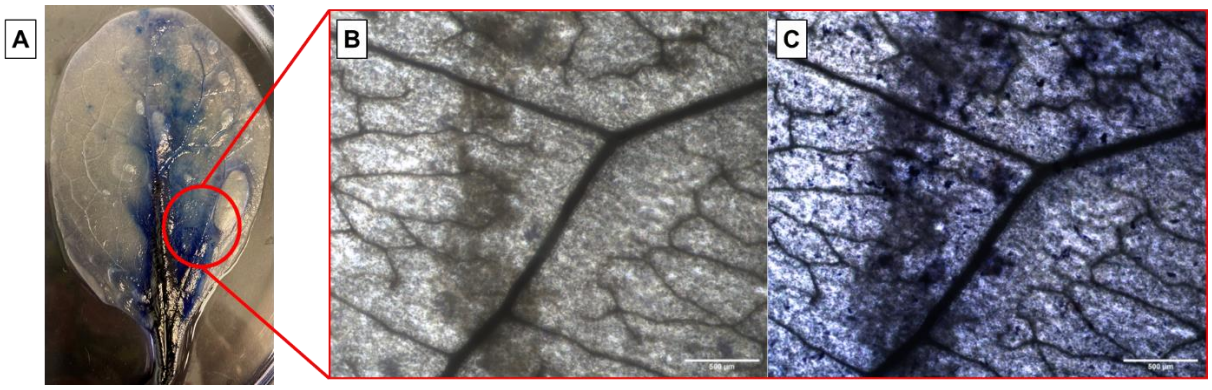

Figure 3-7: Leaf perfusion of trypan blue through hiPS-CM seeded leaf vasculature. (A) Trypan blue dye is present through the vasculature and leaf tissue (blue). hiPS-CM seeding location circled in red. (B) Prior to trypan blue perfusion, hiPS-CMs were adherent, but not viable on leaf. (C) Trypan blue stained adherent hiPS-CMs on leaf surface (blue), demonstrating vasculature is perfusable and can reach adherent non-viable cells. Scale bars 500 μm.

3.4 Discussion

Decellularized spinach leaves are a promising vascularized scaffold for cardiac tissue engineering. An attractive feature of this scaffold is the vascularized network that is inherent within the structure. This research aimed to determine if perfused leaf vasculature is capable of supplying compounds to cells seeded on the leaf surface, indicating a perfusable scaffold for cardiac tissue engineering. We demonstrated that a cardioactive drug significantly affects seeded hiPS-CM function on leaves when perfused through leaf vasculature. Specifically, epinephrine, a drug that increases contractile rate frequency, increased seeded hiPS-CM beat frequency when perfused through the vasculature. Thus, perfusate from the leaf vasculature will permeate the decellularized tissue to the leaf surface, supplying seeded cells with compounds that can alter cell function.

Although hiPS-CM contractile beat frequency was affected by perfused and control doses of epinephrine, hiPS-CM contractile strain was not. This is contradictory to previous studies with static culture epinephrine addition to hiPS-CMs. Contractile strain has previously been found to increase with dosed epinephrine.[13] Our observations may be due to the room temperature conditions in which the cells were exposed. Cardiac cells are temperature sensitive and demonstrate longer action potential duration at room temperature than body temperature.[32] As ambient temperature affects electrophysiology of cardiomyocytes, it may also play a role in the observed hiPS-CM contractile properties. In addition, cold stress of cardiomyocytes has been

found to lead to oxidative stress, autophagy and apoptosis.[33] Conducting experiments at room temperature for 10 minutes, despite using warm media, could have potential implications on the contractility of hiPS-CM clusters. hiPS-CM contractile strain prior to epinephrine addition was within the range we have observed for collagen IV coated TCP and non-coated leaves.[20,34] Future studies should use incubation chambers to maintain equilibration temperatures for environment continuity. Mounted incubation chambers are available on inverted microscopes but would require modification to allow for the current perfusion design system.

Washout of epinephrine did not restore hiPS-CM beat frequency to baseline levels. It is possible that five minutes is not enough time to wash out epinephrine from this model system. Residual epinephrine may remain within the vasculature and continue to flow to the hiPS-CMs during fresh media perfusion. Additional time and media volume is likely required to demonstrate a return in beat frequency to pre-epinephrine drug values. To start, further washout control studies in TCP could be performed to determine the static culture timing conditions in which we observe return to pre-drug beat frequency. There is likely to be a delay in the perfused leaf scaffolds compared to static incubation as the fluid needs to transverse the leaf vascular system prior to arrival at the cell membrane, where it can bind to the appropriate receptor.

We occasionally observed non-contractile hiPS-CMs after cell seeding on leaves, but paired controls were contracting on collagen IV coated TCP plates. This could possibly be due to cell health on the scaffold surface. If there were residual detergents or solutions remaining in the leaf scaffold after decellularization and sterilization, cells would likely respond poorly. We utilized this sample condition for trypan blue perfusion to demonstrate that trypan blue migrates through the leaf vasculature and permeates the unhealthy cell membrane, staining non-viable cells dark blue.

For several years, we have been interested in designing a decellularized spinach leaf perfusion system with the aim to study cell behavior on the leaf surface after leaf vascular perfusion. Previously, the goal of this system was to demonstrate that leaf nutrient perfusion was able to sustain cells on the leaf surface alone. Early work developed a perfusion system in which fibroblast seeded leaves were perfused with 70% ethanol to show perfused cell death.[35] We then moved to create a system that would maintain cell viability of leaves with media perfusion. To do this, we created a closed-loop perfusion and waste collection system that supplied cell media

to human mesenchymal stem cells (hMSCs) on leaves in a hypoxic chamber environment. Perfusion within a hypoxic chamber provided control over ambient conditions and supplied cell nutrients only through the media perfused leaf (**Figure 3-8**). The perfused hMSC seeded leaf, in a chamber purged with nitrogen gas, demonstrated 99% hMSC viability after 24 hours, compared to 69% viability in hypoxic controls.[36] However, it was later hypothesized that a lack of carbon dioxide in the hypoxic chamber could have caused low hMSC control viability. Based on further iterations of this work, we decided to pivot to demonstrate changes in cardiomyocyte functional behavior with cardioactive media perfusion.

Figure 3-8: hMSC seeded decellularized leaf connected to a hypoxic chamber media perfusion device. A decellularized spinach leaf seeded with hMSCs was placed in a closed-loop elevated perfusion system within a hypoxic chamber. Cell media was perfused through the leaf for 24 hours after which viability was measured.

For this research aim, we focused on live cardiac cell behavior in response to perfused stimuli. To do this, we seeded cardiomyocytes on perfused decellularized spinach leaves and induced them with epinephrine, a known stimulus. To reduce complexity and record live cell behavior, the perfusion system was designed to be performed on an inverted microscope at ambient temperature. We aimed to minimize cell disruption once the leaf was positioned on the microscope, so most static media above the seeded hiPS-CMs was removed; however, a small volume of media remained in the cloning wells. This media may have diluted perfused epinephrine, and therefore affected hiPS-CM beat frequency or strain response. In addition, perfusion rate may have affected hiPS-CM response. We calculated a conservative flow rate based on *in vivo* cardiomyocyte blood flow (Section 3.2.6) to reduce the risk of disrupting the leaf vasculature. Although high flow rate would increase delivery rate of epinephrine to seeded hiPS-CMs, high flow rate and internal vascular pressures risk rupture of leaf vasculature and stem. We have not yet characterized the vascular resistance of decellularized spinach leaves, and we are uncertain how it compares to the CV system. Characterization of leaf vasculature, burst

properties, and vessel permeability may be considered for future work. In addition, leaf perfusion characterization using a pressure-based or pulsatile flow system would be of interest in future studies.

In conclusion, we demonstrated that cardioactive dosed media travels through the leaf vasculature and effects hiPS-CM cell function on the leaf surface. Therefore, we conclude that the leaf vasculature can affect cells on the leaf surface via perfusion. The leaf contains an inherent, viable vascular system that can perfuse nutrients to cells on the scaffold surface.

3.5 References

1. Lee PT, Dweck MR, Prasher S, et al. Left ventricular wall thickness and the presence of asymmetric hypertrophy in healthy young army recruits: Data from the LARGE heart study. Circ Cardiovasc Imaging. 2013;6(2):262-267. doi:10.1161/CIRCIMAGING.112.979294
2. Riemenschneider SB, Mattia DJ, Wendel JS, et al. Inosculation and perfusion of pre-vascularized tissue patches containing aligned human microvessels after myocardial infarction. Biomaterials. 2016;97:51-61. doi:10.1016/j.biomaterials.2016.04.031
3. Mao AS, Mooney DJ. Regenerative medicine: Current therapies and future directions. Proc Natl Acad Sci. 2015;112(47):14452-14459. doi:10.1073/pnas.1508520112
4. Kreutziger KL, Muskheli V, Johnson P, Braun K, Wight TN, Murry CE. Developing Vasculature and Stroma in Engineered Human Myocardium. Tissue Eng Part A. 2011;17(9-10):1219-1228. doi:10.1089/ten.tea.2010.0557
5. Coulombe KLK, Murry CE. Vascular perfusion of implanted human engineered cardiac tissue. In: 2014 40th Annual Northeast Bioengineering Conference (NEBEC). Vol April. IEEE; 2014:1-2. doi:10.1109/NEBEC.2014.6972763
6. Masumoto H, Ikuno T, Takeda M, et al. Human iPS cell-engineered cardiac tissue sheets with cardiomyocytes and vascular cells for cardiac regeneration. Sci Rep. 2015;4(1):6716. doi:10.1038/srep06716
7. Novosel EC, Kleinhans C, Kluger PJ. Vascularization is the key challenge in tissue engineering. Adv Drug Deliv Rev. 2011;63(4-5):300-311. doi:10.1016/j.addr.2011.03.004
8. McCulloh KA, Sperry JS, Adler FR. Water transport in plants obeys Murray's law. Nature. 2003;421(6926):939-942. doi:10.1038/nature01444
9. Jansen K, Evangelopoulou M, Casellas CP, et al. Spinach and Chive for Kidney Tubule Engineering: the Limitations of Decellularized Plant Scaffolds and Vasculature. AAPS J. 2021;23(11):1-7. doi:10.1208/s12248-020-00550-0
10. Sack L, Holbrook NM. Leaf Hydraulics. Annu Rev Plant Biol. 2006;57(1):361-381. doi:10.1146/annurev.arplant.56.032604.144141
11. Pittermann J. The evolution of water transport in plants: An integrated approach. Geobiology. 2010;8(2):112-139. doi:10.1111/j.1472-4669.2010.00232.x
12. Gershlak JR, Hernandez S, Fontana G, et al. Crossing kingdoms: Using decellularized plants as perfusable tissue engineering scaffolds. Biomaterials. 2017;125:13-22. doi:10.1016/j.biomaterials.2017.02.011

13. Yokoo N, Baba S, Kaichi S, et al. The effects of cardioactive drugs on cardiomyocytes derived from human induced pluripotent stem cells. Biochem Biophys Res Commun. 2009;387(3):482-488. doi:10.1016/j.bbrc.2009.07.052
14. Nguyen N, Nguyen W, Nguyenton B, et al. Adult human primary cardiomyocyte-based model for the simultaneous prediction of drug-induced inotropic and pro-arrhythmia risk. Front Physiol. 2017;8:1-16. doi:10.3389/fphys.2017.01073
15. Huebsch N, Loskill P, Deveshwar N, et al. Miniaturized iPS-Cell-Derived Cardiac Muscles for Physiologically Relevant Drug Response Analyses. Sci Rep. 2016;6(November 2015):1-12. doi:10.1038/srep24726
16. Sasaki D, Matsuura K, Seta H, Haraguchi Y, Okano T, Shimizu T. Contractile force measurement of human induced pluripotent stem cell-derived cardiac cell sheet-tissue. PLoS One. 2018;13(5):1-21. doi:10.1371/journal.pone.0198026
17. Yang L, Soonpaa MH, Adler ED, et al. Human cardiovascular progenitor cells develop from a KDR+ embryonic-stem-cell-derived population. Nature. 2008;453(7194):524-528. doi:10.1038/nature06894
18. Kattman SJ, Witty AD, Gagliardi M, et al. Stage-Specific Optimization of Activin/Nodal and BMP Signaling Promotes Cardiac Differentiation of Mouse and Human Pluripotent Stem Cell Lines. Cell Stem Cell. 2011;8(2):228-240. doi:10.1016/j.stem.2010.12.008
19. Lundy SD, Zhu W-Z, Regnier M, Laflamme MA. Structural and Functional Maturation of Cardiomyocytes Derived from Human Pluripotent Stem Cells. Stem Cells Dev. 2013;22(14):1991-2002. doi:10.1089/scd.2012.0490
20. Hansen KJ, Laflamme MA, Gaudette GR. Development of a Contractile Cardiac Fiber From Pluripotent Stem Cell Derived Cardiomyocytes. Front Cardiovasc Med. 2018;5(52):1-11. doi:10.3389/fcvm.2018.00052
21. Arts T, Reneman RS. Measurement of deformation of canine epicardium in vivo during cardiac cycle. Am J Physiol - Hear Circ Physiol. 1980;239(8):H432-7. http://www.ncbi.nlm.nih.gov/pubmed/7435589
22. Gaudette GR, Todaro J, Azeloglu EU, Krukenkamp IB, Chiang F-P. Determination of regional stroke work with high spatial resolution in the isolated beating rabbit heart. Cardiovasc Eng An Int J. 2002;2(4):129-137.
23. Kamgoué A, Ohayon J, Usson Y, Riou L, Tracqui P. Quantification of cardiomyocyte contraction based on image correlation analysis. Cytom Part A. 2009;75A(4):298-308. doi:10.1002/cyto.a.20700
24. Czirok A, Isai DG, Kosa E, et al. Optical-flow based non-invasive analysis of cardiomyocyte contractility. Sci Rep. 2017;7(1):10404. doi:10.1038/s41598-017-10094-7
25. Kelly DJ, Azeloglu EU, Kochupura P V., Sharma GS, Gaudette GR. Accuracy and reproducibility of a subpixel extended phase correlation method to determine micron level displacements in the heart. Med Eng Phys. 2007;29(1):154-162. doi:10.1016/j.medengphy.2006.01.001
26. Hansen KJ, Favreau JT, Gershlak JR, Laflamme MA, Albrecht DR, Gaudette GR. Optical Method to Quantify Mechanical Contraction and Calcium Transients of Human Pluripotent Stem Cell-Derived Cardiomyocytes. Tissue Eng Part C Methods. 2017;23(8):445-454. doi:10.1089/ten.tec.2017.0190
27. Formaggia L, Quarteroni A, Veneziani A. Cardiovascular Mathematics. 1st ed. (Quarteroni A, Hou T, Le Bris C, Patera AT, Zuazua E, eds.). Springer-Verlag Italia; 2009.

28. Abi-Gerges N, Indersmitten T, Truong K, et al. Multiparametric Mechanistic Profiling of Inotropic Drugs in Adult Human Primary Cardiomyocytes. Sci Rep. 2020;10(1):18-24. doi:10.1038/s41598-020-64657-2
29. Duncker DJ, Bache RJ. Regulation of coronary blood flow during exercise. Physiol Rev. 2008;88(3):1009-1086. doi:10.1152/physrev.00045.2006
30. Thorp KR, Dierig DA. Color image segmentation approach to monitor flowering in lesquerella. Ind Crops Prod. 2011;34(1):1150-1159. doi:10.1016/j.indcrop.2011.04.002
31. Sarrafzadeh MH, La HJ, Lee JY, et al. Microalgae biomass quantification by digital image processing and RGB color analysis. J Appl Phycol. 2015;27(1):205-209. doi:10.1007/s10811-014-0285-7
32. Wang K, Climent A, Gavaghan D, Kohl P, Bollensdorff C. Room Temperature vs Ice Cold - Temperature Effects on Cardiac Cell Action Potential. Biophys J. 2016;110(3):587a. doi:10.1016/j.bpj.2015.11.3134
33. Ren J, Prentice H, Ge W, et al. Unraveling the Mystery of Cold Stress-Induced Myocardial Injury. Front Physiol. 2020;11:580811. doi:10.3389/fphys.2020.580811
34. Robbins ER, Pins GD, Laflamme MA, Gaudette GR. Creation of a contractile biomaterial from a decellularized spinach leaf without ECM protein coating: An in vitro study. J Biomed Mater Res Part A. 2020;108(10):2123-2132. doi:10.1002/jbm.a.36971
35. Alkhaledi F, Robbins ER, Hansen KJ, Gaudette GR. Designing a Perfusion System for Decellularized Spinach Leaf Scaffolds to Support Cell Function. In: Biomedical Engineering Society; 2017:P-SAT-121.
36. Jones TP, Robbins ER, Jones JD, Gaudette GR. Designing a Device to Evaluate Cell Viability on Perfused Decellularized Leaves. In: Biomedical Engineering Society. ; 2019:P-SAT-800.

4. Specific Aim 2: Determine if Protein Coating is Necessary to Improve Cardiac Scaffold Generation from Decellularized Leaves

The introduction (starting with Section 4.1), methods, results, and discussion presented in this aim are reprinted with permission from *Journal of Biomedical Materials Research Part A*, Volume 108(10), pp. 2123-2132, published by John Wiley and Sons (Appendix).[1]

4.1 Introduction

A tissue engineered implantable patch could improve function of the infarcted heart, providing an early treatment for MI patients. Recently, we demonstrated the use of a decellularized spinach leaf as a perfusable, vascularized cardiac patch scaffold.[2] Spinach leaves are inexpensive, have no associated donor costs, and are biocompatible. The primary remaining scaffold after leaf perfusion based decellularization is cellulose, a biomaterial used for a variety of medical applications.[3–5] As such, decellularized leaves have several properties that make them ideal candidates for a cardiac patch scaffold.

Cardiomyocytes are necessary to functionalize a cardiac tissue engineered patch. Primary adult human cardiomyocytes are non-proliferative, thus they are not a feasible cell source due to the large number of cells required for donation and implantation. Advances in cardiac tissue engineering using human induced pluripotent stem (hiPS) cells as a cell source are promising.[6–10] hiPS cells can be differentiated into cardiomyocytes (hiPS-CMs)[11–14] and are promising for use in cardiac tissue engineered constructs because a patient's own cells can be used without concern of immune rejection.[15]

Initial studies showed that decellularized leaves coated with fibronectin, an extracellular matrix (ECM) protein found in adult cardiac ECM, are effective for cardiomyocyte adherence and function.[2] Proteins such as fibronectin promote cell adhesion and migration due to their Arg-Gly-Asp (RGD) sequence peptide.[16] Furthermore, fibronectin adheres to and is biologically active on hydrophilic materials such as cellulose.[17,18] Other proteins found in cardiac ECM can also be used to coat biomaterials for cardiac applications. We demonstrated collagen IV coated fibrin microthreads provide a surface conducible for cardiomyocyte adherence and function.[19] However, as ECM proteins are sourced from allogeneic donors, protein sourcing and processing are serious concerns that must be considered for clinical translation. Furthermore, minimizing

required materials will reduce production costs, complexity, and potential deviations in the manufacturing process, which are important considerations for clinical translation and product manufacturing. Ideally, tissue scaffolds should not require ECM surface coatings for cardiac function. To determine whether ECM coatings are necessary and improve hiPS-CM behavior on leaf scaffolds, we compared hiPS-CM adherence, maturation, and contractile function on ECM and non-ECM coated decellularized leaves.

4.2 Materials and Methods

4.2.1 Spinach Decellularization

Spinach leaves were cannulated with 27 gauge needles, decellularized, and lyophilized as outlined in Appendix A. Lyophilized leaves were stored at room temperature until used.

4.2.2 Leaf Scaffold Surface Coating

After decellularization and lyophilization, 4 cm^2 sections of decellularized spinach leaves were rehydrated on a shaker plate with 10 mM Tris buffer pH 9.0 solution, rinsed with DI water, and sterilized with 70% ethanol, each for 30 minutes. Leaves in 70% ethanol were transferred into a biosafety cabinet and rinsed three times in sterile 1X PBS. Leaves were incubated at 37°C in RPMI-B27 cell media (RPMI 1640, 2% B-27™, 1% L-glutamine, and 1% Penicillin/Streptomycin) overnight. After incubation, RPMI-B27 media was aspirated from the decellularized leaves and sterile 10 mm diameter Pyrex cloning wells (Corning Inc., Corning, NY) were positioned on the leaf surface. Sterile 100 µL solutions of fibronectin (human plasma, 100 µg/mL, Sigma Aldrich), collagen IV (human placenta, 10 µg/mL, Sigma Aldrich), or 1X PBS (no coating) were pipetted into the cloning wells. Fibronectin and collagen IV protein concentrations were determined by previous studies in which we had successful cardiomyocyte adherence and contraction on decellularized leaves[2] and fibrin microthreads.[19] In preliminary studies, 100 µg/mL fibronectin coating on leaves resulted in improved cardiomyocyte adherence compared to 10 µg/mL; therefore, this study proceeded with 100 µg/mL. Coatings on leaves were air dried at room temperature in a biosafety cabinet until dry.

ECM coatings on leaves were verified with immunofluorescence antibody staining and imaging (Appendix D, E). After coating, samples were fixed in 4% paraformaldehyde (PFA) and immunolabeled for fibronectin (rabbit anti-human, Abcam) or collagen IV (mouse anti-human,

Abcam) primary antibodies and Alexa Fluor 488 goat anti-rabbit or anti-mouse secondary antibodies, respectively. Samples were then imaged with a scanning confocal microscope (Leica Microsystems, Buffalo Grove, IL).

4.2.3 hiPS-CM Differentiation, Isolation, and Seeding on Leaves

A contractile cardiac patch composed of hiPS-CMs on decellularized spinach leaves has the potential to improve diseased cardiac tissue function following MI. hiPS-CMs were differentiated into cardiomyocytes with induction of activin-A and bone morphogenetic protein-4 in the lab of Dr. Michael Laflamme at McEwen Stem Cell Institute (Appendix B).[14,20] Cells were cryopreserved, with cell preparations contained >75% cardiomyocytes.[14,19,21] hiPS-CMs were shipped overnight to Worcester Polytechnic Institute and stored in cryogenic conditions. When they were ready to be used, they were thawed. hiPS-CMs were thawed and seeded in RPMI-B27 media, 10% fetal bovine serum (FBS) (Gibco), and 1% Rho-associated protein kinase (ROCK) inhibitor (Y-27632 dihydrochloride, Sigma Aldrich) (Appendix B). 150,000-200,000 hiPS-CMs were seeded in 10 mm diameter cloning wells (Pyrex®, Corning Inc., Corning NY) (191,000-255,000 cells/cm^2) on ECM coated and non-coated leaves and were incubated for 18 hours at 37°C. As positive controls, 156,250 hiPS-CMs/cm^2 were seeded on ECM coated and non-coated tissue culture plastic (TCP). Cells were cultured in RPMI-B27 media on leaves and controls at 37°C for 7, 14, and 21 days (N=3 biological replicates). RPMI-B27 cell media was replenished every 2-3 days. Samples were fixed in 4% PFA at days 7, 14 and 21.

4.2.4 Effect of FBS on hiPS-CM Adhesion to Decellularized Leaves

To determine if initial hiPS-CM seeding with FBS affected cell binding to leaves, we seeded hiPS-CMs on non-coated decellularized spinach leaves, as previously detailed, with or without FBS. hiPS-CM FBS seeding media contained RPMI-B27, 10% FBS (Gibco), and 1% ROCK inhibitor (Y-27632 dihydrochloride, Sigma Aldrich). hiPS-CM seeding media without FBS was composed of RPMI-B27 and 1% ROCK inhibitor (Y-27632 dihydrochloride, Sigma Aldrich). hiPS-CMs were incubated with or without FBS on leaves (n=6) for 18 hours at 37°C. RPMI-B27 media was replenished after 18 hours, and then every two days. Samples were fixed in 4% PFA after 7 days in culture.

4.2.5 hiPS-CM Contractile Function

Cardiac left ventricular contraction is defined by tissue deformation and strain in the left ventricle *in vivo*.[22] Measuring strain in contracting hiPS-CMs can be accomplished optically and non-invasively under a microscope with a high-speed camera.[23–26] We used high density mapping (HDM), as previously described[26,27], to measure hiPS-CM contractile strain on decellularized spinach leaves. Live hiPS-CM contraction videos were visualized with an inverted microscope (DMIL, Leica Microsystems, Buffalo Grove, IL) and recorded at 60 frames per second with a high-speed camera (HiSpec 4, Fastec Imaging Corp, San Diego, CA). HDM analysis of hiPS-CM contraction was performed using code written in MATLAB (MathWorks, Natick, MA), previously explained in detail.[27] HDM defines a region of interest (ROI) and segments it into smaller subimages (32x32 pixels). Each subimage is transformed into the discrete Fourier domain and calculated to characterize light intensity. The subimage intensity is compared to that of the following frame using phase correlation to determine deformation. An inverse Fourier transform is then applied to find the peak displacement value between the two frames.[26] This process continues across the ROI with an overlap of 16 pixels. Green-Lagrange strain is calculated with reference to the first video frame. Green-Lagrange strain allows us to calculate small tissue deformation based on an initial reference state and is not affected by rigid body motion or rotation.[28] Maximum contractile strain is reported as the peak strain value from initiation of contraction.[27]

Contractile strain measurements of hiPS-CMs on coated and non-coated leaf samples and TCP were collected at one time point, either day 7, 14, or 21. Cardiomyocyte contractions on leaves was visualized over time (**Figure 4-1**). Video data from one to five regions on a sample was analyzed, based on number of observed hiPS-CM contractile areas on a sample. Contractile strain was reported as the maximum contractile principle strain value from initiation of contraction in a determined cell region[27], and sample contractile strain was defined as the mean ± standard deviation of the regions. Immediately after data collection, samples were fixed in 4% PFA and stored in 1X PBS at 4°C.

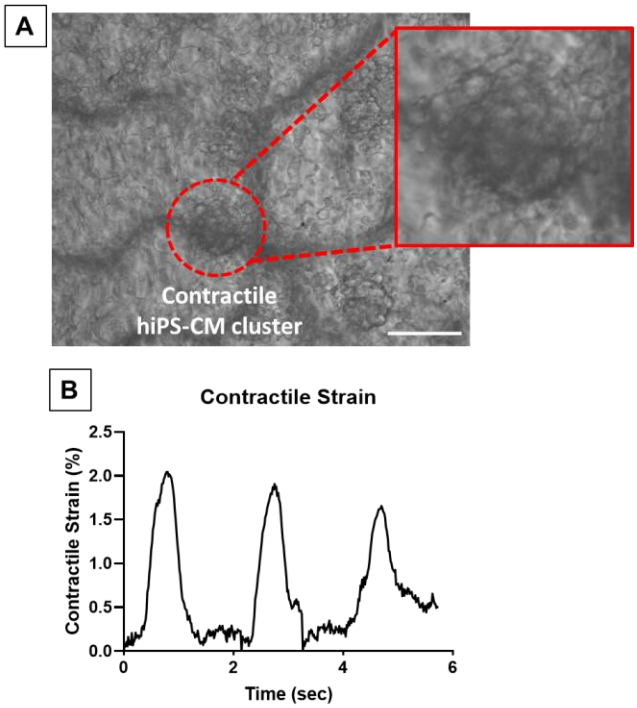

Figure 4-1: High density mapping analysis of hiPS-CM contractile strain on a non-coated decellularized spinach leaf. (A) Single frame of high-speed contraction video of hiPS-CMs on a non-coated decellularized spinach leaf. High density mapping (HDM) strain analysis was performed on contractile hiPS-CM clusters on decellularized leaves, illustrated in red circle. The inset visualizes several cells on the leaf. Scale bar 50 μm. (B) Contractile strain of the hiPS-CM cluster was measured with HDM over time. Peaks in strain plot indicate maximum strain per contraction on the leaf's surface.

4.2.6 Immunofluorescence Image Analysis

hiPS-CM seeded decellularized spinach leaf scaffolds were immunolabeled for sarcomeric α-actinin (mouse or rabbit, Abcam) and connexin-43 (goat, Abcam) primary antibodies to indicate cell adhesion, spreading, sarcomere length and gap junctions. Secondary antibodies Alexa Fluor 488 (Invitrogen) or Alexa Fluor 647 (Invitrogen) were used for sarcomeric α-actinin. Connexin-43 was immunolabeled with Alexa Fluor 568 (Invitrogen) secondary antibody. hiPS-CM nuclei were indicated with Hoescht 33342 nuclear stain (Life Technologies). Antibody host species, vendors, dilution factors, and protocol are specified in Appendices D and E. Samples were imaged with a scanning confocal microscope (Leica Microsystems, Buffalo Grove, IL).

4.2.7 hiPS-CM Sarcomere Length on Leaf Scaffolds

Cardiomyocyte sarcomere length is indicative of cell behavior since length is associated with cardiac muscle contraction mechanics and cell maturity.[29,30] hiPS-CM sarcomere length was calculated by measuring the distance between Z-disks, indicated by positive

immunofluorescence (IF) sarcomeric α-actinin images, using Fourier transform analysis (**Figure 4-2**). Sarcomere length was analyzed in ImageJ (NIH) and MATLAB (MathWorks, Natick, MA). A collected IF image was opened in ImageJ and a random array of visible cell sarcomeres was selected in an α-actinin positive cell. A line was drawn perpendicular to the sarcomere bands, and the grey value peaks were plotted in ImageJ using the "Plot Profile" function (**Figure 4-2A, 4-2B**). Discrete Fourier transforms and power spectrum analysis of the sarcomere grey values were performed in MATLAB (**Figure 4-2C, 4-2D**), calculating the cell's sarcomere length. Sarcomere band data between one and 18 cells on a leaf sample were collected and the sample sarcomere length was defined as the mean ± standard deviation.

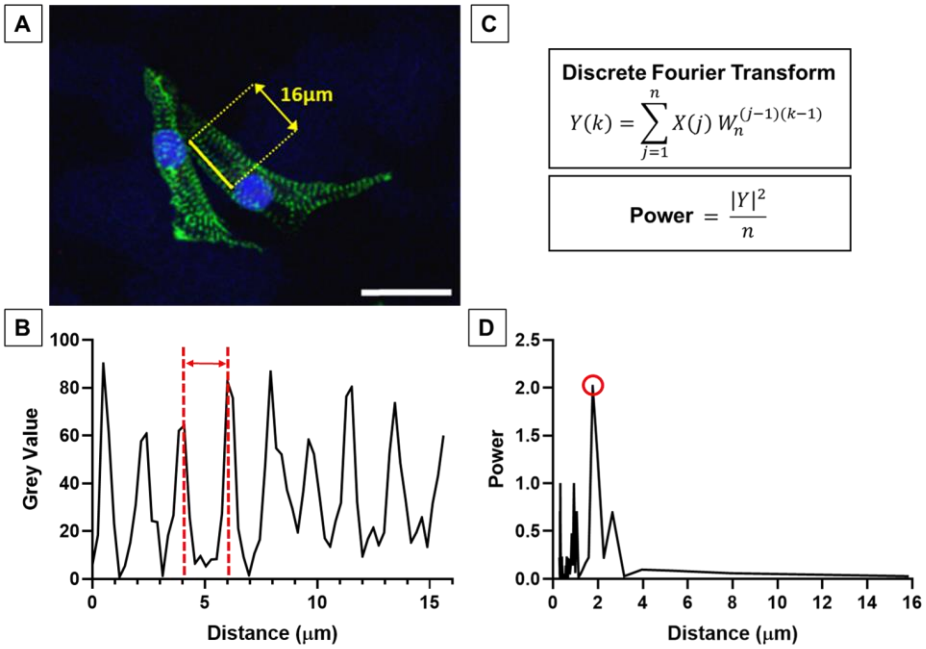

Figure 4-2: Fourier transform analysis to calculate sarcomere lengths on decellularized leaves. (A) A 16 µm line (yellow) was drawn in ImageJ perpendicular to hiPS-CM α-actinin positive bands (green); nuclei (blue). Scale bar 25 µm. (B) Grey values plotted across the length of the line as shown in (A). Grey value peaks correspond to α-actinin positive regions, and the distance between these peaks (red) is the sarcomere length. (C) Sarcomere lengths were calculated with discrete Fourier transform and power spectrum analysis. (D) Cell sarcomere length is equal to the distance value corresponding to the highest power, circled in red.

4.2.8 hiPS-CM Spreading on Leaf Scaffolds

hiPS-CM cell spreading and sarcomeric striation is an indication of cell adherence and eventual maturation.[30] hiPS-CMs were indicated with positive sarcomeric α-actinin staining. Cells were deemed spreading if hiPS-CM sarcomeres extended beyond the circumference of the cell nucleus. Data were collected from between two and six regions on a leaf sample and cell

spreading was defined as the mean ± standard deviation. Data is presented as the percent of elongated hiPS-CMs out of the total hiPS-CM population per mm^2 of leaf surface. Total cell number is the mean number of cells in a sample per mm^2 of leaf surface, or density.

4.2.9 Statistical Analysis

This study analyzed N=3 biological replicates for each time and coating condition, with sample numbers illustrated in results. All results are presented as mean ± standard deviation. Statistical significance between ECM coatings was tested with one-way ANOVA and post-hoc Tukey t-tests ($p<0.05$). Statistical significance between hiPS-CM contractile strain on non-coated leaves with or without FBS in seeding media was tested with an unpaired t-test ($p<0.05$). All statistical analyses were performed in GraphPad Prism 8 (GraphPad Software, San Diego, CA).

4.3 **Results**

4.3.1 ECM Coating Verification on Decellularized Spinach Leaves

Immunofluorescence staining and imaging demonstrated that fibronectin (**Figure 4-3A**) and collagen IV (**Figure 4-3B**) protein coatings adhere to the surface of decellularized spinach leaves. On control coverslips, adherent fibronectin and collagen IV appeared as a porous network of fibers. Adherent fibronectin and collagen IV on the leaf scaffold also appeared porous; however, the fibrous network was not as prominent on the leaf. Visible in the network centers of several ECM pores are leaf stomata, the oblong leaf surface openings for gas and water transport during photosynthesis. ECM on decellularized spinach leaf scaffolds appear to adhere on the topographically diverse surface of the leaf, surrounding stomata pores.

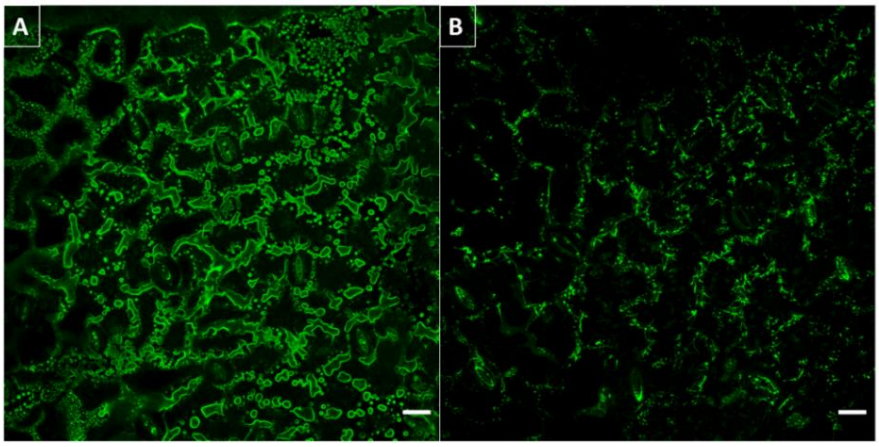

Figure 4-3: ECM coating verification with IF staining and imaging on decellularized spinach leaves. (A) Fibronectin and (B) collagen IV protein coatings adhere to the surface of decellularized spinach leaves. Scale bar 25 μm.

4.3.2 hiPS-CMs Adhere to ECM Coated and Non-Coated Decellularized Spinach Leaves

Spinach leaves were decellularized, sterilized, and coated with either fibronectin or collagen IV ECM protein. Immunofluorescence staining demonstrated that both ECM protein coatings adhered to the surface of decellularized spinach leaves. Furthermore, hiPS-CMs adhered to decellularized spinach leaves with and without ECM coatings for 21 days (**Figure 4-4**), indicating that ECM protein coatings are unnecessary for hiPS-CM adherence on leaves.

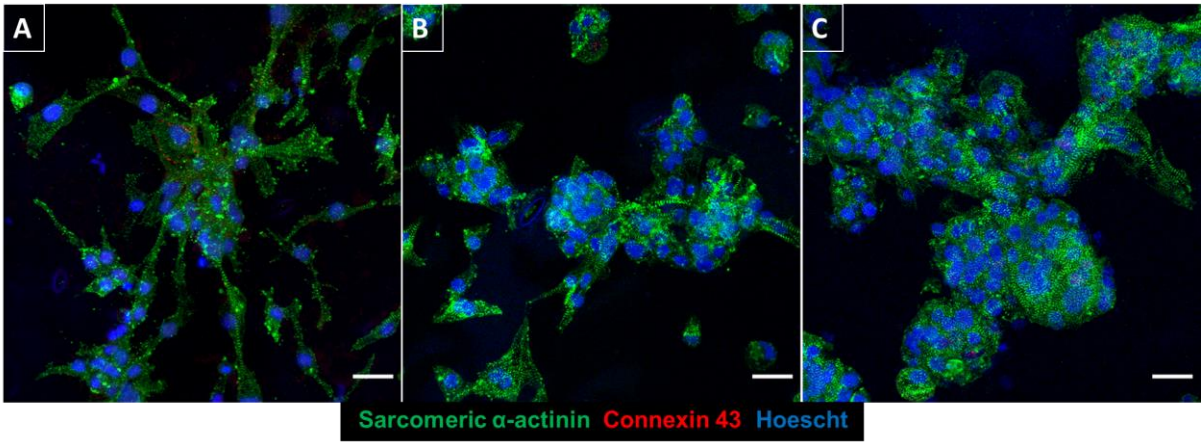

Figure 4-4: hiPS-CMs cultured on decellularized spinach leaves. Cells cultured for 21 days on (A) collagen IV coated decellularized leaf, (B) fibronectin coated decellularized leaf, and (C) non-coated decellularized spinach leaf. Samples were stained for sarcomeric α-actinin (green), connexin-43 (red), and Hoescht 33342 (blue). Scale bar 25 μm.

To study if FBS had an effect on cell adherence to non-coated decellularized spinach leaves, we removed FBS from hiPS-CM seeding media. After 7 days in culture on leaves, hiPS-CMs remained adherent to non-coated leaves with and without FBS at initial cell seeding. Both

seeding conditions had variable cell morphologies on leaf scaffolds, illustrating both elongated sarcomeric bands and round cell clusters. In addition, there were no statistically significant differences in hiPS-CM maximum contractile strain with or without FBS (p=0.22) **(Figure 4-5).**

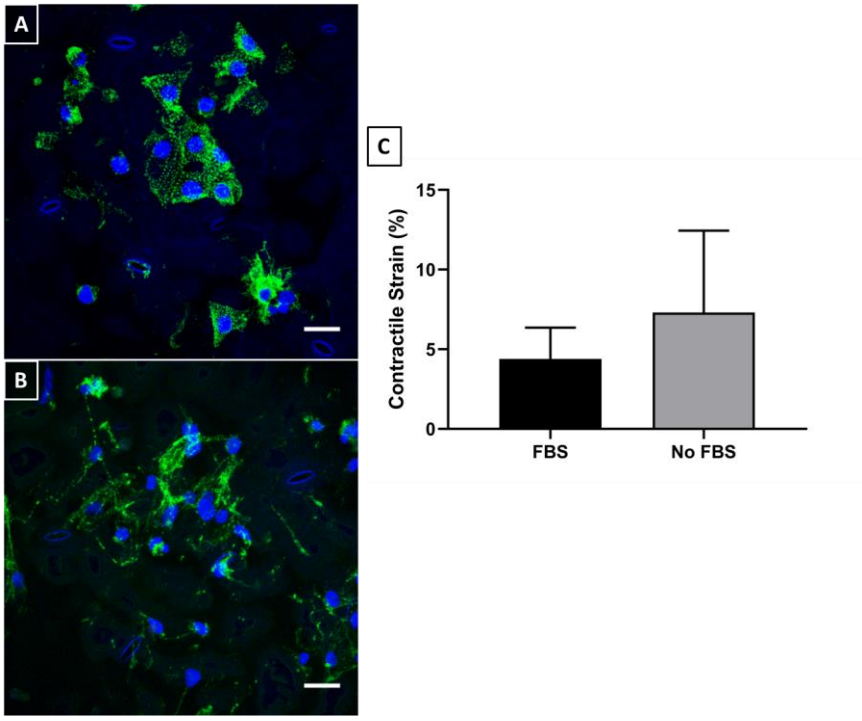

Figure 4-5: hiPS-CMs cultured on non-coated decellularized spinach leaves for 7 days. IF imaging of leaves (A) with FBS and (B) without FBS when hiPS-CMs were seeded. Samples were stained for sarcomeric α-actinin (green) and Hoescht 33342 (blue). Scale bar 25μm. (C) Peak contractile strain analysis for hiPS-CMs on FBS and no FBS seeded on non-coated decellularized spinach leaves for 7 days. There was no significant difference between FBS and no FBS seeded non-coated leaves at day 7 (p=0.22).

4.3.3 hiPS-CMs on Non-Coated Leaves Have Equivalent Contractile Strain as Coated Leaves

hiPS-CMs contracted on spinach leaves and TCP at all time points and under all coating conditions (**Figure 4-6**); however, we did not always observe hiPS-CM contractile behavior with live video imaging. Contractile strain was analyzed in n≥4 samples per condition and time point. We only observed contraction for N=2 of 3 biological replicates of hiPS-CMs on collagen IV coated leaves at day 14 and on fibronectin TCP at day 21. All maximum contractile strains were larger than 1.5%. No statistically significant differences in maximum contractile strain between hiPS-CMs seeded on coated and non-coated leaves and TCP at each time point nor over time were observed (**Figure 4-6A, 4-6B**). There were no significant differences in maximum contractile strain of hiPS-CMs on ECM coated and non-coated leaves at days 7 and 21. However, strain on collagen IV coated leaves (3.25 ± 0.39%) were significantly larger than non-

coated leaves (1.54 ± 0.60%) (p=0.03) at day 14. This observation was the only significant difference for all leaf coatings and time points. No differences in hiPS-CM contractile strain were found between these samples and corresponding collagen IV coated TCP (2.65 ± 0.97%) or non-coated TCP (2.11 ± 0.48%) at day 14.

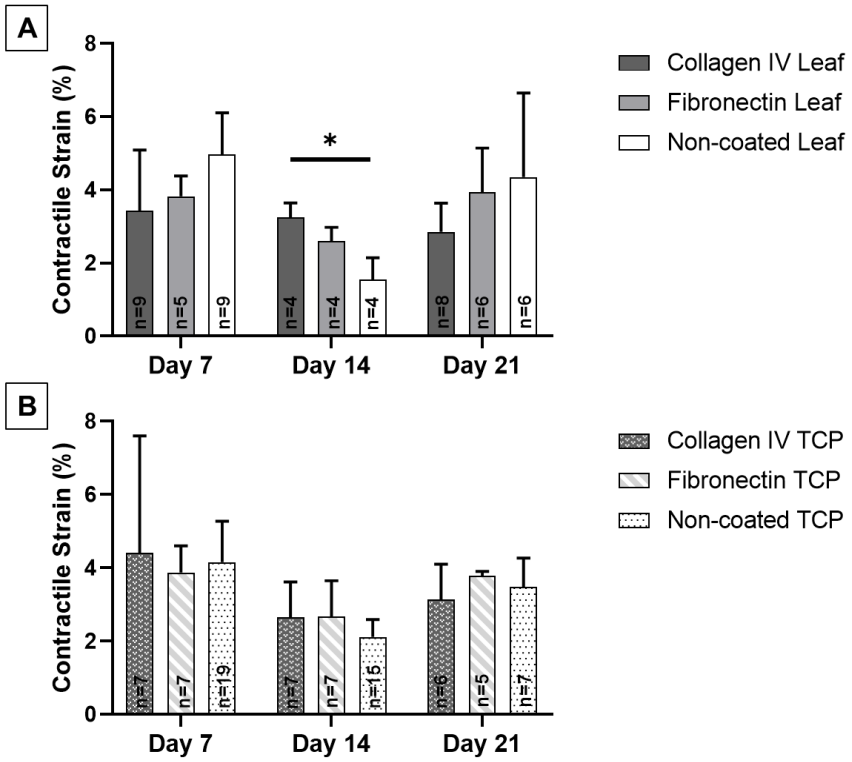

Figure 4-6: Maximum contractile strain analysis for hiPS-CMs on ECM coated and non-coated decellularized spinach leaves for 7, 14, and 21 days. Sample sizes n for each condition are noted within the data. (A) There were no significant differences over time for coated and non-coated leaves. However, collagen IV coated leaves had larger contractile strain than non-coated leaves at day 14 ($p<0.05$). No significance difference was found between coated and non-coated leaves at days 7 and 21. (B) No significant differences were found in contractile strain for hiPS-CMs seeded on ECM coated and non-coated tissue culture plastic (TCP) at 7, 14, and 21 days. (A, B) There were no significant differences between coated and non-coated leaves and TCP.

4.3.4 hiPS-CM Sarcomere Length Approaches Adult Maturity on All Leaf Coating Conditions

Sarcomere length was determined in n≥4 samples per condition. Average hiPS-CM sarcomere lengths ranged from 1.65 ± 0.18 μm on collagen IV coated leaves at day 7 to 2.06 ± 0.06 μm on fibronectin coated leaves at day 14. There were no statistically significant differences in hiPS-CM sarcomere length between leaf coatings at day 7 and day 21 (**Figure 4-7**). In addition, there were no significant differences in collagen IV coated and non-coated leaf samples over time. There was a statistically significant increase in hiPS-CM sarcomere length on fibronectin coated

leaves at day 14 compared to day 7 (p=0.008) and day 21 (p=0.04). In addition, sarcomeres on fibronectin coated leaves were statistically longer than on collagen IV coated leaves at day 14 (p=0.006).

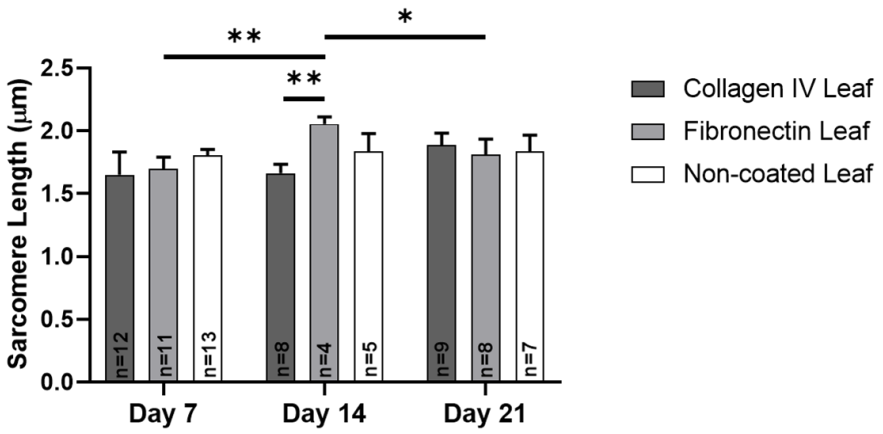

Figure 4-7: Sarcomere length analysis for hiPS-CMs on ECM coated and non-coated decellularized spinach leaves for 7, 14, and 21 days. Sample sizes n for each condition are illustrated within the data. Fibronectin coated leaves had statistically longer sarcomere lengths than collagen IV coated leaves at day 14 ($p<0.01$). Significant difference was also found in fibronectin coated leaves between day 7 and 14 ($p<0.01$), and day 14 and 21 ($p<0.05$).

4.3.5 No Significant Differences in hiPS-CM Spreading Across Leaf Coating Conditions

hiPS-CM cell count and spreading was calculated with $n \geq 8$ samples for each leaf condition. We observed cell spreading and elongation in more than 37% of hiPS-CMs on ECM coated and non-coated leaves, observed by IF imaging. There were no significant differences in spreading between leaf coatings and time points (**Figure 4-8**).

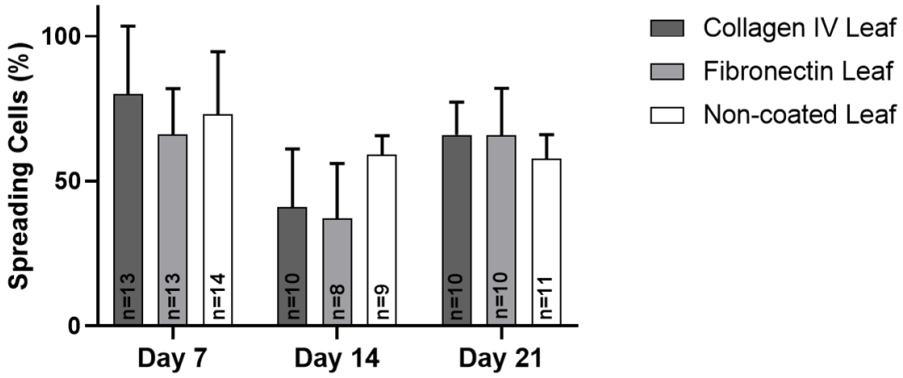

Figure 4-8: Cell spreading analysis for hiPS-CMs on ECM coated and non-coated decellularized spinach leaves for 7, 14, and 21 days. Sample sizes n for each condition are illustrated within the data. There were no significant differences in cell spreading between culture time or coatings.

However, at day 14, we observed decreased average sample cell density compared to day 7 (not significant) and day 21 ($p=0.03$) on fibronectin coated leaves (**Figure 4-9**). At day 14, fibronectin coated leaves also had decreased cell spreading compared to day 7 and 21 (not significant).

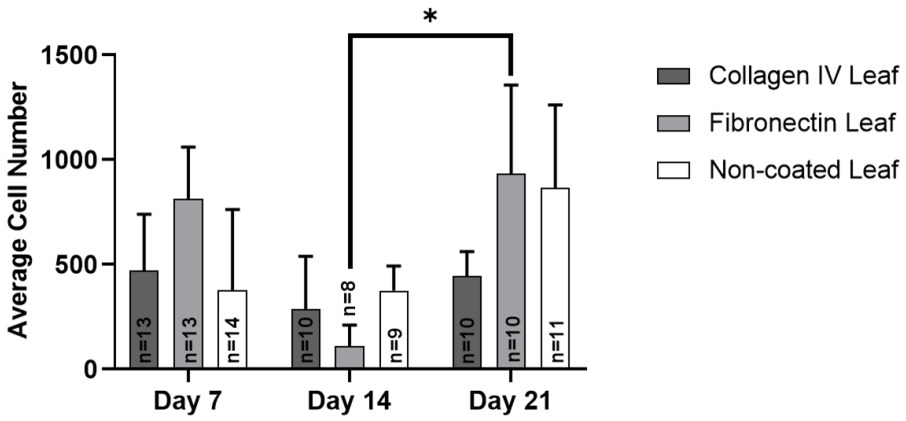

Figure 4-9: Average cell number per mm^2 of IF sarcomeric α-actinin positive hiPS-CMs on coated and non-coated leaves over time. Sample sizes n for each condition are illustrated within the data. Fibronectin coated leaves had statistically less cells at day 14 compared to day 21 ($p<0.05$).

4.4 Discussion

Decellularized leaves are primarily composed of cellulose, a biocompatible biomaterial commonly used in tissue engineering. Cellulose is used in other fields of tissue engineering research and in FDA-approved surgical hemostatic wound dressings.[3,5,31,32] Cellulose scaffolds modified with ECM proteins before cell seeding have been found to change cell behavior. For example, seeding C2C12 mouse myoblasts in type I collagen hydrogels increased cell adhesion on plant-derived cellulose.[33] For cardiac tissue engineering application, fibronectin coated cellulose polymer scaffolds promote maturation of neonatal cardiomyocytes by sarcomere organization and increased gap junction density.[3] This can be explained by the observation that cardiomyocytes bind to ECM with cell integrin receptors and form focal adhesions to the matrix[34,35], which in turn can influence cardiomyocyte behavior and maturation.[36] Our previous studies coated decellularized spinach leaves with ECM proteins found in the adult heart.[2] We were interested in removing the ECM coating from the leaf scaffold while retaining similar cell behavior on the scaffold. Herein, we determined that ECM coatings are not necessary for hiPS-

CM adherence and function on decellularized leaves. We hypothesize that cells bind to non-coated decellularized leaves due to the scaffold's cellulose composition. Cellulose's polysaccharide structure may positively interact with the cell surface glycocalyx[3], reducing the need for ECM coatings on the scaffold's surface. FBS proteins, present during hiPS-CM seeding, may bind directly to non-coated leaves and provide a substrate for cell adhesion; however, including FBS is not necessary for hiPS-CM adhesion or contraction on the leaf scaffold. We observed that hiPS-CMs adhere to non-coated decellularized spinach leaves with and without FBS in the seeding media. Furthermore, we found no functional significant differences in contractile behavior between the two seeding conditions after 7 days, indicating that FBS is not necessary to culture contractile hiPS-CMs on leaves.

Eliminating the ECM coating step has several advantages in creating a tissue engineered cardiac patch for implantation. First, the preparation time and steps to manufacture the tissue would be reduced, which therefore decreases manufacturing complexity. This would eliminate additional contamination risks during manufacturing and increase speed of manufacturing. Faster manufacturing could then lead to decreased production and product costs. Furthermore, including ECM coatings on the tissue would add an additional concern for FDA approval. The sources of the ECM would have to be controlled and qualified, increasing time and cost of approval. Removal of the ECM would eliminate this testing and allow for a faster regulatory approval process.

When evaluating novel scaffolds for cardiac tissue engineering, it is important to consider tissue deformation, or contractile strain, which is indicative of left ventricular function. In this study, we found no statistically significant differences in contractile strain between hiPS-CMs seeded on ECM coated and non-coated leaves and TCP over 21 days. In addition, contractile strains were not significantly different from the TCP controls. We also observed a trend toward decreased contractile strain from day 7 to day 14 for all conditions, although this did not reach statistical significance. This corresponded with decreased cell spreading (not significant) and cell number (not significant) from day 7 to day 14. The decreasing trend could be related to the drastic difference between the substrate stiffnesses of leaves and TCP. We previously determined that the maximum tangent modulus for decellularized spinach leaves is 0.3 MPa[2], within the range of adult human myocardium (20-500 kPa).[37] Whereas, polystyrene plastic has an elastic

modulus of 3 GPa[38], three orders of magnitude larger. Neonatal cardiomyocytes cultured on stiff substrates have been found to have less sarcomere definition and alignment than those cultured on substrates with stiffnesses similar to native myocardium. This can interrupt cardiomyocyte maturation, decrease contractile forces, and cardiomyocytes can form actin stress fibers as they mature.[39] We hypothesize that decreased hiPS-CM cell contractility observed at day 14, specifically in TCP culture, may be due to its stiff surface substrate. With long-term culture on TCP, differences in hiPS-CM contractile and morphology behavior could become more evident over time.

This study observed larger cardiomyocyte contractile strain values on decellularized spinach leaves than previous findings.[2] Previous contractile strain analysis determined stem cell derived CM strain on fibronectin coated decellularized spinach leaves to be 0.6% at day 21. Our findings demonstrate 3.94 ± 1.20% contractile strain on fibronectin coated leaves at day 21. This could be due to changes in decellularization techniques compared to previous findings.[2] We found that using 1% SDS is as effective as 10% SDS to decellularize spinach leaves. Higher SDS concentrations may affect leaf substrate stiffness and reduce the contractility of adherent cardiomyocytes. Although cardiomyocyte contractility increased, hiPS-CMs' contractile strains on decellularized leaves were still less than the human myocardium (15.9-22.1%).[40] This is likely due to several factors. Strain depends on cardiomyocyte orientation. Aligned hiPS-CMs show improved contractile performance versus non-aligned hiPS-CMs.[41] This study focused on the ability for decellularized leaves to support hiPS-CM function with and without ECM surface coatings. We will continue to focus on improving contractility of the seeded hiPS-CMs with cell alignment. Another factor to contribute to differences in strain magnitudes is the thickness of the cell layer. The scaffolds presented here are monolayers, whereas human myocardium is hundreds of cell layers thick. These extra cells help deform the substrate, resulting in increased contractile strain.

Variability in strain measurements or average cell number could also be explained, in part, by exposure to room temperature conditions during data acquisition. Image-based strain data collection is performed at room temperature and can take as long as 10 minutes per sample. Samples were cultured in multi-well plates and therefore, contractile samples could have been exposed to room temperature for longer than 10 minutes. To minimize the effects of temperature,

plates were returned to the 37°C incubator after data collection of three samples for at least 15 minutes before continuing with data collection. Furthermore, this study used unpaired samples to avoid performing repeated data collection, potentially affecting strain results over time. Future studies may consider returning multi-well plates to the incubator after one sample data collection to minimize any temperature effects on strain data or cell number.

hiPS-CMs contain a mixed cell population of atrial, ventricular and nodal cardiomyocytes after cardiac differentiation.[15,42] Nodal cells propagate action potentials, stimulating cardiomyocyte contraction. We found that a majority of hiPS-CMs on leaves contracted. However, some sarcomeric α-actinin positive samples were not contractile during strain data collection. This helps explains the different sample sizes of measured strain compared to IF image analysis. For example, there were less contractile hiPS-CM samples on collagen IV coated leaf scaffolds at day 14 (N=2, n=4) for strain analysis than sarcomeric α-actinin positive samples for sarcomere length analysis (N=3, n=8).

Culture time is linked to increased sarcomere length and maturation. If cell spreading data indicated no significant differences in spreading and maturity between leaf coatings. Furthermore, sarcomere lengths of hiPS-CMs on leaves were comparable to previous findings. Resting sarcomere length of human embryonic stem cell-derived cardiomyocytes (hES-CMs) in culture dishes has been found to increase from an average of 1.65 μm in early-stage hES-CMs to 1.81 μm ($p<0.001$) in late-stage hES-CMs.[30] hiPS-CM sarcomere lengths on non-coated decellularized spinach leaves were similar to or exceeded these findings. Average sarcomere lengths of hiPS-CMs cultured on non-coated decellularized leaf scaffolds for 21 days ranged from 1.80 ± 0.05 μm to 1.84 ± 0.14 μm, comparable to late-stage hES-CMs in culture dishes. Overall, average hiPS-CM sarcomere length on leaves approaches average sarcomere length of adult cardiomyocytes (1.8 μm to 2.2 μm).

Too much of an increase in sarcomere length (above 2.2 μm) is associated with the pathophysiology of heart disease and heart failure since chronic dilation in the diseased ventricle results in increased cardiomyocyte lengths. This length increase is associated with loss of function by decreased cardiac contractility, according to the Frank-Starling mechanism.[43,44] We did not observe hiPS-CM sarcomere lengths larger than 2.2 μm on coated or non-coated decellularized spinach leaves. Furthermore, we did not observe increases in hiPS-CM sarcomere

length and decreased contractile strain values on non-coated leaves, which corresponds to the pathophysiology of heart failure.

In conclusion, when seeded with hiPS-CMs, non-coated decellularized leaves have comparable hiPS-CM contractile function as fibronectin and collagen IV coated leaves. ECM protein coatings are not necessary to improve cardiomyocyte cell adhesion, behavior, and contractility on decellularized leaf scaffolds. Decellularized spinach leaves can serve as inexpensive, abundant, and sustainable pre-vascularized scaffolds for cardiac tissue engineering. Non-coated decellularized leaf surfaces allow for simple cell attachment for an engineered tissue patch, and we are able to provide the appropriate environment for hiPS-CMs to adhere. The decellularized leaf holds significant potential as a scaffold for a cardiac tissue engineered patch to refunctionalize diseased cardiac tissue.

4.5 References

1. Robbins ER, Pins GD, Laflamme MA, Gaudette GR. Creation of a contractile biomaterial from a decellularized spinach leaf without ECM protein coating: An in vitro study. J Biomed Mater Res Part A. 2020;108(10):2123-2132. doi:10.1002/jbm.a.36971
2. Gershlak JR, Hernandez S, Fontana G, et al. Crossing kingdoms: Using decellularized plants as perfusable tissue engineering scaffolds. Biomaterials. 2017;125:13-22. doi:10.1016/j.biomaterials.2017.02.011
3. Entcheva E, Bien H, Yin L, Chung C-Y, Farrell M, Kostov Y. Functional cardiac cell constructs on cellulose-based scaffolding. Biomaterials. 2004;25(26):5753-5762. doi:10.1016/j.biomaterials.2004.01.024
4. Czaja WK, Young DJ, Kawecki M, Brown RM. The future prospects of microbial cellulose in biomedical applications. Biomacromolecules. 2007;8(1):1-12. doi:10.1021/bm060620d
5. Modulevsky DJ, Cuerrier CM, Pelling AE. Biocompatibility of Subcutaneously Implanted Plant-Derived Cellulose Biomaterials. Zhao F, ed. PLoS One. 2016;11(6):e0157894. doi:10.1371/journal.pone.0157894
6. Lesman A, Habib M, Caspi O, et al. Transplantation of a Tissue-Engineered Human Vascularized Cardiac Muscle. Tissue Eng Part A. 2010;16(1):115-125. doi:10.1089/ten.tea.2009.0130
7. Stevens KR, Pabon L, Muskheli V, Murry CE. Scaffold-Free Human Cardiac Tissue Patch Created from Embryonic Stem Cells. Tissue Eng Part A. 2009;15(6):1211-1222. doi:10.1089/ten.tea.2008.0151
8. Guyette JP, Charest JM, Mills RW, et al. Bioengineering Human Myocardium on Native Extracellular Matrix. Circ Res. 2016;118(1):56-72. doi:10.1161/CIRCRESAHA.115.306874

9. Masumoto H, Ikuno T, Takeda M, et al. Human iPS cell-engineered cardiac tissue sheets with cardiomyocytes and vascular cells for cardiac regeneration. Sci Rep. 2015;4(1):6716. doi:10.1038/srep06716
10. Zhang B, Montgomery M, Chamberlain MD, et al. Biodegradable scaffold with built-in vasculature for organ-on-a-chip engineering and direct surgical anastomosis. Nat Mater. 2016;15(6):669-678. doi:10.1038/nmat4570
11. Eschenhagen T, Bolli R, Braun T, et al. Cardiomyocyte Regeneration. Circulation. 2017;136(7):680-686. doi:10.1161/CIRCULATIONAHA.117.029343
12. Zhu W-Z, Van Biber B, Laflamme MA. Methods for the Derivation and Use of Cardiomyocytes from Human Pluripotent Stem Cells. In: Schwartz PH, Wesselschmidt RL, eds. Methods Mol Biol. Vol 767. Methods in Molecular Biology. Humana Press; 2011:419-431. doi:10.1007/978-1-61779-201-4_31
13. Burridge PW, Keller G, Gold JD, Wu JC. Production of De Novo Cardiomyocytes: Human Pluripotent Stem Cell Differentiation and Direct Reprogramming. Cell Stem Cell. 2012;10(1):16-28. doi:10.1016/j.stem.2011.12.013
14. Kattman SJ, Witty AD, Gagliardi M, et al. Stage-Specific Optimization of Activin/Nodal and BMP Signaling Promotes Cardiac Differentiation of Mouse and Human Pluripotent Stem Cell Lines. Cell Stem Cell. 2011;8(2):228-240. doi:10.1016/j.stem.2010.12.008
15. Zhang J, Wilson GF, Soerens AG, et al. Functional Cardiomyocytes Derived From Human Induced Pluripotent Stem Cells. Circ Res. 2009;104(4). doi:10.1161/CIRCRESAHA.108.192237
16. Ruoslahti E, Pierschbacher MD. New Perspectives in Cell Adhesion: RGD and Integrins. Science (80-). 1987;238(4826):491-497.
17. Grinnell F, Feld MK. Fibronectin Adsorption on Hydrophilic and Hydrophobic Surfaces Detected By Antibody-Binding and Analyzed During Cell-Adhesion in Serum-Containing Medium. J Biol Chem. 1982;257(9):4888-4893.
18. Macdonald DE, Markovic B, Allen M, Somasundaran P, Boskey AL. Surface analysis of human plasma fibronectin adsorbed to commercially pure titanium materials. J Biomed Mater Res. 1998;41(1):120-130.
19. Hansen KJ, Laflamme MA, Gaudette GR. Development of a Contractile Cardiac Fiber From Pluripotent Stem Cell Derived Cardiomyocytes. Front Cardiovasc Med. 2018;5(52):1-11. doi:10.3389/fcvm.2018.00052
20. Yang L, Soonpaa MH, Adler ED, et al. Human cardiovascular progenitor cells develop from a KDR+ embryonic-stem-cell-derived population. Nature. 2008;453(7194):524-528. doi:10.1038/nature06894
21. Lundy SD, Zhu W-Z, Regnier M, Laflamme MA. Structural and Functional Maturation of Cardiomyocytes Derived from Human Pluripotent Stem Cells. Stem Cells Dev. 2013;22(14):1991-2002. doi:10.1089/scd.2012.0490
22. Arts T, Reneman RS. Measurement of deformation of canine epicardium in vivo during cardiac cycle. Am J Physiol - Hear Circ Physiol. 1980;239(8):H432-7. http://www.ncbi.nlm.nih.gov/pubmed/7435589
23. Gaudette GR, Todaro J, Azeloglu EU, Krukenkamp IB, Chiang F-P. Determination of regional stroke work with high spatial resolution in the isolated beating rabbit heart. Cardiovasc Eng An Int J. 2002;2(4):129-137.

24. Kamgoué A, Ohayon J, Usson Y, Riou L, Tracqui P. Quantification of cardiomyocyte contraction based on image correlation analysis. Cytom Part A. 2009;75A(4):298-308. doi:10.1002/cyto.a.20700
25. Czirok A, Isai DG, Kosa E, et al. Optical-flow based non-invasive analysis of cardiomyocyte contractility. Sci Rep. 2017;7(1):10404. doi:10.1038/s41598-017-10094-7
26. Kelly DJ, Azeloglu EU, Kochupura P V., Sharma GS, Gaudette GR. Accuracy and reproducibility of a subpixel extended phase correlation method to determine micron level displacements in the heart. Med Eng Phys. 2007;29(1):154-162. doi:10.1016/j.medengphy.2006.01.001
27. Hansen KJ, Favreau JT, Gershlak JR, Laflamme MA, Albrecht DR, Gaudette GR. Optical Method to Quantify Mechanical Contraction and Calcium Transients of Human Pluripotent Stem Cell-Derived Cardiomyocytes. Tissue Eng Part C Methods. 2017;23(8):445-454. doi:10.1089/ten.tec.2017.0190
28. Formaggia L, Quarteroni A, Veneziani A. Cardiovascular Mathematics. 1st ed. (Quarteroni A, Hou T, Le Bris C, Patera AT, Zuazua E, eds.). Springer-Verlag Italia; 2009.
29. Rodriguez ML, Graham BT, Pabon LM, Han SJ, Murry CE, Sniadecki NJ. Measuring the Contractile Forces of Human Induced Pluripotent Stem Cell-Derived Cardiomyocytes With Arrays of Microposts. J Biomech Eng. 2014;136(5):051005. doi:10.1115/1.4027145
30. Lundy SD, Zhu W-Z, Regnier M, Laflamme MA. Structural and Functional Maturation of Cardiomyocytes Derived from Human Pluripotent Stem Cells. Stem Cells Dev. 2013;22(14):1991-2002. doi:10.1089/scd.2012.0490
31. Helenius G, Bäckdahl H, Bodin A, Nannmark U, Gatenholm P, Risberg B. In vivo biocompatibility of bacterial cellulose. J Biomed Mater Res Part A. 2006;76A(2):431-438. doi:10.1002/jbm.a.30570
32. Hart J, Silcock D, Gunnigle S, Cullen B, Light ND, Watt PW. The role of oxidised regenerated cellulose/collagen in wound repair: effects in vitro on fibroblast biology and in vivo in a model of compromised healing. Int J Biochem Cell Biol. 2002;34(12):1557-1570. doi:10.1016/S1357-2725(02)00062-6
33. Hickey RJ, Modulevsky DJ, Cuerrier CM, Pelling AE. Customizing the Shape and Microenvironment Biochemistry of Biocompatible Macroscopic Plant-Derived Cellulose Scaffolds. ACS Biomater Sci Eng. 2018;4(11):3726-3736. doi:10.1021/acsbiomaterials.8b00178
34. Stevens MM, George JH. Exploring and Engineering the Cell Surface Interface. Science (80-). 2005;310:1135-1138. doi:10.1126/science.1106587
35. Wu X, Sun Z, Foskett A, Trzeciakowski JP, Meininger GA, Muthuchamy M. Cardiomyocyte contractile status is associated with differences in fibronectin and integrin interactions. Am J Physiol Circ Physiol. 2010;298(6):H2071-H2081. doi:10.1152/ajpheart.01156.2009
36. Baharvand H, Azarnia M, Parivar K, Ashtiani SK. The effect of extracellular matrix on embryonic stem cell-derived cardiomyocytes. J Mol Cell Cardiol. 2005;38(3):495-503. doi:10.1016/j.yjmcc.2004.12.011
37. Reis LA, Chiu LLY, Feric N, Fu L, Radisic M. Biomaterials in myocardial tissue engineering. J Tissue Eng Regen Med. 2016;10(1):11-28. doi:10.1002/term.1944
38. Gilbert PM, Havenstrite KL, Magnusson KEG, et al. Substrate elasticity regulates skeletal muscle stem cell self-renewal in culture. Science (80-). 2010;329(5995):1078-1081. doi:10.1126/science.1191035

39. Jacot JG, McCulloch AD, Omens JH. Substrate stiffness affects the functional maturation of neonatal rat ventricular myocytes. Biophys J. 2008;95(7):3479-3487. doi:10.1529/biophysj.107.124545
40. Yingchoncharoen T, Agarwal S, Popović ZB, Marwick TH. Normal Ranges of Left Ventricular Strain: A Meta-Analysis. J Am Soc Echocardiogr. 2013;26(2):185-191. doi:10.1016/j.echo.2012.10.008
41. Ribeiro AJS, Ang Y-S, Fu J-D, et al. Contractility of single cardiomyocytes differentiated from pluripotent stem cells depends on physiological shape and substrate stiffness. Proc Natl Acad Sci. 2015;112(41):12705-12710. doi:10.1073/pnas.1508073112
42. Shiba Y, Hauch K, Laflamme M. Cardiac Applications for Human Pluripotent Stem Cells. Curr Pharm Des. 2009;15(24):2791-2806. doi:10.2174/138161209788923804
43. Opie LH, Commerford PJ, Gersh BJ, Pfeffer M a, England N. Controversies in ventricular remodelling. Lancet. 2006;367(9507):356-367.
44. Sahli Costabal F, Choy JS, Sack KL, Guccione JM, Kassab GS, Kuhl E. Multiscale characterization of heart failure. Acta Biomater. 2019;86:66-76. doi:10.1016/j.actbio.2018.12.053

5. Specific Aim 3A: Align Cardiomyocytes with Fibrin Microthreads on Leaf Scaffold

As demonstrated in Specific Aim 2, contractile strain of unorganized hiPS-CMs on decellularized spinach leaves was a fraction of an *in vivo* contracting ventricle.[1] To manufacture a clinically applicable engineered cardiac patch, hiPS-CMs' contractile strain must be similar to that of *in vivo* conditions. It has been determined that hiPS-CMs contractile performance improves on aligned substrates compared to non-aligned substrates.[2,3] Therefore, aligning hiPS-CMs on the leaf may improve contractile strain. This aim seeks to align human induced pluripotent stem cell-derived cardiomyocytes (hiPS-CMs) on decellularized spinach leaves to promote directional behavior and improve contractility.

5.1 Introduction

Cardiac tissue alignment is essential for appropriate contractile function.[4,5] Cardiomyocyte alignment has been extensively studied in order to mimic native cell function. Cardiomyocytes *in vivo* are exposed to physical stimuli and directional anisotropy that maintains their elongated shape, which regulates sarcomere alignment.[4,6,7] Cell alignment also dictates healthy cardiac tissue's proper electromechanical function. Ventricular contraction is controlled by a highly timed electrical signal that propagates from the atria, through anisotropic cardiac muscle, to the ventricle.[5] Native heart tissue directionally propagates ion flow and action potential to adjacent cardiomyocytes, thus contracting cells in tandem and pumping blood out of the ventricle.

Fibrin is a biocompatible natural material commonly used as a tissue engineering scaffold due to its high cell adhesion and potential for autologous clinical use.[8] Fibrin occurs in nature by tissue injury, in which blood coagulation and platelets form a fibrin rich clot that serves as a provisional matrix so that migrating cells such as monocytes, fibroblasts, and endothelial cells can interact with the tissue injury.[9] Fibrin is a biopolymer of fibrinogen cleaved by thrombin. Thrombin-mediated cleavage of the fibrinopeptide creates conformation changes and exposes polymerization sites, generating a fibrin monomer and formation of insoluble fibrin.[10] In *in vitro* culture conditions, fibrin can degrade rapidly by fibrinolysis. Previous research has demonstrated that fibrin degradation can be reduced when the plasmin inhibitor, aprotinin, is dosed into the cell culture media.[11] In these *in vitro* culture conditions, fibrin can serve as a tissue scaffold.

Previous research has studied the use of fibrin microthreads as a tissue scaffold for cell seeding and delivery.[12–14] Seeded cells elongate along the fibrin microthread surface, providing a

physical structure for cells to reference.[15,16] Our laboratory has previously shown that hiPS-CMs adhere and align on extruded fibrin microthreads to form contractile cardiac fibers.[3] The mechanical contractile properties of these hiPS-CM seeded threads are also compatible to that of the human heart. Furthermore, cell seeded fibrin microthreads remain viable after *in vivo* cardiac transplantation in rats.[3,17]

As demonstrated in Specific Aims 1 and 2, hiPS-CMs adhere to and contract on decellularized spinach leaves, a vascularized biocompatible scaffold. In this aim, we will utilize hiPS-CM seeded fibrin microthreads to transfer aligned cells to decellularized spinach leaves, forming contractile hiPS-CMs arrays on leaf scaffolds. Exploiting fibrinolytic culture conditions, cells will transfer from fibrin microthreads onto decellularized spinach leaves and form aligned cell arrays on leaves.

5.2 Materials and Methods

5.2.1 Fibrin Microthread Manufacturing

Fibrin microthreads were formed with fibrinogen (70 mg/mL, bovine plasma, MP Biomedicals) and thrombin (8 U/mL, bovine plasma, Sigma-Aldrich) by previously detailed methods[3,18] (Appendix G). Fibrinogen and thrombin solutions were coextruded through a blending tip connector into 10 mM HEPES buffered bath (pH 7.4). Threads polymerized in the HEPES bath, then removed and air dried overnight. Each thread construct was composed of three, 2 cm long dry thread sections that were silicone glued to the surface of a polydimethylsiloxane (PDMS) (10:1, Dow SYLGARD™ 184 Silicone Elastomer Kit) washer (inner hole diameter 1.2 cm). PDMS thread constructs were placed in 6 well plates and ethylene oxide (EO) gas sterilized for 12 hours in sterilization pouches. Sterile thread constructs were stored at room temperature until used.

Either human mesenchymal stem cells (hMSCs) or hiPS-CMs were seeded onto fibrin microthreads. Prior to cell seeding, sterile fibrin microthreads constructs were hydrated in sterile 1X PBS for 20 minutes. hMSC seeding occurred after PBS hydration. Microthread constructs and tissue culture plastic (TCP) control wells for hiPS-CM seeding were additionally coated with collagen IV (human placenta, 10 μg/mL, Sigma Aldrich) solution. Collagen IV solution was

incubated on microthreads after hydration on elevated 12 mm round glass coverslips or in control TCP wells for 2 hours at 37°C.[3]

5.2.2 Cell Preparation and Seeding on Fibrin Microthreads

5.2.2.1 hMSC Seeding

Human mesenchymal stem cells (hMSCs) derived from bone marrow (Lonza, Inc.) were thawed and expanded in T-75 flasks in hMSC growth media (MSCGM; Lonza, Inc.) for use (Appendix H). Prior to cell seeding, P8 hMSCs were loaded with 8.2 nM Qdot 655 ITK carboxyl quantum dots (Qdots; Invitrogen) to track the cells.[19] Qdots in MSCGM were incubated on confluent hMSCs in T-75 flasks for 24 hours at 37°C with 5% carbon dioxide (Appendix H).

After microthread hydration in PBS, each thread construct was moved to an elevated glass coverslip and seeded with 200,000 Qdot loaded hMSCs in 150 µL of 50 µg/mL aprotinin (AP) supplemented MSCGM (**Figure 5-1**). Aprotinin is a proteolytic enzyme inhibitor that has been shown to slow fibrinolysis. In standard media without aprotinin, fibrin microthreads decrease in diameter.[11] Cells were incubated on threads on coverslips at 37°C, 5% carbon dioxide for 18 hours. After 18 hours, constructs were moved to new wells containing fresh AP supplemented MSCGM. AP media was replaced every 2-3 days.

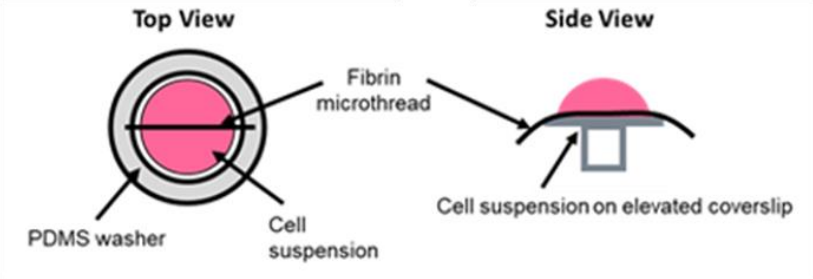

Figure 5-1: Fibrin microthread cell seeding mechanism on elevated coverslips. Hydrated fibrin microthreads adherent to PDMS washers were placed on elevated coverslips for cell suspension seeding.

5.2.2.2 hiPS-CM Seeding

hiPS-CMs were differentiated as previously described in Specific Aims 1 and 2 (Appendix B). hiPS-CMs were shipped overnight to Worcester Polytechnic Institute and stored in cryogenic conditions. When hiPS-CMs were ready to be used, they were thawed (Appendix B). Collagen IV coated fibrin microthread constructs were moved to elevated glass coverslips and seeded with 150,000 hiPS-CMs in 150 µL of 50 µg/mL aprotinin (AP) supplemented RPMI-B27 media

(RPMI 1640, 2% B-27™, 1% L-glutamine, and 1% Penicillin/Streptomycin) with 10% fetal bovine serum (FBS) (Gibco) and 1% ROCK inhibitor (Y-27632 dihydrochloride, Sigma Aldrich). Cells were incubated on threads on elevated coverslips at 37°C, 5% carbon dioxide for 18 hours. After 18 hours, constructs were placed in new wells containing fresh AP supplemented RPMI-B27. AP media was replaced every 2-3 days.

5.2.3 Decellularizing Leaves and Scaffold Preparation

Spinach leaves were obtained, decellularized, lyophilized, and stored as previously outlined in Specific Aims 1 and 2 (Appendix A). Lyophilized decellularized leaf sections were rehydrated and sterilized on a shaker plate, as previously described in Specific Aim 2. Prior to cell seeding, leaves were incubated at 37°C in the appropriate cell seeding media overnight. After incubation, media was aspirated off the decellularized leaves. Leaf surfaces were coated with sterile solutions of fibronectin (human plasma, 100 μg/mL, Sigma Aldrich). Coatings on leaves were air dried at room temperature in a biosafety cabinet until dry.

5.2.4 Microthread Adhesion to Leaves and Controls

Cell seeded fibrin microthreads for leaf application were cultured in AP supplemented media in 6 well plates for 24 hours, after which cell seeded microthreads were positioned on fibronectin coated leaves so that the threads were in contact with the leaf. A custom weight was applied to the outside edge of each PDMS washer to hold the thread on the leaf. The leaf-thread construct was cultured in media without aprotinin to intentionally degrade the fibrin microthreads and transfer the cells from the threads to the leaves (**Figure 5-2**).

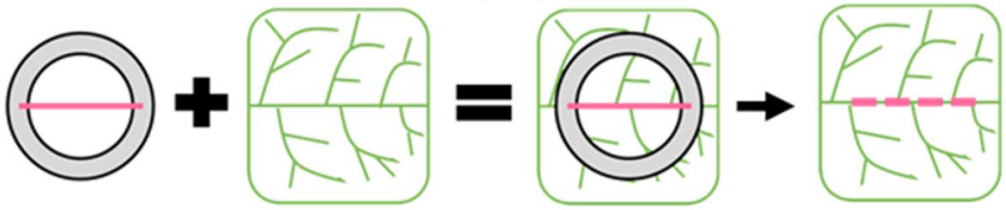

Figure 5-2: Cell seeded fibrin microthread positioned on decellularized spinach leaves to transfer cells. Cell seeded microthreads were placed on decellularized leaves in contact with weights. After 7 days, threads were removed from leaves. In fibrinolytic culture conditions, it was hypothesized that cells would transfer from the microthreads to leaves.

Controls for Qdot hMSCs were seeded on fibronectin coated leaves, fibrin microthreads in AP supplemented media, and tissue culture plastic (TCP). Controls for hiPS-CMs were seeded on fibronectin coated leaves, collagen IV coated fibrin microthreads in AP supplemented media, and

10 μg/mL collagen IV coated TCP. Cell seeded microthreads on leaves and controls were cultured for 7 days. At day 7, all constructs were fixed in 4% paraformaldehyde (PFA) for 10 minutes, followed by three rinses in 1X PBS.

5.2.5 Immunofluorescence Staining and Imaging

Cell seeded microthreads on leaves were separated from leaves after fixation and stained and imaged individually. hMSC seeded microthreads and leaves were immunolabeled with Alexa Fluor™ 488 Phalloidin (Thermo Fisher Scientific) and Hoescht 33342 (Appendix E). hiPS-CM seeded microthreads and leaves were stained for sarcomeric α-actinin, Alexa Fluor™ 488 Phalloidin (Thermo Fisher Scientific), and Hoescht 33342 (Appendix D, E). Imaging was conducted on a laser scanning confocal microscope (Leica Microsystems, Buffalo Grove, IL).

5.2.6 Nuclear Alignment Quantification

Cell alignment on leaves was quantified by calculating relative nuclei orientation angle to the applied microthread. Nuclear orientation is a product of cell orientation.[20] Intracellular forces, due to extracellular cues, can deform and displace the nucleus by cytoskeletal organization. hMSC nuclei orientation information was analyzed from the blue nuclei channel of immunofluorescent images using nuclear orientation angle. One image per sample was used for analysis. Nuclear orientation was measured using the particle analysis function within ImageJ (NIH) to obtain the orientation of the long axis of the nucleus, with respect to the long axis of the fibrin microthread location[16,19] (Appendix I). Using the circstat toolbox in MATLAB (MathWorks, Natick, MA), average angle of nuclei was calculated with respect to the direction of the thread position. Control leaf samples used the horizonal direction as a reference position. Cells were considered aligned if their orientation angle was within 0 and 20 degrees of the reference axis.[20]

5.2.7 Statistical Analysis

Results are presented as mean ± standard deviation for nuclear orientation angle for cells on control leaves, fibrin microthreads, and aligned hMSCs on leaves (n=2 samples).

5.3 **Results**

5.3.1 hMSCs Adhere and Align to Decellularized Leaves with Fibrin Microthreads

At day 7, aligned hMSCs were found on leaves after microthreads were removed from fibrinolytic conditions (n=2) (**Figure 5-3**). The hMSCs' cytoskeleton, illustrated by F-actin, were aligned on the leaves along the direction of the removed microthread. After 7 days, the fibrin microthreads that had been cultured on the leaf were noticeably thinner than initial application, and few cells remained on the threads (data not shown).

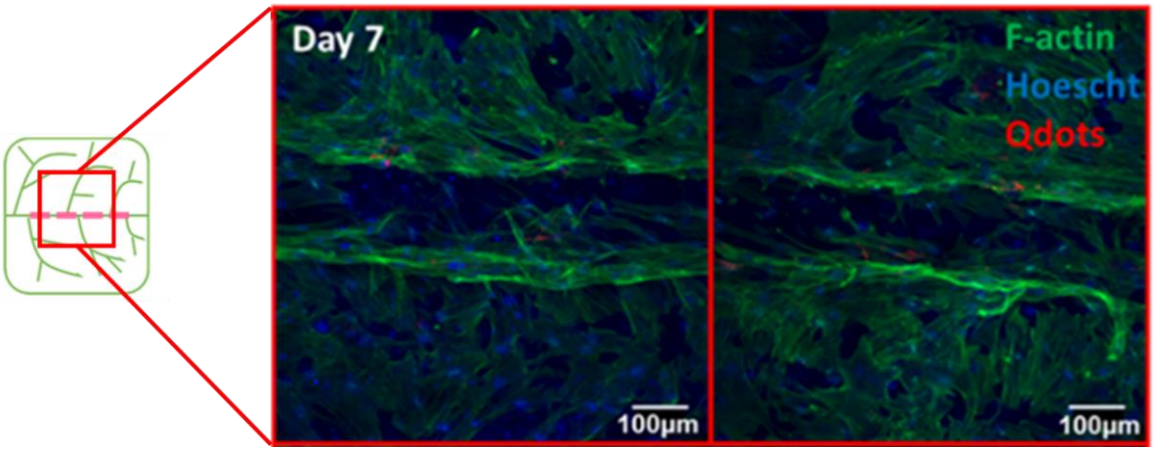

Figure 5-3: hMSCs migrate from microthreads to the leaf in the aligned direction of the removed microthread after 7 days. Microthreads were located in the center of the sample in the horizontal direction. Samples were stained for F-actin (green), Qdots (red), and Hoescht 33342 (blue). Scale bar 100 μm.

Immunofluorescent imaging illustrated hMSCs adherent to control fibrin microthreads (n=2) and fibronectin coated leaves (n=2) after 7 days of culture. hMSCs on control decellularized leaves were not visibly organized in a specific orientation. On fibrin microthreads, hMSCs were aligned along the length of the thread.

With respect to control conditions, average hMSC nuclei angle on control fibrin microthreads were more aligned (11.06° ± 0.85) compared to hMSCs on control leaves (27.8° ± 0.24) and microthread aligned leaf samples (26.0° ± 0.91) (**Figure 5-4A**). Average nuclear angle of microthread aligned hMSCs on leaves were similar to control leaf samples. In addition, average nuclear orientation angles were 26.0° ± 0.91 on the aligned leaves and 17.8° ± 7.7 for hMSCs on the corresponding removed microthread samples (n=2) (**Figure 5-4B**).

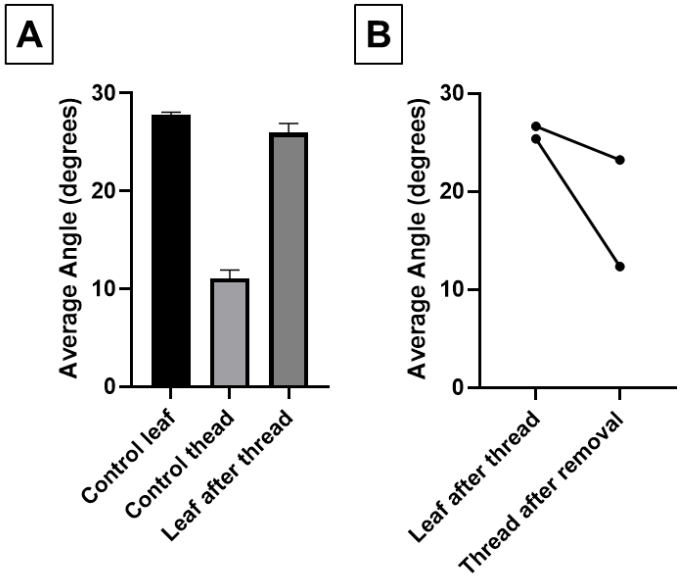

Figure 5-4: hMSC nuclear orientation after fibrin microthread removal from decellularized leaf. (A) Average nuclear orientation angles along fibrin thread controls compare to control leaves and thread-aligned leaves (n=2); (B) Nuclear orientation on threads after removal from leaf and nuclei remaining on leaves (n=2).

5.3.2 hiPS-CMs Did Not Adhere to Decellularized Leaves with Microthreads

We did not observe any transferred hiPS-CMs on leaves after removing hiPS-CM seeded threads at day 7. Few hiPS-CMs also remained on degraded fibrin microthreads. hiPS-CMs were found on control samples for threads and leaves. Since no cells were observed on the aligned leaf samples for hiPS-CMs, no nuclear alignment was observed or calculated.

5.4 **Discussion**

This aim was a preliminary study to determine if using fibrin microthreads on decellularized spinach leaves was a feasible method to induce hiPS-CM alignment. However, our results do not support using this method moving forward since hiPS-CMs did not adhere or align upon application of microthreads on leaves.

After 7 days, hMSCs transferred onto decellularized spinach leaves from fibrin microthreads when cultured in fibrinolytic conditions. Furthermore, hMSCs appeared to align along the microthread position on the leaf. However, few Qdots were present in the aligned hMSCs on leaves. Qdots were loaded into hMSCs to track cell migration, and should remain within the cell for 7 days.[14,19,22] Cells lacking Qdots on leaves may indicate that they had proliferated from

hMSCs. As hMSCs proliferate, the Qdots transfer to the daughter cells; however, because the density of Qdots is less, they may be more difficult to see. We hypothesize that hMSCs aligned on leaves because a select number of hMSCs transferred to the leaf during initial thread application, and then proliferated around the microthread during fibrinolytic degradation over 7 days. The fibrin microthread that remained in contact with the leaf provided a topographical barrier in which the cells were limited to in culture. Topography can induce cell alignment on substrates.[2,23–25] We demonstrated in this aim that hMSCs can migrate from fibrin microthreads and form aligned cell arrays on decellularized leaf scaffolds; however, the way in which this occurred was adjudicated. This could be further confirmed by shortening the culture time to observe if proliferation is the main cause of alignment, or if cells transfer onto the leaf due to fibrin microthread degradation.

We did not observe hiPS-CM transfer from fibrin microthreads onto decellularized spinach leaves in fibrinolytic conditions after 7 days. This may have been due to poor cell seeding on the fibrin microthreads. However, we hypothesize that as microthread degradation occurred in fibrinolytic conditions and cell media was replenished, hiPS-CMs detached from the microthreads, and were aspirated during media changes. Because hiPS-CMs do not proliferate, any cells that may have stuck to the leaf would not multiply, unlike hMSCs. To modify this study for future work, we would consider seeding more hiPS-CMs on individual threads to achieve transfer. However, we have deemed that this method is not efficient for hiPS-CM alignment on leaves since cardiomyocytes do not proliferate.

Overall, this study was a preliminary step to demonstrate that topography and aligned three-dimensional substrates such as fibrin microthreads can induce cell alignment on leaves. It is well established that topographical cues induce cell behavior. Further study requires modified materials and approach to induce cardiac cell alignment on leaves.

5.5 References

1. Robbins ER, Pins GD, Laflamme MA, Gaudette GR. Creation of a Contractile Biomaterial From a Decellularized Spinach Leaf Without ECM Protein Coating: An in vitro study. *J Biomed Mater Res Part A*. Published online April 22, 2020. doi:10.1002/jbm.a.36971
2. Ribeiro AJS, Ang Y-S, Fu J-D, et al. Contractility of single cardiomyocytes differentiated

from pluripotent stem cells depends on physiological shape and substrate stiffness. *Proc Natl Acad Sci*. 2015;112(41):12705-12710. doi:10.1073/pnas.1508073112
3. Hansen KJ, Laflamme MA, Gaudette GR. Development of a Contractile Cardiac Fiber from Pluripotent Stem Cell Derived Cardiomyocytes. *Front Cardiovasc Med*. 2018;5(52):1-11. doi:10.3389/fcvm.2018.00052
4. Pijnappels DA, Schalij MJ, Atsma DE, De Vries AAF. Cardiac anisotropy, regeneration, and rhythm. *Circ Res*. 2014;115(4):e6-e7. doi:10.1161/CIRCRESAHA.115.304644
5. Severs NJ. The cardiac muscle cell. *BioEssays*. 2000;22(2):188-199. doi:10.1002/(SICI)1521-1878(200002)22:2<188::AID-BIES10>3.0.CO;2-T
6. Guyette JP, Charest JM, Mills RW, et al. Bioengineering Human Myocardium on Native Extracellular Matrix. *Circ Res*. 2016;118(1):56-72. doi:10.1161/CIRCRESAHA.115.306874
7. Vunjak-Novakovic G, Tandon N, Godier A, et al. Challenges in Cardiac Tissue Engineering. *Tissue Eng Part B Rev*. 2010;16(2):169-187.
8. Ahmed TAE, Dare E V., Hincke M. Fibrin: A Versatile Scaffold for Tissue Engineering Applications. *Tissue Eng Part B Rev*. 2008;14(2):110306231744007. doi:10.1089/teb.2007.0435
9. Clark RAF. Fibrin and Wound Healing. *Ann N Y Acad Sci*. 2006;936(1):355-367. doi:10.1111/j.1749-6632.2001.tb03522.x
10. Mosesson MW. Structure and Functions of Fibrinogen and Fibrin. *Recent Adv Thromb Hemost 2008*. Published online 2009:3-26. doi:10.1007/978-4-431-78847-8_1
11. Coffin ST, Gaudette GR. Aprotinin extends mechanical integrity time of cell-seeded fibrin sutures. *J Biomed Mater Res - Part A*. 2016;104(9):2271-2279. doi:10.1002/jbm.a.35754
12. Cornwell KG, Pins GD. Discrete crosslinked fibrin microthread scaffolds for tissue regeneration. *J Biomed Mater Res - Part A*. 2007;82(1):104-112.
13. Guyette JP, Fakharzadeh M, Burford EJ, et al. A novel suture-based method for efficient transplantation of stem cells. *J Biomed Mater Res - Part A*. 2013;101 A(3):809-818. doi:10.1002/jbm.a.34386
14. Hansen KJ, Favreau JT, Guyette JP, et al. Functional Effects of Delivering Human Mesenchymal Stem Cell-Seeded Biological Sutures to an Infarcted Heart. *Biores Open Access*. 2016;5(1):249-260. doi:10.1089/biores.2016.0026
15. Grasman JM, Page RL, Dominko T, Pins GD. Crosslinking strategies facilitate tunable structural properties of fibrin microthreads. *Acta Biomater*. 2012;8(11):4020-4030. doi:10.1016/j.actbio.2012.07.018
16. Grasman JM, Pumphrey L, Dunphy M, Perez-Rogers J, Pins GD. Static Axial Stretching Enhances the Mechanical Properties and Cellular Responses of Fibrin Microthreads. *Acta Biomater*. 2014;10(10):4367-4376. doi:10.1038/jid.2014.371
17. Hansen KJ, Favreau JT, Guyette JP, et al. Functional Effects of Delivering Human Mesenchymal Stem Cell-Seeded Biological Sutures to an Infarcted Heart. *Biores Open Access*. 2016;5(1):249-260. doi:10.1089/biores.2016.0026
18. Proulx MK, Carey SP, Ditroia LM, et al. Fibrin microthreads support mesenchymal stem cell growth while maintaining differentiation potential. *J Biomed Mater Res - Part A*. 2011;96 A(2):301-312. doi:10.1002/jbm.a.32978
19. Rosen AB, Kelly DJ, Schuldt AJT, et al. Finding Fluorescent Needles in the Cardiac Haystack: Tracking Human Mesenchymal Stem Cells Labeled with Quantum Dots for Quantitative In Vivo Three-Dimensional Fluorescence Analysis. *Stem Cells*.

2007;25(8):2128-2138. doi:10.1634/stemcells.2006-0722
20. Bray M-A, Adams WJ, Geisse NA, Feinberg AW, Sheehy SP, Parker KK. Nuclear Morphology and Deformation in Engineered Cardiac Myocytes and Tissues. *Biomaterials*. 2010;31(19):5143-5150. doi:10.1016/j.physbeh.2017.03.040
21. Carnes ME, Pins GD. Etching anisotropic surface topography onto fibrin microthread scaffolds for guiding myoblast alignment. *J Biomed Mater Res - Part B Appl Biomater*. 2020;108B(5):2308-2319. doi:10.1002/jbm.b.34566
22. Salick MR, Napiwocki BN, Sha J, et al. Micropattern Width Dependent Sarcomere Development in Human ESC-Derived Cardiomyocytes. *Biomaterials*. 2014;35(15):4454-4464. doi:10.1038/jid.2014.371
23. Muller-Borer BJ, Collins MC, Gunst PR, Cascio WE, Kypson a P. Quantum dot labeling of mesenchymal stem cells. *J Nanobiotechnology*. 2007;5:9. doi:1477-3155-5-9 [pii]\r10.1186/1477-3155-5-9
24. McCain ML, Desplantez T, Geisse NA, et al. Cell-to-cell coupling in engineered pairs of rat ventricular cardiomyocytes: relation between Cx43 immunofluorescence and intercellular electrical conductance. *AJP Hear Circ Physiol*. 2012;302(2):H443-H450. doi:10.1152/ajpheart.01218.2010
25. McDevitt TC, Angello JC, Whitney ML, et al. In vitro generation of differentiated cardiac myofibers on micropatterned laminin surfaces. *J Biomed Mater Res*. 2002;60(3):472-479. doi:10.1002/jbm.1292
26. English EJ. Micropatterned Fibrin Hydrogels for Increased Cardiomyocyte Alignment. Published online 2019. doi:10.1017/CBO9781107415324.004

6. Specific Aim 3B: Manipulate Decellularized Leaf Topography to Align Cardiomyocytes

6.1 Introduction

Cardiomyocyte (CM) culture systems should aim to mimic *in vivo* microenvironmental topographical cues.[1] We have previously demonstrated in Specific Aims 1 and 2 that human induced pluripotent stem cell derived cardiomyocytes (hiPS-CMs) adhere to and contract on a decellularized spinach leaf. Micropatterned, or microcontact printed, topographical cues could provide signals for hiPS-CMs to align in arrays on the leaf, similar to *in vivo* behavior. Stamp micropatterning uses a patterned elastomeric stamp to transfer an inked material by pressing the stamp directly onto that substrate.[2] Micropatterning can be conducted using proteins, hydrogels, or synthetic materials. Micropatterned designs are often used to model cell maturity, alignment, and response to different surface templates and designs. Furthermore, CMs adhere and conform to micropatterned protein topographical cues on substrates. When elongated micropatterned cues are applied, CMs display increased maturity in elongation than on non-patterned surfaces.[3–5]

In this aim, we develop and test a method to form rows of aligned hiPS-CMs using micropatterned topographical cues[5] on decellularized spinach leaf scaffolds, and then determine if this method leads to hiPS-CM alignment. To micropattern leaves, we pursued fibrin hydrogel as a substrate due to its rapid formation and structural integrity on the leaf surface. Previous work has demonstrated that primary and stem cell-derived cardiomyocytes adhere to and contract on fibrin hydrogel scaffolds.[6–10] In addition, when micropatterned fibrin hydrogels are seeded with hiPS-CMs, hiPS-CMs demonstrate improved contractile and aligned behavior when compared to non-patterned controls.[7]

However, fibrin hydrogels alone have low mechanical integrity[11] compared to heart tissue. Adding structural reinforcement to fibrin hydrogels could enhance its ability to serve as a tissue engineered cardiac patch scaffold. Decellularized spinach leaves have mechanical properties similar to that of decellularized heart tissue. In addition, decellularized leaves have a perfusable vascular system, which is difficult to construct in fibrin hydrogels. Micropatterned fibrin hydrogel on decellularized spinach leaves may be the solution to align CMs on the leaf surface. In this aim, we develop a method to micropattern stamp fibrin on the surface of decellularized leaves to align cardiomyocytes.

Based on previous work, hiPS-CMs should adhere to and align along the direction of the fibrin micropatterns, improving their functional behavior. Contractile performance of aligned cardiomyocytes is improved when compared to non-aligned.[5] We have previously shown that hiPS-CMs adhere, align, and improve their performance, comparable to the adult human myocardium, on elongated scaffolds compared to non-aligned controls.[12,13] We expect to observe longitudinal alignment behavior along the micropatterned arrays. Aligned hiPS-CMs on micropatterned leaves should follow the structural cues of the micropatterns.

6.2 Materials and Methods

6.2.1 Decellularizing Leaves and Preparation

Leaf decellularization and lyophilization was conducted using methods described in Specific Aims 1 and 2 (Appendix A).

6.2.2 Micropatterned Stamp Manufacturing

Micropatterning fibrin on leaves was conducted using micropatterned stamp molds. Micropatterned molds were manufactured with photolithographic methods to create a master silicon wafer (**Figure 6-1**). Photoresist (SU-8 2035) was coated on a silicon wafer template with square stamp templates of 1 cm^2 (Appendix J). Each stamp template was designed to contain 100 μm deep rectangular rows with widths of 10, 15, 25, 50 or 100 μm. The mask containing the stamp template was placed over the wafer and exposed to UV light. Exposure time and energy used to form the rows was determined based on the UV light wattage and lamp power. After UV exposure, the wafer was exposed to photoresist developer solution for 15 minutes to dissolve the unexposed negative photoresist. The wafer was then baked at 150°C for 90 minutes to harden the photoresist. PDMS was mixed at a ratio of 10:1 base and curing agent (Dow SYLGARD™ 184 Silicone Elastomer Kit) and poured onto the manufactured photoresist wafer template to create the stamp mold. The mold was degassed and cured on the template at 60°C for 2 hours. The cured PDMS mold was cut out from the template and washed with deionized (DI) water. Individual PDMS mold stamps were trimmed on both sides perpendicular to the patterned rows so that the cut edges exposed the row grooves.

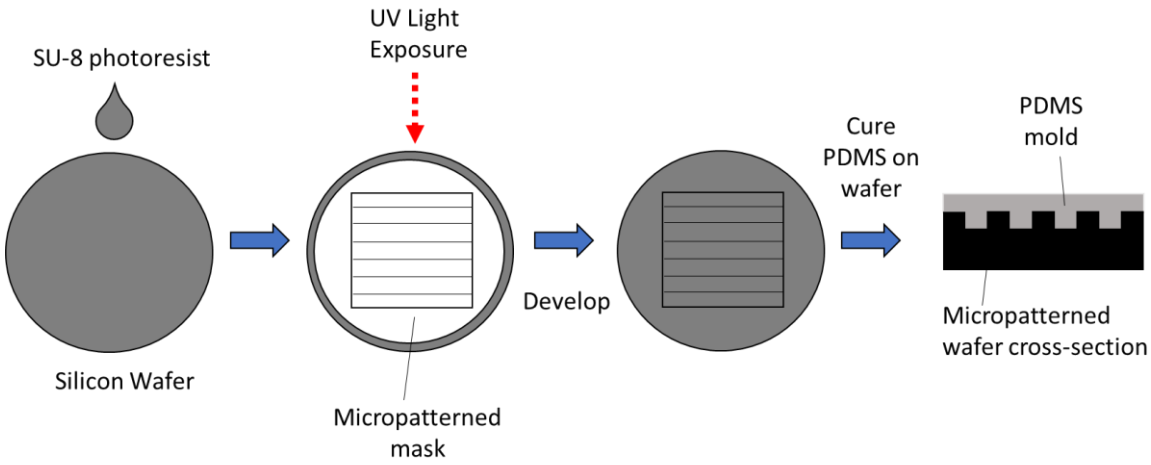

Figure 6-1: Process to manufacture micropatterned wafer and PDMS molds using photolithography. SU-8 photoresist was coated on the silicon wafer. The micropattern design mask containing the stamp template was placed over the wafer and subject to UV light to form the micropattern. The wafer was then exposed to developer solution to remove unexposed photoresist. PDMS was then cured on the wafer to create the stamp mold for micropatterning.

6.2.3 Verifying Stamp Pattern Geometry

Manufactured PDMS stamp geometry was verified by cutting a 1 mm thick stamp cross-section at its center, perpendicular to the rectangular rows, and measuring the geometry of each micropattern width (10, 15, 25, 50, and 100 μm). PDMS cross-sections were imaged on an upright microscope (Leica Microsystems, Buffalo Grove, IL) on a coverslip, with two sample images taken per pattern design. Measurements for row depth, peak width, and valley width were taken at three random locations per image using the line tool in ImageJ (NIH). Data were represented as mean ± standard deviation.

6.2.4 Fibrin Micropatterning on Leaf and Coverslips

Prior to patterning, 100 μm row width PDMS molds were sterilized with autoclave steam or EO gas sterilization. PDMS stamps were coated in sterile 1% Pluronics F-127 for one hour and air dried in a biosafety cabinet prior to use.

Micropatterning substrates included glass coverslips (for controls) and decellularized spinach leaves. For fibrin micropatterning on coverslips, 22x22 mm glass coverslips were first incubated overnight in sterile 0.67% gelatin solution (porcine, Sigma-Aldrich) at 37°C. Gelatin coverslips were adhered to the bottom of 6 well plates with vacuum grease and air dried in a biosafety cabinet prior to patterning. Coverslip controls included non-patterned fibrin hydrogel on gelatin coated coverslips and gelatin coated coverslips.

Prior to micropatterning, decellularized spinach leaves were rehydrated and sterilized as described in Specific Aim 2, rinsed with 1X PBS, and incubated in the appropriate cell media overnight (Appendix A). Leaf control conditions included decellularized leaves with non-patterned fibrin hydrogel and non-coated leaves.

Fibrin hydrogels (10 mg/mL) were composed of 90.7% 11 mg/mL fibrinogen (bovine plasma, MP Biomedicals), 4.0% 40 U/mL thrombin (bovine plasma, Sigma-Aldrich), and 5.3% RPMI 1640 basal media (Appendix L). Fibrinogen, thrombin, and RPMI basal media were thawed and sterile filtered individually with 0.2 µm syringe filters prior to mixing in a biosafety cabinet. All components were maintained on ice prior to mixing. When mixed, this solution cures rapidly. In addition, 10 mg/mL fibrin hydrogel has shown successful hiPS-CM adhesion and micropatterned cell alignment.[7]

After mixing of fibrinogen, thrombin, and RPMI basal media, 30 µL of fibrin solution was immediately pipetted onto the leaf or coverslip surface. For micropatterned samples, the 100 µm PDMS stamp was placed on the substrate parallel to a reference edge, and pattern surface in contact with fibrin (**Figure 6-2**). Sterile forceps were used to lightly tap down the stamp onto the substrate surface. After 30 minutes at room temperature, the PDMS mold was removed with forceps in the direction of the row pattern. Fibrin patterns were verified by visual observation on the leaf or coverslip surface. Non-patterned fibrin coatings were left to cure on leaves or coverslips for 30 minutes without stamps.

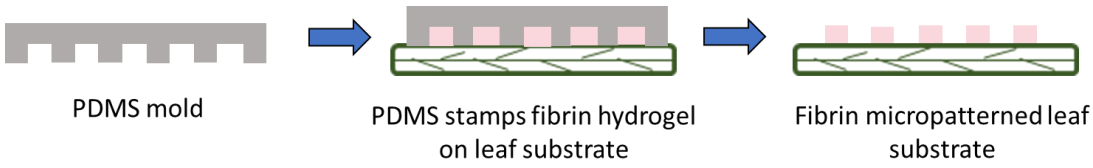

Figure 6-2: Process to fibrin micropattern the substrate surface. Fibrin hydrogel was pipetted onto the substrate surface, then the PDMS stamp was gently placed on the fibrin to micropattern the substrate. After 30 minutes, the PDMS stamp was removed in the direction of the row pattern, depositing the fibrin micropattern on the substrate surface.

To verify 100 µm fibrin rows on leaves, two patterned leaves were fixed with 4% paraformaldehyde (PFA), processed, and embedded in paraffin wax blocks using a custom protocol (Appendix K). Micropatterned leaves were sectioned at 15 µm thickness on a microtome perpendicular to the row direction. Fibrin on leaf samples were stained with eosin (Appendix K). Fibrin micropatterns on leaves were measured for peak, valley, and depth using

ImageJ's linear measuring tool, as explained in Section 6.2.3. Per leaf sample, five measurements were collected from distinct patterns (N=2, n=10). The sample mean and standard deviation of measured fibrin patterns were calculated for row peak width, valley width, and row depth.

6.2.5 Cell Seeding and Culture Time

6.2.5.1 hMSC Seeding and Culture

Human mesenchymal stem cells (hMSCs) derived from bone marrow (Lonza, Inc.) were thawed and expanded in T-75 flasks in hMSC growth media (MSCGM; Lonza, Inc.) for use (Appendix H). Following 100 µm fibrin micropatterning, 50,000 P8 hMSCs in 50 µg/mL aprotinin supplemented MSCGM were seeded on each patterned or non-patterned leaf and gelatin coverslip substrate in 10 mm cloning wells (Pyrex®, Corning Inc., Corning NY) (Appendix L). Aprotinin, a proteolytic enzyme inhibitor shown to slow fibrinolysis[14], was added to maintain the structural integrity of the patterned fibrin. Seeded hMSC samples included fibrin micropatterned leaves (N=3, n=11), fibrin non-patterned control leaves (N=3, n=8), uncoated leaves (N=3, n=9), fibrin micropatterned coverslips (N=3, n=9), fibrin non-patterned control coverslips (N=3, n=7), and gelatin coated coverslips (N=3, n=9). hMSCs were cultured on substrates at 37°C, 5% carbon dioxide. After 24 hours, cloning wells were removed from the leaf or coverslip substrates, and cells on fibrin coated samples were replenished with aprotinin supplemented MSCGM. Samples without fibrin were fed with MSCGM. Media was replenished in constructs every other day. After 5 days, samples were fixed in 4% PFA and rinsed three times in 1X PBS.

6.2.5.2 hiPS-CM Seeding and Culture

hiPS-CMs were differentiated as previously described in Specific Aims 1 and 2 (Appendix B). hiPS-CMs were shipped overnight to Worcester Polytechnic Institute and stored in cryogenic conditions. When hiPS-CMs were ready to be used, they were thawed (Appendix B). hiPS-CMs were seeded on leaf and 0.67% gelatin coverslip substrates to compare cardiac cell behavior (Appendix L). 150,000 hiPS-CMs in 50 µg/mL aprotinin supplemented RPMI-B27 media (RPMI 1640, 2% B-27™, 1% L-glutamine, and 1% Penicillin/Streptomycin) with 10% fetal bovine serum (FBS) (Gibco) and 1% Rho-associated protein kinase (ROCK) inhibitor (Y-27632 dihydrochloride, Sigma Aldrich) were seeded onto each patterned and non-patterned substrate in 10 mm cloning wells. Seeded hiPS-CM leaf samples included fibrin micropatterned leaves (N=3,

n=10), fibrin non-patterned control leaves (N=3, n=6), and uncoated leaves (N=3, n=16). hiPS-CMs on substrates were cultured at 37°C, 5% carbon dioxide. After 18 hours, cells on fibrin coated samples were replenished with aprotinin supplemented RPMI-B27. Samples that did not contain fibrin were fed with RPMI-B27. Media was replenished every day. After 7 days, samples were fixed in 4% PFA and rinsed three times in 1X PBS.

6.2.6 hMSC Behavior Analysis

6.2.6.1 Immunofluorescence Labeling and Imaging

hMSC samples were immunofluorescence (IF) labeled with Alexa Fluor™ 488 Phalloidin (Thermo Fisher Scientific) and Hoescht 33342 (Appendix E) and imaged with the 40X objective on a scanning confocal microscope (Leica Microsystems, Buffalo Grove, IL). Maximum projection images were obtained from the scanning confocal microscope by image collection every 1 µm. Samples were positioned on 24 x 60 mm coverslips so the substrate pattern was parallel to the edge of the coverslip. Therefore, the fibrin micropattern would be aligned to the edge of coverslip and parallel with the horizontal direction in the image. For each sample, images were collected in two locations at the center of the cell seeded region. Image analysis was performed on the maximum projection images collected.

6.2.6.2 Nuclear Orientation

Nuclear orientation is a product of cell orientation. Intracellular forces, due to extracellular cues, can deform and displace the nucleus by cytoskeletal organization. Specifically, in cardiomyocytes, the filaments in sarcomeric Z-lines are mechanotransductive and couple myocyte shape to nuclear shape.[15,16] When cardiomyocytes elongate, both sarcomere length and nuclear length increases. Furthermore, nuclear alignment is a function of cardiac anisotropy in that cardiomyocyte nuclei alignment can occur from changes in anisotropic substrates.[16] Although nuclear alignment is a function of cell alignment, it is limited in that it is not a direct measurement as it is a result of intracellular cytoskeleton behavior.

hMSC nuclei orientation information was analyzed from the blue nuclei channel of IF images using nuclear orientation angle. Nuclei orientation indicates cell alignment on a substrate where cells are considered aligned if their orientation angle is within 0 and 20 degrees of the reference axis.[17] Nuclear orientation angle was measured using the particle analysis function within ImageJ (NIH) to obtain the orientation of the long axis of the nucleus, with respect to the long axis of the

micropattern (Appendix I).[18,19] Image nuclei data was saved as a .csv file and angles were normalized from 0 to 90 degrees, with the horizontal pattern direction referenced at 0 degrees. Using the circstat toolbox in MATLAB (MathWorks, Natick, MA), average angle of nuclei were calculated with respect to the horizontal direction.

6.2.7 hiPS-CM Behavior Analysis

6.2.7.1 hiPS-CM Contractile Strain and Beat Frequency

After 7 days, hiPS-CM live cell behavior on leaf scaffolds was evaluated with contractile strain analysis from image-based strain measurements. hiPS-CM contractile strain was measured using high density mapping (HDM) strain analysis[20,21], as previously described in Specific Aims 1 and 2 (Appendix C). In addition, we conducted contractile beat frequency analysis of micropatterned fibrin leaves in distinct regions of interest (ROIs) to determine if fibrin micropatterned leaf samples contained synchronized hiPS-CM contraction (n=7 samples). Three ROIs within a sample were selected in the following locations: the original ROI from contractile strain analysis, a ROI within the same fibrin micropatterned row as the original, and a ROI in a parallel row from the original. Contractile strain velocity between ROIs was measured by first calculating ROI centroid locations and distance between the original and parallel or within row ROI centroids. Then, we determined the time difference in contraction initiation between parallel and within row ROIs, relative to the original ROI. Contractile strain velocity (in millimeters per second) was calculated by the distance between centroids divided by the time difference to contraction initiation.

6.2.7.2 hiPS-CM Immunofluorescence Labeling and Imaging

Cell adhesion and alignment on leaves and coverslips were analyzed with immunofluorescence (IF) labeling and imaging. Samples were IF labeled for sarcomeric α-actinin (mouse monoclonal, Abcam), Alexa Fluor™ Phalloidin (Thermo Fisher Scientific) and Hoescht 33342, and imaged on a scanning confocal microscope (Leica Microsystems, Buffalo Grove, IL) with the 40X objective (Appendix D, E). Maximum projection images were obtained with vertical image collection every 1 μm. During imaging, leaf samples were positioned on 24 x 60 mm coverslips and aligned so that the substrate was parallel to the edge of the coverslip. Therefore, the fibrin micropattern would be aligned to the edge of coverslip and parallel with the horizontal direction in the image. For each sample, images were collected in two locations at the center of the cell seeded region. Image analysis was performed on the maximum projection images collected.

6.2.7.3 hiPS-CM Adherence to Fibrin Micropatterns

hiPS-CM adherence to fibrin micropatterned region of the leaf was measured using Fast Fourier transform (FFT) analysis of hiPS-CM F-actin channel images to detect the spacing in which cells are patterned on the leaf. As FFT analysis with power spectrum analysis determines the peak frequency of a pattern, this analysis determined if cell adhesion occurred in 100 μm spaced rows. First, perpendicular lines were drawn at 25%, 50% and 75% (left, center and right) across the width of an image in ImageJ (NIH) (**Figure 6-3A)**, and gray scale peaks were plotted for each line using the "Plot Profile" function (**Figure 6-3B**). Using the custom code written in MATLAB (MathWorks, Natick, MA) to measure sarcomere spacing in Specific Aim 2 (Appendix F)[22], we analyzed the distance between patterns of cell F-actin using Fourier transform and power analysis.

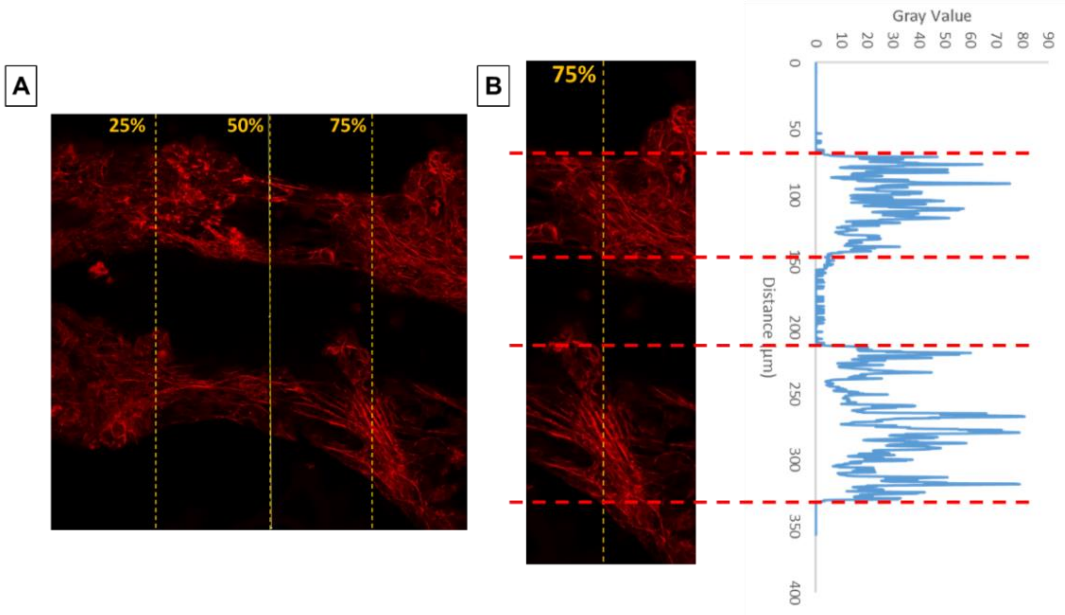

Figure 6-3: Fast Fourier transform (FFT) analysis of hiPS-CM F-actin channel images to detect cell spacing on micropatterned leaves. (A) Perpendicular lines were drawn at 25%, 50% and 75% (left, center and right, yellow) across the width of a F-actin channel IF image (red). (B) Across the length of a perpendicular line (ex. 75%), gray value intensity plots indicate F-actin presence. The most frequent distance between F-actin patterns is the micropatterned cell spacing.

The most frequent pattern distance in microns was calculated between hiPS-CM patterns at each image measurement (25%, 50% and 75%). An outlier calculation was removed where power analysis was not able to detect more than one cell pattern per perpendicular line. The average distance between rows per sample was calculated, and then the mean of all hiPS-CM patterned leaf samples was determined (N=3, n=9).

6.2.7.4 hiPS-CM Nuclear and F-actin Orientation

Nuclear orientation analysis was performed as with hMSCs described in Section 6.2.6.2 (Appendix I). Nuclear orientation angle was measured in nuclei channel images using the particle analysis function within ImageJ to obtain the orientation of the long axis of the nucleus, with respect to the long axis of the micropattern.[18,19] We calculated mean nuclear angle of each image to compare nuclei orientation angle alignment between surface conditions. Using the circstat toolbox in MATLAB, average nuclei angle was calculated with respect to the direction of the horizontal axis.

hiPS-CM cytoskeletal orientation on micropatterned and non-patterned substrates was measured with F-actin channel image data. F-actin orientation was calculated using the Directionality plugin feature in ImageJ (NIH). The Directionality plugin is used to calculate the preferred orientation of structures present within an image, calculating a histogram of the number of structures in given angle directions. The method uses Fourier spectrum analysis to calculate the orientation and power for each angle direction.[23] The plugin calculates each sample's F-actin primary direction by fitting a Gaussian function to the direction output, where the primary angle is the center of the Gaussian. Primary directions in degrees were compiled, and the mean orientation angle and standard deviation of F-actin was calculated per condition. Angle data were binned by 15 degree increments and plotted in a histogram for each condition.

6.2.8 Statistical Analysis

Data are presented as mean ± standard deviation values from three biological replicates (N=3) for each hMSC and hiPS-CM seeded samples. From these biological replicates, there were at least six cell seeded samples (n=6) per patterned or non-patterned condition. One-way ANOVAs for multiple comparisons with post-hoc Tukey t-tests ($p<0.05$) were performed to determine the effect of micropatterned compared to control conditions for cell contractile strain, nuclear alignment, and F-actin alignment. Regional beat frequency analysis of micropatterned leaves was performed using a one-way ANOVA for multiple comparisons with post hoc paired Dunnett t-test ($p<0.05$). Contractile velocity analysis was analyzed using a paired t-test ($p<0.05$). All analyses were performed in GraphPad Prism 9 (GraphPad Software, San Diego, CA).

6.3 **Results**

6.3.1 100 µm Row Stamp Best Represents Designed Micropattern

PDMS molds were constructed from a photolithography template for five different micropattern width conditions. PDMS molds were designed to have depth of 100 µm and equal peak and valley widths of 100, 50, 25, 15, or 10 µm. Molds were easily removed from wafer templates. PDMS row widths (peak and valley) and depths were measured per design (n=6) (**Figure 6-4**).

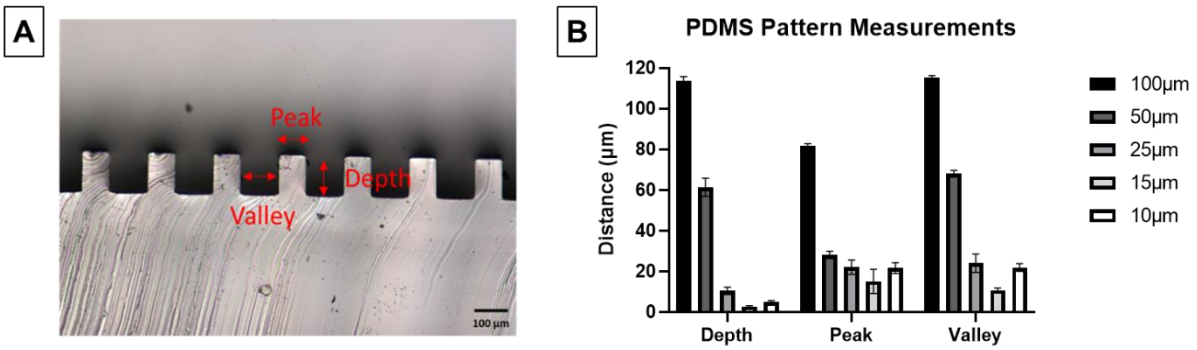

Figure 6-4: PDMS mold measurements of depth and width (peak and valley) for micropatterned row cross-sections. (A) Cross section of 100 µm width row pattern, with examples of peak, valley, and depth measured locations. Scale bar 100 µm. (B) Measured depth, peak, and valley for 100, 50, 25, 15, and 10 µm PDMS molds (n=6).

The designed row depth for all patterns was 100 µm. The measured average depth for 50, 25, 15, and 10 µm row width values were all less than 100 µm (**Table 1**). The row depths in these designs appeared to represent the width more than the designed depth. The only stamp that resembled the designed depth was the 100 µm width design.

	Depth	**Peak**	**Valley**
100µm	113.7 ± 2.0	81.6 ± 1.1	115.3 ± 0.9
50µm	61.3 ± 4.5	28.0 ± 1.8	68.0 ± 1.6
25µm	10.3 ± 1.8	22.0 ± 3.5	24.0 ± 4.5
15µm	2.6 ± 0.4	15.0 ± 6.0	10.6 ± 1.1
10µm	4.8 ± 0.7	21.6 ± 2.6	21.8 ± 1.9

Table 1: Average ± standard deviation of PDMS mold pattern rows for depth, peak, and valley measurements.

Furthermore, peak and valley width measurements should be like that of the designed row widths (100, 50, 25, 15 or 10 µm). In Table 1, valley row widths measured values were similar to the designed value, except for 10 µm widths. Measured peak widths were close to the design for 100, 25 and 15 µm design rows. The measured dimensions of the PDMS mold with 100 µm pattern

spacing provided the most consistent rectangular measurements closest to the designed value. Therefore, 100 μm row patterns were pursued for micropatterning leaves.

6.3.2 Micropatterned Fibrin Represents Designed Pattern on Leaf

Fibrin hydrogel micropatterned rows were manufactured on decellularized spinach leaves using 100 μm PDMS stamps. Fibrin topographical patterns were present across the leaf surface, visible to the naked eye. The leaves were fixed in 4% PFA, embedded in paraffin, sectioned, stained with eosin to distinguish fibrin, and fibrin micropattern dimensions were measured from imaged sections (**Figure 6-5**). Mean ± standard deviation measurements of fibrin rows on 100 μm micropatterned leaves were measured in ImageJ (N=2, n=10). Average valley depth (80.3 ± 19.9 μm) and peak width (86.3 ± 17.3 μm) of fibrin rows on leaves approached 100 μm. However, micropatterned fibrin depth on leaves (22.4 ± 9.9 μm) was considerably less than average PDMS mold depth dimensions (113.7 ± 2.0 μm) and the designed depth value (100 μm).

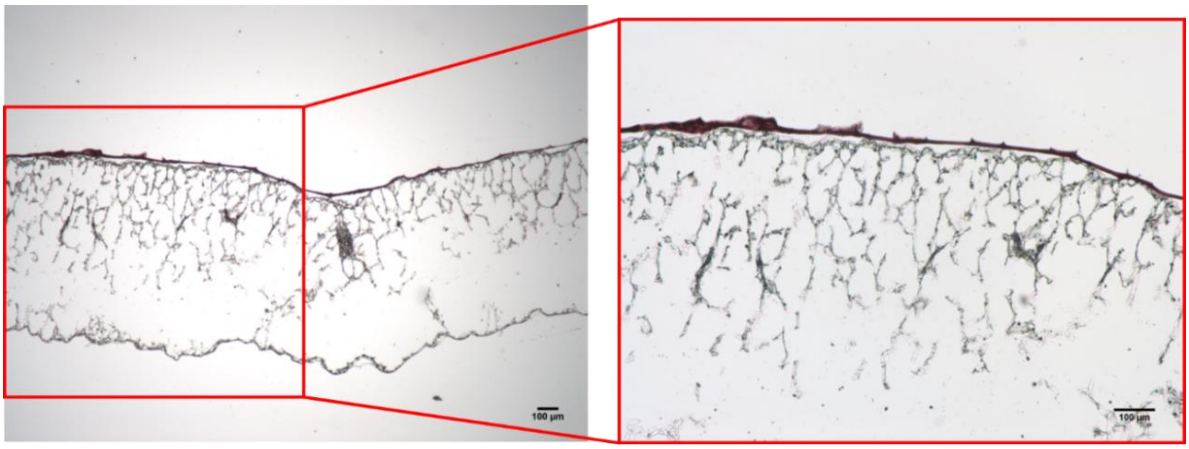

Figure 6-5: Cross sectioned 100 μm fibrin micropatterned leaf stained with eosin. Zoomed in view of cross section illustrates eosin-stained fibrin (pink) rows across the leaf surface. Scale bars 100 μm.

6.3.3 hMSCs Follow Topographical Cues on Fibrin Micropatterned Leaves

6.3.3.1 hMSC Cytoskeleton Aligns in Direction of Micropattern

Human MSCs appeared to form confluent layers on leaf surfaces after 5 days (**Figure 6-6**). Non-patterned hMSCs demonstrate unorganized behavior on the surface of the leaf (**Figure 6-6A**). Whereas micropatterned cells are organized and F-actin are oriented in the horizontal direction (**Figure 6-6B**), suggesting alignment with the micropatterned rows. Furthermore, F-actin bands appeared with increased density in widths of 100 μm on patterned leaves, indicating that hMSCs are on top of or within the fibrin rows.

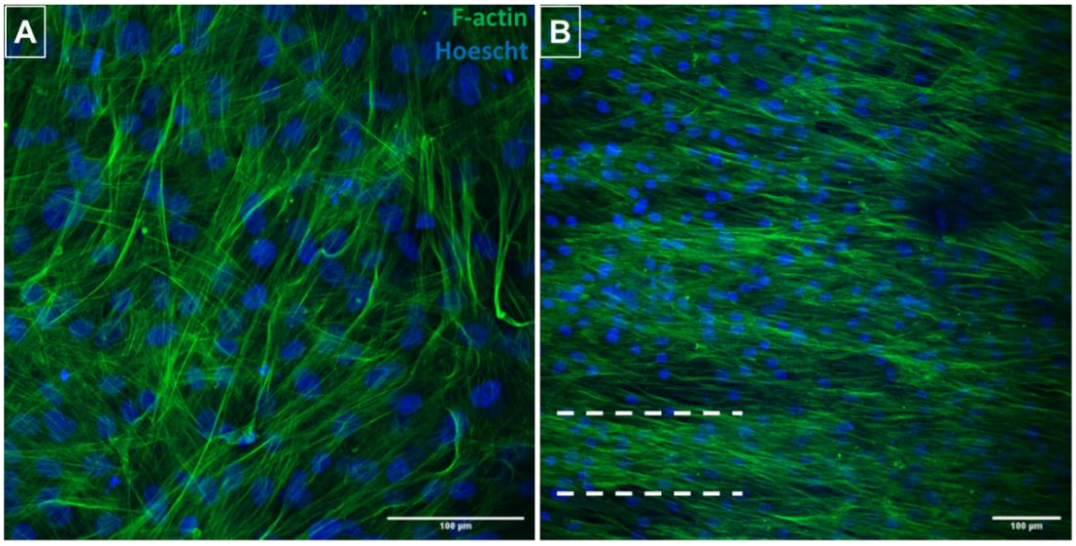

Figure 6-6: hMSC alignment on fibrin micropatterned and non-patterned leaf surface. Samples were immunolabeled for F-actin (green) and Hoescht 33342 (blue). (A) hMSCs on non-patterned fibrin coated leaf spread randomly and display no cytoskeletal organization after 5 days. (B) hMSCs on micropatterned fibrin leaf are aligned in the orientation of the 100 µm rows (white dotted lines), visualized in the cytoskeleton organization after 5 days. Scale bars 100 µm.

6.3.3.2 hMSC Nuclei Align in the Direction of Micropatterned Fibrin

Hoechst staining of hMSC nuclei on fibrin micropatterned leaves demonstrated alignment with the patterned rows (**Figure 6-7**). Average hMSC nuclear angle on fibrin micropatterned leaves was significantly lower, relative to the row direction, compared to hMSCs on non-patterned leaves ($p<0.0001$) (**Figure 6-7B**). The same results were true for hMSC nuclei on patterned versus non-patterned fibrin ($p=0.0001$) and gelatin ($p<0.0001$) coverslips **(Figure 6-7A)**. Therefore, micropatterned hMSCs demonstrate more nuclear alignment than their respective controls.

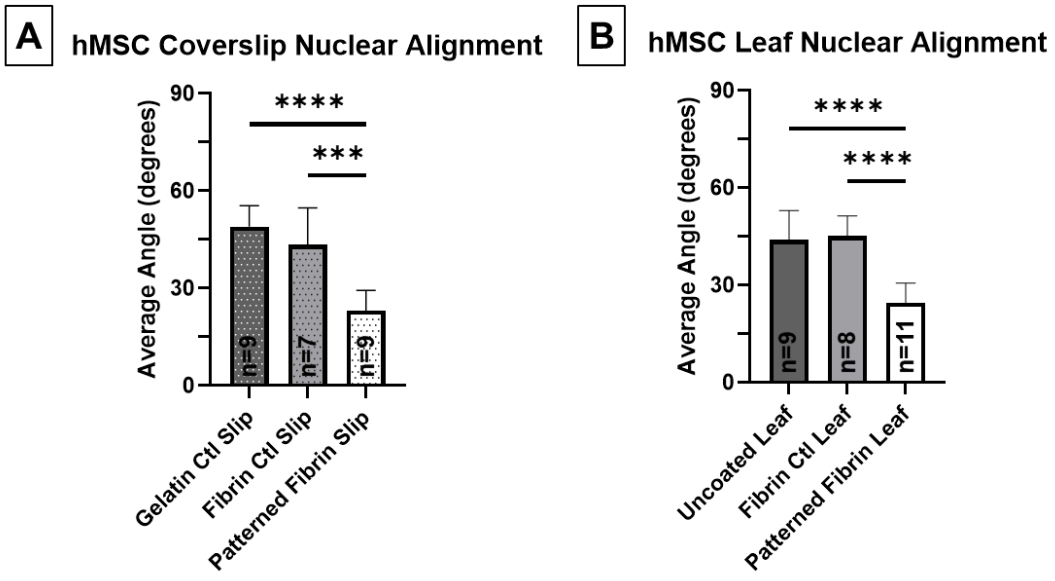

Figure 6-7: Fibrin micropatterned hMSCs have lower nuclear angle than non-patterned samples on coverslips and leaf substrates. Sample sizes n for each condition are illustrated within the data. (A) Average hMSC nuclear angle on fibrin micropatterned coverslips is significantly lower than hMSCs on non-patterned fibrin control ($p=0.0001$) and gelatin ($p<0.0001$) coverslips. (B) Average hMSC nuclear angle on fibrin micropatterned leaf substrates is significantly lower than hMSCs on non-patterned fibrin ($p<0.0001$) and uncoated ($p<0.0001$) leaf substrates.

6.3.4 hiPS-CM Follow Topographical Cues on Fibrin Micropatterned Leaves

hiPS-CMs adhered to fibrin micropatterned and control leaves and coverslips. However, after two days in culture, hiPS-CMs lifted off fibrin micropatterned coverslips. hiPS-CM contraction appeared to dislodge the micropatterned fibrin off the coverslips. As the cells were no longer attached to the substrates, data from hiPS-CM seeded coverslips were not obtained.

6.3.4.1 hiPS-CMs on Micropatterned Leaves Demonstrate Higher Contractile Strain Than Non-Patterned Leaves

After 7 days of hiPS-CM culture on leaves, n=4 out of 10 micropatterned, n=3 out of 6 fibrin control, and n=12 out of 16 uncoated leaf samples were contracting. Average contractile strain measurements of hiPS-CMs on fibrin micropatterned decellularized spinach leaves (8.7%) was significantly higher than non-coated leaves (4.7%; $p<0.05$) (**Figure 6-8**). In addition, although not significant, micropatterned fibrin leaves had slightly higher average contractile strain than fibrin non-patterned control leaves. There were no significant differences in contractile strain in fibrin coated leaves compared to non-coated leaves. The data suggest micropattern-induced hiPS-CM alignment improves cardiac contractile function.

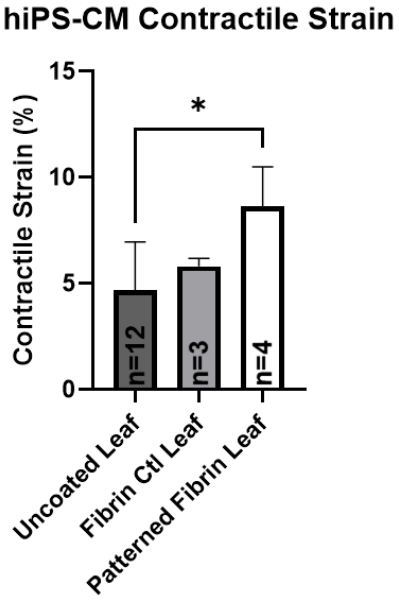

Figure 6-8: Average contractile strain of hiPS-CMs on micropatterned and non-patterned leaf substrates. Sample sizes n for each condition are illustrated within the data. hiPS-CMs on micropatterned leaves demonstrated significantly higher contractile strain ($p<0.05$) than on uncoated leaves.

6.3.4.2 hiPS-CM Micropatterned Leaves Demonstrate Coupled Contractile Function

Regional hiPS-CM beat frequency was measured in three ROI locations on fibrin micropatterned leaves (original ROI, in a parallel row, or within the same micropatterned row) (**Figure 6-9**). Examples of ROI locations in a single sample are displayed in **Figure 6-9A**. No significant differences were found in beat frequency between original and paired within row or parallel ROIs, suggesting that hiPS-CMs contractions are synchronous within and across patterns (n=7) (**Figure 6-9B**). In addition, average beats per minute values vary little across patterned leaf samples, demonstrating consistent beat frequency in the micropatterned leaf condition.

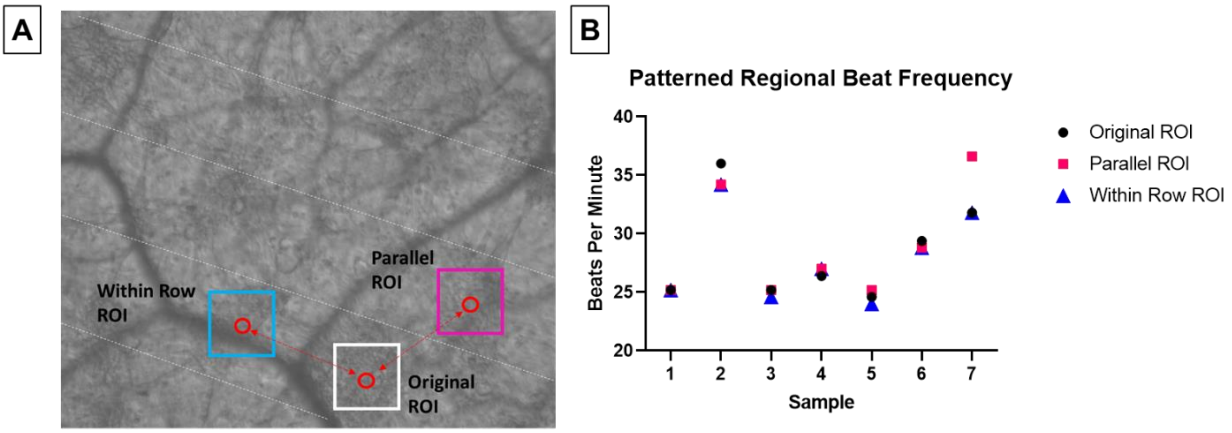

Figure 6-9: Beat frequency of micropatterned samples in three ROI locations. White lines represent micropatterned fibrin rows on leaves. (A) Highlighted squares represent selected ROIs in a sample. The distance between ROIs was calculated by determining the centroid location of the ROI, then calculating the distance between original and other ROI. (B) Beat frequency at original, parallel, and within row ROIs per sample are not significantly different within or between samples.

Synchronized contraction indicates that micropatterned hiPS-CMs are branched within and across a patterned sample. To further investigate this phenomenon, we calculated contraction velocities (in mm/sec) from the original ROI to parallel and within row ROIs (**Figure 6-10**). Three parallel ROIs and one within row ROI did not display synchronized contraction behavior to the original ROI; therefore, these samples were removed from contraction velocity analysis. hiPS-CM contraction velocities were similar from the original ROI to parallel and within row ROIs (**Figure 6-10A**). The average difference in time between synced initiation of contractions was 0.05 seconds from original ROI to both parallel and within row ROIs. However, more within row ROI samples (n=6) were synchronized with the original ROI, compared to parallel ROIs (n=4). Furthermore, average hiPS-CM contractile velocity of parallel ROIs was lower (3.1 ± 2.2 mm/sec) than within row ROIs (8.8 ± 10.7 mm/sec) (**Figure 6-10B**). But, there were no significant differences found between velocity of paired samples (p=0.3).

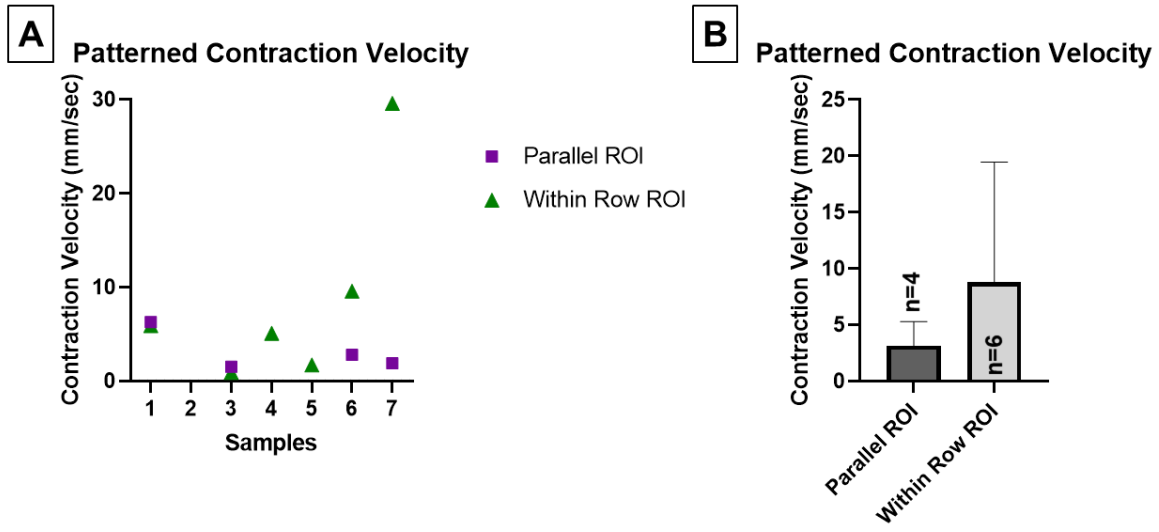

Figure 6-10: hiPS-CM contraction velocity across micropatterned leaves from original ROI to parallel or within the same row ROI. Sample sizes n for each condition are illustrated within the data. (A) Contraction velocity (mm/sec) from the original ROI to parallel or within row ROIs across all samples were not significantly different per sample. ROIs in samples 2, 4 and 5 were removed because ROIs were not synchronized. (B) Average contraction velocity from original ROI to parallel ROI and within row ROI.

6.3.4.3 hiPS-CMs Adhere and Align on 100 µm Micropatterned Leaves

hiPS-CMs on patterned leaves adhere to fibrin microchannels on leaves, non-patterned fibrin-coated leaves, and non-coated leaves. On the non-patterned fibrin control leaves and uncoated leaves, hiPS-CM nuclei and cytoskeleton spread in all directions without any noticeable alignment (**Figure 6-11A**). On micropatterned leaves, cardiac cells appeared to adhere within the 100 µm rows of fibrin (**Figure 6-11B**). Micropatterned hiPS-CMs' cytoskeletons spread along the axis of the fibrin rows.

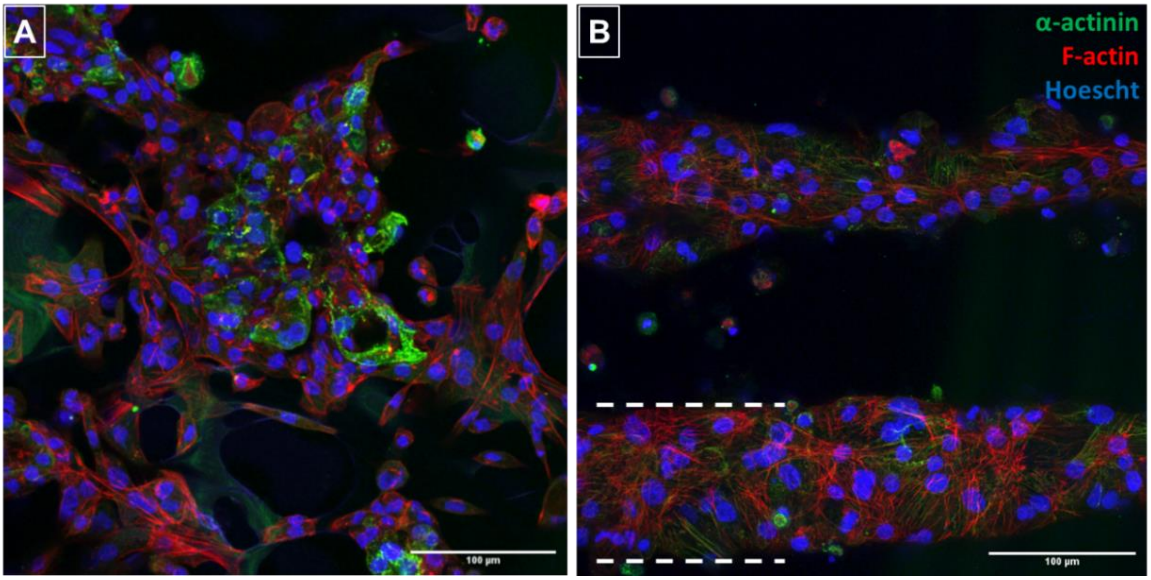

Figure 6-11: hiPS-CM cytoskeletal alignment on fibrin micropatterned and non-patterned leaf surface. Samples were stained for sarcomeric α-actinin (green), F-actin (red), and Hoescht 33342 (blue). (A) hiPS-CMs on non-patterned fibrin coated leaves spread randomly and display no cytoskeletal organization. (B) hiPS-CMs on micropatterned fibrin leaf are aligned in the orientation of the 100 µm rows (white dotted lines), visualized in the cytoskeleton organization. Scale bars 100 µm.

When hiPS-CM spacing between rows was measured with cell cytoskeleton FFT analysis, the average distance between hiPS-CM patterns was 80.3 ± 29.1 µm (N=3, n=9). This spacing value is like the fibrin measurements widths found in Section 6.3.2 and approaches the designed row width of 100 µm for fibrin micropatterning on the leaf.

6.3.4.4 hiPS-CM Nuclei and Cytoskeleton Align in the Direction of the Micropattern

hiPS-CM nuclear orientation analysis shows a significant decrease in nuclear angle in patterned leaves versus uncoated ($p<0.01$) and non-patterned fibrin control leaves ($p<0.05$), relative to the horizontal (and patterned) axis (**Figure 6-12**).

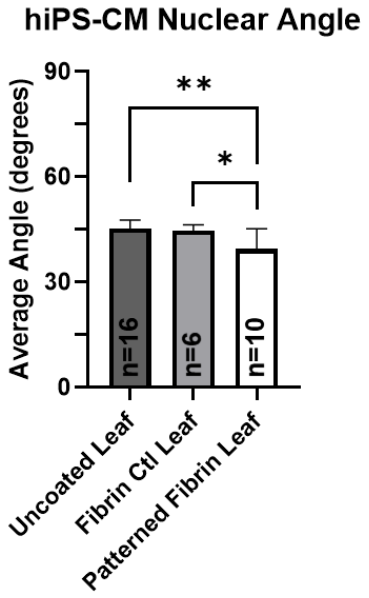

Figure 6-12: Nuclear angle of hiPS-CMs on fibrin micropatterned leaves. Sample sizes n for each condition are illustrated within the data. Average hiPS-CM nuclei angle on micropatterned leaves was significantly lower than nuclei angle on uncoated ($p<0.01$) and non-patterned fibrin leaves ($p<0.05$).

In addition, average hiPS-CM F-actin orientation angle relative to the horizontal axis was slightly lower on micropatterned leaves than non-patterned control leaves (not significant) **(Figure 6-13A)**. The cytoskeletal orientation distribution illustrates that hiPS-CM F-actin on micropatterned leaves have a skewed distribution of primary direction angles, with most sample angles aligned within 0 to 15 degrees of the horizontal axis, and all samples oriented less than 45 degrees from the pattern direction (**Figure 6-13B)**. Uncoated leaves also showed a skewed distribution in which a majority of samples have primary direction angle located at less than 15 degrees, with all samples oriented within 60 degrees. However, fibrin control leaves display most samples oriented from 30 to 45 degrees of the horizontal axis, and maximum up to 75 degrees.

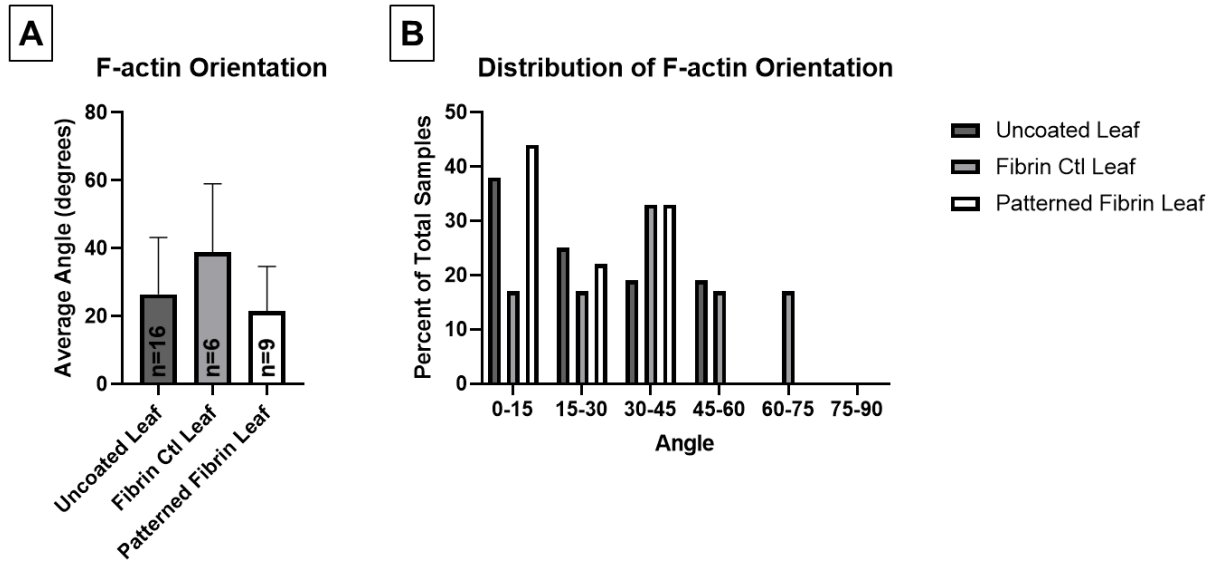

Figure 6-13: Cytoskeletal orientation of hiPS-CMs on micropatterned leaves. (A) Average nuclear angle relative to micropatterned direction. No significant differences were found between conditions, however patterned had the lowest average angle. Sample sizes n for each condition are illustrated within the data. (B) Distribution histogram of F-actin orientation by binned 15 degree angles. Micropatterned leaves demonstrate that a majority of samples are aligned within 15 degrees of the micropatterned axis.

6.4 **Discussion**

The objective of this aim was to improve cardiac cell contractile function on decellularized leaves by inducing cell alignment, which is observed in adult cardiac muscle. Aligned hiPS-CMs have demonstrated improved contractile performance versus non-aligned hiPS-CMs.[5] In this aim, we demonstrated the capability to induce topographical cues on leaf scaffolds using fibrin hydrogel micropatterning, and successfully induced hMSC and hiPS-CM cell alignment on the leaf. In doing so, cardiac cell alignment improved contractile function across the patterned leaf region, closer to contraction function of *in vivo* cardiac behavior.

We constructed a micropattern stamp with photolithography techniques and demonstrated fibrin rows could be micropatterned on decellularized spinach leaves. Stamps of 100 µm depth and width can create fibrin patterns on leaves. When additional PDMS designs were measured, stamp cross section widths only approached the designed value in the 100 µm wide row design. In smaller width row designs (10, 15, 25, and 50 µm), PDMS mold cross sections illustrated triangular peak patterns instead of rectangular. In addition, we did not observe depth of 100 µm in these PDMS molds. Wafers with 100 µm deep rectangular row designs are limited by the

fabrication parameters. For instance, during wafer fabrication, the exposure was calculated by $T = \frac{D * 1.5}{23.4 * Y}$, where T is the exposure time (seconds), D is the dosage (millijoules/cm^2), Y is the lamp power, and the additional constants account for the UV light wattage and the glass film on the mask in contact with the wafer. In manufacturing our photoresist wafer, the calculated exposure did not appropriately create all designed row widths and depth. In designs containing parallel rectangular rows separated by narrow distances, as in our stamp design, UV light can spill out of the mask windows during exposure and affect the depth and shape of the wafer pattern. Therefore, the PDMS mold is altered. In addition, low resolution during wafer manufacturing may form sharp edges within the wafer rows, resulting in low PDMS feature height and width. To increase the precision of the design, future iterations of the wafer should modify exposure time and energy to form wider and deeper channels. The manufacturing process described in Section 6.2.2 used a relatively long exposure with low energy (Appendix J). Future iterations of the design could increase the exposure energy but shorten time. Based on the data acquired (Section 6.3.1), there does not appear to be a linear relationship between width of rows constructed on mask, PDMS stamps, and resulting fibrin row width. A more systematic analysis may produce a well-defined relationship allowing for more accurate production of fibrin rows on decellularized leaves. Future work should refine the lithography manufacturing protocols to allow for deep row design with small widths to determine if smaller widths improve upon our results, since hiPS-CMs cultured on fibrin hydrogels with small width micropatterned channels have demonstrated higher maximum contractile strains compared to larger widths.[7]

Using 100 μm width and depth PDMS stamps, we successfully patterned fibrin on the leaves with 100 μm spacing. Previous work has demonstrated that PDMS molds with less than 20 μm depth are adequate for forming micropatterned hydrogels to induce myoblast or cardiac cell alignment[7,24]; however, when these patterns were utilized as stamps on leaves, they did not provide sufficient topography to align hMSCs (data not shown). Hence, we redesigned the stamp depth to 100 μm to induce more defined topographical rows. When fibrin micropatterned leaves were cross-sectioned and measured, the average row valley and peak widths were similar to PDMS cross-section measurements. However, the depth of fibrin of the leaf (22.4 ± 9.9 μm) was much smaller than that observed in the PDMS mold (113.7 ± 2.0 μm). This indicates we may need larger initial volumes of fibrin for patterning to create depths of 100 μm. In addition, the

leaf is a soft substrate when compressed and does not respond as plastic when applied. Based on initial geometry calculations, 30 µL was used to fill the row spaces within the stamp, but larger volumes may be required to achieve 100 µm depths and overcome any leaking of fibrin through the leaf. This also may indicate that lightly tapping the stamp on the leaf displaces fibrin through the leaf. In cross sections of fibrin patterned leaves, fibrin was occasionally observed, through eosin staining, within the leaf scaffold itself. Cellulose polymer, the main component of leaves, is hydrophilic[25]; however, fibrin is a hydrophobic material.[26] Decellularization of biological tissues has previously been observed to induce large pores in collagen matrix and increase water absorption.[27] This may also occur within the decellularized spinach leaf tissue, increasing pore size and allowing fibrin to polymerize within the leaf tissue. For future studies, it would be interesting to explore how to reduce fibrin displacement through the leaf scaffold. Future work could explore decellularized spinach leaf surface properties and how fibrin adheres and polymerizes on the leaf surface.

Micropatterned fibrin on decellularized leaves resulted in hiPS-CM adhesion approximately spaced as the designed row width. Cardiac cell adherence on leaves, informed by measured cell cytoskeletal patterns, corresponds to the fibrin micropatterned widths measured in additional micropatterned leaf cross sections. Our previous work demonstrated that hiPS-CMs do not require a protein coating to adhere to decellularized leaves. The data here suggests that cells may preferentially adhere to fibrin rather than uncoated regions of the leaf.

When hMSCs were seeded on fibrin micropatterned and control coverslips, hMSC nuclei aligned along the patterned axes similar to leaf conditions. However, hiPS-CM seeding on fibrin patterned coverslips led to cells dislodging off the coverslips after two days. This phenomenon has been previously observed after cardiac cells were seeded on laminin patterns on polystyrene and glass.[28] We believe that this was due to the contractile forces of the hiPS-CMs acting on the fibrin gel when adherent to the gelatin coated coverslips. Whereas the leaf scaffold is compliant, the glass coated coverslips are extremely stiff, and therefore the cells may have pulled (via contraction) the hydrogel substrate off the coverslip. In addition to matching the compliance of normal cardiac myocardium, the compliance of the leaf scaffold may be advantageous in growing contractile cells.

hiPS-CMs on fibrin micropatterned decellularized spinach leaves demonstrated improved contractile functional behavior compared to non-patterned samples after seven days. Specifically, hiPS-CM contractile strain on micropatterned leaves (8.7%) was significantly higher than non-coated leaves (4.7%; $p<0.05$); however, it was not yet equivalent to human adult myocardial strain *in vivo* (15.9-22.1%). Further culture time of hiPS-CMs on micropatterned leaves may improve contractile strain. This has previously been demonstrated when hiPS-CMs are cultured on aligned fibrin microthread substrates.[12]

Furthermore, hiPS-CMs on fibrin micropatterned leaves demonstrated synchronized beat frequency and rapid contraction velocity within and across micropatterned rows. Contraction velocity was calculated from the frame at which contraction initiated. We determined that three separate parallel ROIs and one within row ROI of the total samples were not synchronized based on an initiation time delay compared to the original ROI. Therefore, we removed those samples from analysis in order to detect contraction velocity of the synchronized ROIs. In addition, we observed slightly faster average contraction velocity within row ROIs (8.8 ± 10.7 mm/sec) compared to parallel ROIs (3.1 ± 2.2 mm/sec) (not significant). This anisotropy correlates with measured *in vivo* longitudinal and transverse conduction velocities, where conduction velocity is defined as the speed of action potential propagation across cardiomyocytes.[29] It has been determined that *in vivo* healthy adult human ventricular tissue longitudinal conduction velocity (65 cm/sec) is faster than transverse conduction velocity (51 cm/sec) *in vivo*.[30] Compared to 3D engineered tissues, hiPS-CM cultured cardiac patches have demonstrated conduction velocities up to 41 cm/sec *in vitro*[31], approaching the range of mature human cardiac tissue. Whereas, two-dimensional monolayers of immature hiPS-CMs have achieved conduction velocities of approximately 25 cm/sec.[32] Our measured contraction velocity of a monolayer of hiPS-CMs on micropatterned leaves was over an order of magnitude slower. In future studies, we would aim to increase contraction velocity through increased incubation time, increased cell density, and observed electromechanical coupling of cells especially through gap junctions.

Although measured contraction velocities of hiPS-CMs on micropatterned leaves are orders of magnitude less than reported conduction velocity of mature human tissue, we did observe what appeared to be anisotropic synchronized contraction of hiPS-CMs on micropatterned leaves. Micropatterning hiPS-CMs presents the opportunity to form anisotropic electromechanical

networks across the leaf, which was not observed in hiPS-CMs on non-patterned control leaf scaffolds. Micropatterning leaves appeared to increase lengthwise orientation of hiPS-CMs, which can result in cell anisotropy and end-to-end gap junction coupling.

hMSC and hiPS-CM nuclear orientation on micropatterned fibrin leaves demonstrated significant alignment in the direction of the topographical protein pattern. hMSC nuclei and cytoskeleton aligned along micropatterned rows and confirmed that hMSCs align along topographical cues in culture, as previously published.[33] Micropatterned hMSC nuclei on leaves demonstrate alignment in the direction of the fibrin rows compared to non-patterned control leaves (**Figure 6-6**). Micropatterned hiPS-CM nuclei also demonstrated alignment (**Figure 6-11**), although not as aligned as that of hMSCs. In healthy myocardium, adult cardiomyocytes are aligned within 13° of one another[34] and cells exhibit high degree of anisotropy in ventricular tissue (**Figure 2-1**). hiPS-CMs lack many attributes of adult cardiomyocytes, such as morphology, and are immature in behavior.[29] hiPS-CMs in 2D culture lack the rod structure of adult cardiomyocytes and cluster together without structural guidance.[29] Topographical cue guidance assists alignment of hiPS-CMs, and a cardiac tissue patch should aim to achieve under 20 degrees of cell alignment to mimic *in vivo* fiber arrangement. As this aim found improved hMSC and hiPS-CM nuclear alignment with micropatterned leaves compared to non-patterned controls, additional time in micropatterned culture may allow for hiPS-CM to re-organize its cytoskeletal structure, as previously seen in longer culture[5,7], to better align with the fibrin micropatterned rows. The cytoskeletal structure of micropatterned hiPS-CMs demonstrated improved alignment compared to non-patterned leaves, although this was not significant. In addition, the majority of micropatterned hiPS-CMs' F-actin primary orientation angles occur within 0 to 15 degrees of the fibrin micropatterned rows. These data suggest fibrin micropatterning of decellularized leaves provide structural cues for alignment of hiPS-CMs.

Overall, aligning hiPS-CMs on micropatterned leaves improved cell contractile function after seven days compared to controls. We also observed synchronized hiPS-CM contraction between different regions on micropatterned leaves. These results indicate that patterned hiPS-CMs are connected through an aligned and branching row network, verified in part by IF imaging (**Figure 6-14**).

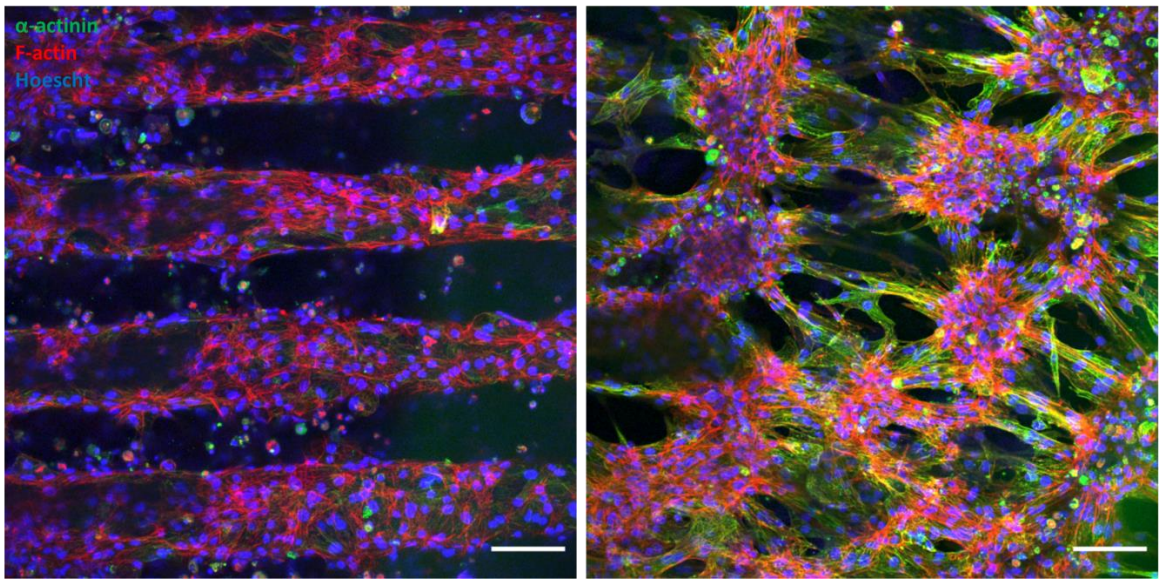

Figure 6-14: hiPS-CMs on micropatterned leaves are aligned and branching within and across rows. hiPS-CMs on micropatterned leaf samples were stained for sarcomeric α-actinin (green), F-actin (red), and Hoescht 33342 (blue). Scale bar 100 μm.

Additional future studies should investigate the presence of connexin-43 in micropatterned hiPS-CMs by immunofluorescence labeling. Connexin-43 is a gap junction protein that demonstrates intercellular communication between adjacent cells[35–37] and is observed in mature CMs (**Figure 2-1**). Gap junctions are present at the end-to-end connections between mature CMs for directional ion flow between cells. If connexin-43 is present between micropatterned hiPS-CMs on leaves, this suggests that hiPS-CMs contain intercellular junctions and efficient for ion transfer may occur between cells. Aligned and synchronized contractile hiPS-CMs represent *in vivo* cardiac muscle physiology and this behavior is promising for cardiac patch scale-up. With additional culture time, we may observe further improvement of hiPS-CM orientation and contractile function along the micropatterned axis of decellularized spinach leaves.

6.5 References

1. Yang X, Pabon L, Murry CE. Engineering Adolescence: Maturation of Human Pluripotent Stem Cell-derived Cardiomyocytes. Circ Res. 2014;114(3):511-523. doi:10.1161/CIRCRESAHA.114.300558.Engineering
2. Alom Ruiz S, Chen CS. Microcontact printing: A tool to pattern. Soft Matter. 2007;3(2):168-177. doi:10.1039/b613349e
3. McCain ML, Desplantez T, Geisse NA, et al. Cell-to-cell coupling in engineered pairs of rat ventricular cardiomyocytes: relation between Cx43 immunofluorescence and intercellular

electrical conductance. AJP Hear Circ Physiol. 2012;302(2):H443-H450. doi:10.1152/ajpheart.01218.2010
4. McDevitt TC, Angello JC, Whitney ML, et al. In vitro generation of differentiated cardiac myofibers on micropatterned laminin surfaces. J Biomed Mater Res. 2002;60(3):472-479. doi:10.1002/jbm.1292
5. Ribeiro AJS, Ang Y-S, Fu J-D, et al. Contractility of single cardiomyocytes differentiated from pluripotent stem cells depends on physiological shape and substrate stiffness. Proc Natl Acad Sci. 2015;112(41):12705-12710. doi:10.1073/pnas.1508073112
6. Chrobak MO, Hansen KJ, Gershlak JR, et al. Design of a Fibrin Microthread-Based Composite Layer for Use in a Cardiac Patch. ACS Biomater Sci Eng. 2017;3(7):1394-1403. doi:10.1021/acsbiomaterials.6b00547
7. English EJ. Micropatterned Fibrin Hydrogels for Increased Cardiomyocyte Alignment. Published online 2019. doi:10.1017/CBO9781107415324.004
8. Wendel JS, Ye L, Tao R, et al. Functional Effects of a Tissue-Engineered Cardiac Patch From Human Induced Pluripotent Stem Cell-Derived Cardiomyocytes in a Rat Infarct Model. Stem Cells Transl Med. 2015;4(11):1324-1332. doi:10.5966/sctm.2015-0044
9. Zhang D, Shadrin I, Lam J, Xian H-Q, Snodgrass R, Bursac N. Tissue-engineered Cardiac Patch for Advanced Functional Maturation of Human ESC-derived Cardiomyocytes. Biomaterials. 2013;34(23):5813-5820. doi:10.1109/TMI.2012.2196707.Separate
10. Liau B, Christoforou N, Leong K, Bursac N. Pluripotent Stem Cell-derived Cardiac Tissue Patch with Advanced Structure and Function. Biomaterials. 2011;32(35):9180–9187. doi:10.1016/j.biomaterials.2011.08.050
11. Ahmed TAE, Dare E V., Hincke M. Fibrin: A Versatile Scaffold for Tissue Engineering Applications. Tissue Eng Part B Rev. 2008;14(2):199-215. doi:10.1089/ten.teb.2007.0435
12. Hansen KJ, Laflamme MA, Gaudette GR. Development of a Contractile Cardiac Fiber From Pluripotent Stem Cell Derived Cardiomyocytes. Front Cardiovasc Med. 2018;5(52):1-11. doi:10.3389/fcvm.2018.00052
13. Taylor RJ, Moody WE, Umar F, et al. Myocardial strain measurement with feature-tracking cardiovascular magnetic resonance: normal values. Eur Hear J – Cardiovasc Imaging. 2015;16(8):871-881. doi:10.1093/ehjci/jev006
14. Coffin ST, Gaudette GR. Aprotinin extends mechanical integrity time of cell-seeded fibrin sutures. J Biomed Mater Res - Part A. 2016;104(9):2271-2279. doi:10.1002/jbm.a.35754
15. Bloom S, Lockard VG, Bloom M. Intermediate filament-mediated stretch-induced changes in chromatin: A hypothesis for growth initiation in cardiac myocytes. J Mol Cell Cardiol. 1996;28(10):2123-2127. doi:10.1006/jmcc.1996.0204
16. Bray M-A, Adams WJ, Geisse NA, Feinberg AW, Sheehy SP, Parker KK. Nuclear Morphology and Deformation in Engineered Cardiac Myocytes and Tissues. Biomaterials. 2010;31(19):5143-5150. doi:10.1016/j.physbeh.2017.03.040
17. Salick MR, Napiwocki BN, Sha J, et al. Micropattern Width Dependent Sarcomere Development in Human ESC-Derived Cardiomyocytes. Biomaterials. 2014;35(15):4454-4464. doi:10.1038/jid.2014.371
18. Carnes ME, Pins GD. Etching anisotropic surface topography onto fibrin microthread scaffolds for guiding myoblast alignment. J Biomed Mater Res - Part B Appl Biomater. 2020;108B(5):2308-2319. doi:10.1002/jbm.b.34566

19. Grasman JM, Pumphrey L, Dunphy M, Perez-Rogers J, Pins GD. Static Axial Stretching Enhances the Mechanical Properties and Cellular Responses of Fibrin Microthreads. Acta Biomater. 2014;10(10):4367-4376. doi:10.1038/jid.2014.371
20. Kelly DJ, Azeloglu EU, Kochupura P V., Sharma GS, Gaudette GR. Accuracy and reproducibility of a subpixel extended phase correlation method to determine micron level displacements in the heart. Med Eng Phys. 2007;29(1):154-162. doi:10.1016/j.medengphy.2006.01.001
21. Hansen KJ, Favreau JT, Gershlak JR, Laflamme MA, Albrecht DR, Gaudette GR. Optical Method to Quantify Mechanical Contraction and Calcium Transients of Human Pluripotent Stem Cell-Derived Cardiomyocytes. Tissue Eng Part C Methods. 2017;23(8):445-454. doi:10.1089/ten.tec.2017.0190
22. Robbins ER, Pins GD, Laflamme MA, Gaudette GR. Creation of a contractile biomaterial from a decellularized spinach leaf without ECM protein coating: An in vitro study. J Biomed Mater Res Part A. 2020;108(10):2123-2132. doi:10.1002/jbm.a.36971
23. Liu Z-Q. Scale space approach to directional analysis of images. Appl Opt. 1991;30(11):1369. doi:10.1364/ao.30.001369
24. Tanaka N, Moriguchi H, Sato A, et al. Microcasting with agarose gel via degassed polydimethylsiloxane molds for repellency-guided cell patterning. RSC Adv. 2016;6(60):54754-54762. doi:10.1039/c6ra11563b
25. Khazraji AC, Robert S. Interaction Effects between Cellulose and Water in Nanocrystalline and Amorphous Regions : A Novel Approach Using Molecular Modeling. J Nanomater. 2013;2013:1-10. doi:http://dx.doi.org/10.1155/2013/409676
26. van Oss CJ. Surface Properties of Fibrinogen and Fibrin. Vol 9.; 1990. Accessed June 30, 2021. papers3://publication/uuid/5B64080D-D6DC-4CEA-A21A-325957F72C2C
27. Zhang Y, Iwata T, Nam K, Kimura T, Wu P. Water absorption by decellularized dermis. Heliyon. 2018;(February):e00600. doi:10.1016/j.heliyon.2018.e00600
28. McDevitt TC, Woodhouse KA, Hauschka SD, Murry CE, Stayton PS. Spatially organized layers of cardiomyocytes on biodegradable polyurethane films for myocardial repair. J Biomed Mater Res - Part A. 2003;66(3):586-595. doi:10.1002/jbm.a.10504
29. Karbassi E, Fenix A, Marchiano S, et al. Cardiomyocyte maturation: advances in knowledge and implications for regenerative medicine. Nat Rev Cardiol. 2020;17(6):341-359. doi:10.1038/s41569-019-0331-x
30. Taggart P, Sutton PM, Opthof T, et al. Inhomogeneous transmural conduction during early ischaemia in patients with coronary artery disease. J Mol Cell Cardiol. 2000;32(4):621-630. doi:10.1006/jmcc.2000.1105
31. Querdel E, Reinsch M, Castro L, et al. Human Engineered Heart Tissue Patches Remuscularize the Injured Heart in a Dose-Dependent Manner. Circulation. 2021;143(20):1991-2006. doi:10.1161/CIRCULATIONAHA.120.047904
32. Herron TJ, Da Rocha AM, Campbell KF, et al. Extracellular matrix-mediated maturation of human pluripotent stem cell-derived cardiac monolayer structure and electrophysiological function. Circ Arrhythmia Electrophysiol. 2016;9(4):1-12. doi:10.1161/CIRCEP.113.003638
33. Tijore A, Irvine SA, Sarig U, Mhaisalkar P, Baisane V, Venkatraman S. Contact guidance for cardiac tissue engineering using 3D bioprinted gelatin patterned hydrogel. Biofabrication. 2018;10(2). doi:10.1088/1758-5090/aaa15d

34. Wei-Ning Lee, Pernot M, Couade M, et al. Mapping Myocardial Fiber Orientation Using Echocardiography-Based Shear Wave Imaging. IEEE Trans Med Imaging. 2012;31(3):554-562. doi:10.1109/TMI.2011.2172690
35. Severs NJ. Gap junction remodeling in heart failure. J Card Fail. 2002;8(6):S293-S299. doi:10.1054/jcaf.2002.129255
36. Goodenough DA, Paul DL. Gap junctions. Cold Spring Harb Perspect Biol. 2009;1(a002576):1-19. doi:10.1101/cshperspect.a002576
37. Lundy SD, Zhu W-Z, Regnier M, Laflamme MA. Structural and Functional Maturation of Cardiomyocytes Derived from Human Pluripotent Stem Cells. Stem Cells Dev. 2013;22(14):1991-2002. doi:10.1089/scd.2012.0490

7. Conclusions and Future Work

7.1 Conclusions

Cardiovascular disease is the leading cause of death worldwide. Patients who suffer from a MI can develop heart failure and rapid decline of heart functional health. Few treatments exist to prevent health decline after MI, and the available immediate treatment options do not restore cardiac tissue function. A tissue engineered cardiac patch composed of an engineered scaffold and cardiomyocytes could be a solution to prevent functional decline. This dissertation examined the use of a decellularized spinach leaf scaffold with hiPS-CMs to create a functional tissue engineered patch for cardiac tissue after MI. The research was completed in three aims. The first aim characterized the leaf's ability to utilize its inherent vasculature to perfuse cardiac cells on its surface. The second aim characterized cardiac cell function on the leaf with different substrate conditions. The third aim developed topographical cues on the leaf to mimic cardiac tissue anatomy and improve functional cell behavior.

7.1.1 Specific Aim 1

Utilization of a scaffold that contains a mature vascular system is one of the major design challenges in tissue engineering, but necessary for thick engineered tissues. We demonstrated that decellularized spinach leaf vasculature is perfusable and capable of supplying cells with compounds on the leaf surface. Following leaf vascular perfusion of 50 μM epinephrine in hiPS-CM media, seeded hiPS-CMs' function on the leaf surface was affected. Epinephrine perfusion demonstrated increased hiPS-CM beat frequency on the leaf surface comparable to that of static drug incubation on TCP. However, we did not observe any significant changes in contractile strain after perfusion or in static culture upon epinephrine addition. In addition, trypan blue perfusion demonstrated dye dispersion throughout the vasculature, leaf tissue, and in non-viable cells on the leaf surface. We conclude that the decellularized spinach leaf is a vascularized, perfusable scaffold capable of being utilized to impact seeded cell behavior.

7.1.2 Specific Aim 2

ECM proteins found in cardiac basement membrane such as fibronectin and collagen IV are commonly used in tissue engineering to promote cell adhesion. We had previously coated fibronectin on decellularized spinach leaves for cell adhesion but had not determined if ECM use was necessary for cell function. In Specific Aim 2, we demonstrated that coating decellularized

spinach leaves with ECM proteins is not necessary to demonstrate equivalent hiPS-CM function to non-coated leaves. We determined hiPS-CMs can adhere to and contract on a decellularized spinach leaf without ECM protein coatings. In fact, there were no significant difference between ECM coated and non-coated leaf surfaces in contractile strain after 21 days in culture. Furthermore, hiPS-CM sarcomere length and cell elongation also showed no meaningful differences between coating or culture time.

7.1.3 Specific Aim 3A

To mimic cardiac tissue behavior, we aimed to align cells on decellularized spinach leaves using cell seeded fibrin microthreads in Specific Aim 3A. We observed that hMSCs successfully migrated and adhered to leaves from fibrin microthreads in fibrinolytic culture conditions. During culture, hMSCs proliferated and aligned around the fibrin microthread on leaves. However, when this method was implemented with hiPS-CMs, we did not observe hiPS-CM adhesion or alignment on leaves. This was hypothesized to be due to the non-proliferative nature of the cardiac cells. Although microthread induced alignment on leaves was unsuccessful with hiPS-CMs, we demonstrated that microthread topographical cues can induce hMSC alignment on the leaf surface.

7.1.4 Specific Aim 3B

In Specific Aim 3B, we aimed to induce cell alignment on decellularized spinach leaves by micropatterned topographical cues on the leaf surface. We successfully designed and micropatterned 100 μm wide fibrin hydrogel rows on spinach leaves. Both seeded hMSCs and hiPS-CMs on micropatterned leaves demonstrated aligned behavior, shown by nuclear and cytoskeletal orientation in the direction of the micropatterned rows. Furthermore, micropatterned hiPS-CMs on leaves demonstrated significantly increased maximum contractile strain compared to controls and synchronized beat frequency within the patterned rows. Overall, micropatterning spinach leaves is a promising technique to enhance hiPS-CM function on the leaf, and therefore cardiac patch function.

7.2 **Future Work**

The data presented in this dissertation demonstrates that the decellularized spinach leaf has the potential for use as a vascularized scaffold for a tissue engineered cardiac patch. Furthermore, we

demonstrated we can modify leaf surface properties to improve adherent hiPS-CM performance and better represent *in vivo* cardiac tissue. In addition to the experiments presented in this research, there are several opportunities for future research that could be explored to further develop this technology.

7.2.1 Specific Aim 1

First, since spinach leaves are obtained at the grocery store, the leaves are inherently variable based on the store, distributor, and where the spinach was grown. In addition, there are three different types of spinach based on leaf texture: savoy (crinkled), semi-savoy and smooth. These types likely affect leaf size and shape, vasculature, surface topography, and material properties, which could influence leaf decellularization, sterilization, perfusion, and cell adhesion outcomes. This research used smooth textured leaves but studying decellularization of different strains of spinach has not yet been pursued. If spinach leaves are to be used as a scaffold for medical application, future work should grow spinach in a controlled environment to ensure consistent production. This would also allow control over what leaf strain is used for scaffold manufacturing and quality control. Consistent leaf quality would also allow us to adjust decellularization and sterilization methods to ensure good cell adhesion and function, allowing us to pinpoint other sources of variability within the process.

In Specific Aim 1, we demonstrated that perfusion of 50 µM epinephrine media travels through the leaf vasculature and increases hiPS-CM contractile beat frequency when seeded on the leaf surface. Our results demonstrated that hiPS-CMs' beat frequency significantly increased after epinephrine addition to cells, but contractile strain did not. This is contrary to previous results in which hiPS-CMs exposed to 50 µM epinephrine were found to improve contractile index to 200% of pre drug conditions.[1] One limitation in this aim is that data were collected at room temperature. Cardiac cells are temperature sensitive, and cold stress has been linked to cardiomyocyte increased oxidative stress, autophagy, and apoptosis.[2] Furthermore, room temperature conditions affect action potential duration in cardiac cells and pacing kinetics.[3] Room temperature conditions are potentially one explanation for why we did not observe increased contractile strain with epinephrine addition. For future studies, we suggest modifying the current microscopy set-up to execute leaf perfusion and function analysis within an attached incubated chamber or on a temperature-controlled heating stage to combat hiPS-CM temperature

sensitivity. In this environment, there may be an increased response to contractile strain and beat frequency compared to room temperature conditions. In addition, future work should explore epinephrine washout methods for hiPS-CM seeded leaves to return normal contractile behavior. Following leaf perfusion washout in this aim, we did not observe a reduction in hiPS-CMs' contractile beat frequency or strain. This may be due to the perfusion time employed, and if so, longer time periods may be necessary. These experiments should also be adjusted to 37°C to reduce adverse effects on hiPS-CMs.

Vascular hydraulics have been well characterized in living plants[4,5], however transport in decellularized leaf vasculature is not. In Specific Aim 1, we demonstrated that fluid flow through the vasculature can affect cells on the leaf surface. Despite this, we do not have a complete understanding of how fluid travels from the perfused decellularized spinach leaf vasculature through the leaf tissue and to the leaf surface, nor the permeability characteristics of the vasculature. Future work could explore and characterize decellularized leaf vasculature further by developing computational fluid flow models of its vasculature. Specifically, fluid flow models of vasculature permeability and fluid dispersion through the decellularized leaf tissue would allow for better understanding how decellularized leaf vasculature transports small molecules through fluid to cells on its surface. Permeability experimental model data could utilize microbead solutions and track their diffusion throughout the leaf over time. Also, pulsatile flow conditions could be applied to the computational fluid model to demonstrate the effect of flow pattern after leaf anastomosis to an artery.

7.2.2 Specific Aim 2

We demonstrated in Specific Aim 2 that coating decellularized leaf scaffolds with ECM proteins was not necessary for hiPS-CM adhesion and function. We hypothesized that cell surface glycocalyx[6] may positively interact with the non-coated leaves' cellulose structure, not requiring ECM to be present on the leaf surface. However, we did not explore cell binding to the leaf. Cardiomyocytes bind to ECM proteins with cell integrin receptors and form focal adhesions to the matrix[7,8], which in turn can influence cardiomyocyte behavior and maturation.[9] Future work should explore hiPS-CM adhesion to decellularized leaves, both ECM coated and non-coated, by examining cell integrin and adhesion markers. Specifically, staining for intracellular markers such as talin, vinculin, and kindlin would provide information about cardiac

mechanotransduction function[10] on the leaf. Information about hiPS-CM expression on leaves would help us understand how hiPS-CMs adhere to different leaf surfaces in addition to cell function.

7.2.3 Specific Aim 3A

In Specific Aim 3A, we utilized fibrin microthreads to induce hMSC alignment on decellularized spinach leaves by cell transfer. Based on the results, we believe that hMSCs aligned on leaves due to cell proliferation after adhesion. Therefore, with hiPS-CMs, this technique was not successful as hiPS-CMs do not proliferate on leaves. To improve this technology for cardiac cell alignment, future work could increase cell seeding efficiency by direct seeding onto the leaf with fibrin microthreads. Direct seeding would allow cells to adhere to the leaf and thread simultaneously, instead of stepwise. Second, adhering threads to the leaf using fibrin glue may assist cell topographical guidance for longer time periods prior to thread fibrinolysis. Fibrin glue is a biologic adhesive commonly used in surgical cases to promote wound healing.[11] This would allow for controlled fibrin microthread placement to create multiple rows of aligned cells on the leaf. These techniques would rely less on the transfer of cells to the leaf, and instead, use fibrin microthreads to guide cell alignment.

7.2.4 Specific Aim 3B

In Specific Aim 3B, we demonstrated that fibrin micropatterned rows align and improve hiPS-CM behavior on decellularized spinach leaves. Although wafer photolithography techniques demonstrated an effective method of creating fibrin hydrogel micropatterns on the leaf, we did recognize several challenges and limitations using PDMS stamps on leaves in which future work could improve upon. First, when stamping the pattern on the leaves, fibrin hydrogel can leach through the leaf scaffold, observed with sectioned micropatterned leaf eosin staining. This is likely due to the porosity of decellularized leaf material. Micropatterning is typically conducted on plastic or glass, where proteins or gels do not permeate through the substrate. At the same time, there is inherent variability when manually tapping the stamp onto the leaf. The microcontact patterning process relies on the pressure applied onto the PDMS stamp to deposit the pattern. Since leaves are pliable, contact pressure plays a large role in how the pattern deposits onto the leaf. In addition, pressure can alter the geometry of the PDMS channels and induce stamp deformation if high loads are applied. Future work could investigate methods to

control and automate stamping to deliver an appropriate contact load to the leaf, while at the same time reducing fibrin leaching through the leaf scaffold. Stamping is a scalable approach based on pattern size, but stamp pressure and application need to be consistent.

An alternative to stamp micropatterning is vacuum assisted patterning. Previous work investigating vacuum assisted patterning has been demonstrated with agarose and cell seeding.[12] This technique avoids contact load, and initial studies in our lab using vacuum patterned fibrin hydrogel on leaves showed promise in non-sterile conditions. Future development of this technology could be implemented for leaves by developing a sterile vacuum system to consistently deliver fibrin hydrogel and cells across the stamp on leaves. Furthermore, scale-up of this technology should be considered for patterned cells on leaves. In this, either the stamp patterning or vacuum patterning technique would need to be modified and qualified for large surface areas across the leaf surface.

An additional challenge we observed during micropatterning was fibrin adhesion to the PDMS stamp during fibrin polymerization. This resulted in fibrin dislodging from the substrate when the stamp was removed. Further investigation into PDMS coating or fibrin polymerization time to avoid fibrin adhesion to the stamp should be considered. An alternative method could consider enhancing leaf adhesion by coating the leaf with an additional thin film of fibrin or matrix prior to micropatterning. This technique may also reduce the number of lost hiPS-CMs on micropatterned coverslips. Dislodged patterned gels on coverslips has previously been observed in other cardiomyocyte micropatterned studies; however, with the addition of elastomer films to coverslips, CMs remained adherent.[13] Moving forward, coating coverslips with additional films may allow for better micropatterned cell adhesion.

To better understand cell response to leaf substrate and topography, future work could also explore the gene expression shift between patterned and non-patterned samples on decellularized spinach leaves. Cell alignment has been associated with maturation and, as mentioned in Section 7.2.2, cardiomyocyte binding to a substrate can influence cell maturity.[9] Specifically, future work related to this aim should also investigate changes in focal adhesion kinase (FAK), cardiac myosin light chain, and cardiac troponin I gene expression in micropatterned versus non-patterned hiPS-CMs using reverse transcription-polymerase chain reaction (RT-PCR). FAK expression has been demonstrated to be essential for maturation of human cardiac cells[14], and

enhanced expression of cardiac myosin light chain and cardiac troponin I are related to cardiac maturation.[15] Expression of genes related to sarcomere structure, calcium handling, filament proteins, and integrins would allow us a more comprehensive understanding of the effects of hiPS-CM alignment on function and maturity on the micropatterned leaf substrate.

Cardiomyocytes are one of several cell populations in the heart that includes fibroblasts, endothelial cells and vascular smooth muscle cells. While myocytes occupy the majority of the volume of the heart[16], non-myocyte cells comprise about 70% of the total heart cell population, and a majority of these are cardiac fibroblasts.[17] In the myocardium, cardiac fibroblasts secrete components of the extracellular matrix (ECM) and transmit mechanical force by the receptor-mediated connections to the ECM.[18] As fibroblasts compose a substantial percentage of cells in the heart with cardiomyocytes and act as support cells for mechanotransduction, inclusion of fibroblasts in a cardiac patch may improve patch function. Cardiac fibroblasts have been successfully cultured with stem cell derived CMs to improve function and maturation of engineered tissues.[19–21] However, culturing the appropriate ratio of fibroblasts to cardiomyocytes is important as to not impede contractility, as previously determined.[22] Future study developing a micropatterned decellularized leaf cardiac patch should explore the use of co-culturing cardiac fibroblasts with hiPS-CMs to induce increased cell anisotropy and contractile performance.

Electrical propagation across the cardiac tissue patch is essential to mimic *in vivo* cardiac function. Future work should also investigate hiPS-CM electrophysiology on micropatterned leaves. First, micropatterned hiPS-CMs should be studied for the presence of connexin-43 by immunofluorescence labeling. Connexin-43 is a widely studied gap junction protein that demonstrates intercellular communication and ion transfer between adjacent cells, and is observed in mature CMs (**Figure 2-1**).[23–25] In Specific Aim 2, we did not observe connexin-43 within hiPS-CMs on leaves, likely due to hiPS-CMs' immature phenotype. If connexin-43 is present between micropatterned hiPS-CMs on leaves, it suggests that hiPS-CMs on a leaf patch may be able to electrically integrate with cardiac tissue. In Specific Aim 3B, we observed that micropatterned hiPS-CMs were elongated along rows and synchronized during contraction, displaying a more mature phenotype than non-patterned cells. From this information, we believe that connexin-43 could be present in micropatterned hiPS-CMs on leaves.

Finally, future work could explore alternative methods to micropatterning leaves and avoid the use of fibrin. Although fibrin is a widely-used biocompatible material[25], additional biologic materials increase the manufacturing complexity of a cardiac patch, as discussed in Specific Aim 2. Alternative methods to induce alignment could include crimping[26] or etching[27] patterns onto the leaf itself, or laser cutting microchannels in the leaf scaffold for cardiac cell seeding. If topographical cues can be etched onto the leaf itself, this may be preferable for clinical regulation to decrease cardiac patch complexity.

7.3 **Discussion**

Decellularized spinach leaf scaffolds present an opportunity to utilize a scaffold with inherent vasculature for use with hiPS-CMs as a cardiac patch. In this work, we demonstrated that the decellularized spinach leaf is perfusable and its perfusate can affect hiPS-CM function on the leaf surface. Second, hiPS-CMs adhere and function on the leaf surface without ECM protein coatings; and finally, micropatterning the leaf surface initiates hiPS-CM anisotropy.

7.3.1 Regulatory Guidance

Although the decellularized spinach leaf scaffold is a long way from consideration for FDA approval submission, regulatory guidance should be considered while developing the scaffold. Several FDA approved tissue engineered solutions exist on the market for skin or wound[29–31] applications and orthopedic[32] implantation. Specifically, decellularized tissue scaffolds have received FDA approval for use in humans, including dermis tissue (Alloderm®; Allergan™), porcine heart valves (Synergraft®; Cryolife) and porcine urinary bladder (MatriStem UBM™; Acell®).[33] The FDA's guidance documents related to Human Cells, Tissues, and Cellular and Tissue-Based Products (HCT/Ps) are located under Title 21 of the Code of Federal Regulations (CFR) Part 1271. These guidance documents require tissue donor screening, industry tissue processing, and the requirement for the tissue to undergo minimal manipulation that does not alter its original characteristics for utility for reconstruction, repair, or replacement.[34]

Decellularization of mammalian tissue can be performed with a variety of techniques including chemical or enzymatic, mechanical, or a combination of both.[35] For example, sodium dodecyl sulfate (SDS), an ionic detergent, is commonly used for tissue decellularization since it can remove cellular content while maintaining ECM components.[33,36–38] Spinach leaves were

decellularized with low concentrations of SDS and Triton X-100, a non-ionic detergent. This technique maintains the structural properties of the leaf, while removing the plant cell material from the scaffold.[39] Although tissues are decellularized with chemicals to remove native cells, the leaf tissue structure is preserved and decellularization does not alter the characteristics of the leaf scaffold as laid out by the FDA guidelines. Our research demonstrated that human cells adhere to the decellularized leaf scaffold, indicating the leaf surface is habitable for cells; however, we have not yet tested for the presence of residual detergents remaining in the leaf after multiple rinsing steps. As a future course of action, this should be pursued. Although, from this body of research and prior successful *in vivo* biocompatibility studies, we believe that the decellularized spinach leaf should pose no harm to patients if implanted.

7.3.2 Cardiac Patch Design Specifications

7.3.2.1 Cardiac Patch Size and Cell Population

In Chapter 2, we presented design characteristics for our cardiac tissue patch including patch size, cell seeding density, and functional outcomes *in vitro* and *in vivo*. Estimates of infarct size indicate that a patch needs to repopulate a minimum surface area of 1 cm^2. Most of the studies here used a 1 cm diameter cloning well (0.78 cm^2 seeding area) which closely matched the minimal surface area design requirement. However, the entire leaf scaffold was significantly larger. With larger seeding wells and cell number, the 1 cm^2 area can easily be met through this seeding method.

Cell population on a cardiac patch should contain 10% of the total heart cell population to refunctionalize cardiac tissue. However, small animal model cardiac patch implantations have demonstrated muscle engraftment[40] and improved LV function[41] with fewer CMs per cm^2 than this standard. In Specific Aim 3B, micropatterned decellularized spinach leaves were seeded 150,000 hiPS-CMs per cm^2 patterned region. The seeded number of hiPS-CMs in this study was substantially lower than our design parameters; however, we aimed to demonstrate that monolayers of hiPS-CMs align on micropatterned leaves. In addition, we limited hiPS-CM seeding number since cloning cylinders were deemed necessary to remain on leaves during culture. The 10 mm cloning cylinders only allowed for a maximum culture media volume of approximately 400 µL and increasing hiPS-CM population may starve the cells of nutrients, despite changing the cell media every day. To increase cell number on the leaf scaffold for

clinical application, future studies should use larger cylinders to increase both cell population and media volume during hiPS-CM seeding and culture.

7.3.2.2 Cardiac Patch Contractility

Cell contractile strain was used as a measure to compare our leaf cardiac patch to *in vivo* cardiac tissue contractile strain. hiPS-CMs on micropatterned leaves demonstrated improved average contractile strain peak values (8.7%) compared to non-coated leaves (4.7%) after seven days. However, contractile strain was still significantly lower than *in vivo* conditions (15.9-22.1%). At this time, the leaf cardiac patch does not meet the clinical design specifications. Despite this, we believe that increased culture time, as previously demonstrated with cultured hiPS-CMs on aligned fibrin microthreads[42], on micropatterned leaves will demonstrated further improved contractile function and approach clinically relevant contractile strain values on the patch.

7.3.2.3 Cardiac Patch Synchronized Function

We demonstrated synchronized function in micropatterned hiPS-CMs on leaves. A standard variable for synchronized CM function is conduction velocity, an electrophysiology measure of cell depolarization speed, which indicates presence of ion channels and gap junction formation between cells. Current engineered cardiac tissue patches have demonstrated *in vitro* conduction velocities ranging from 24 cm/sec [42] to a maximum of 41 cm/sec.[43] Conduction velocity corresponds to contraction velocity, as ion conduction initiates cell contraction.

The average contraction velocity measured in hiPS-CMs seeded on leaves within micropatterned fibrin was 0.88 ± 0.107 cm/sec after seven days of culture. In this, our engineered patch does not yet meet benchmarks for clinical application. Increasing culture time of hiPS-CMs on aligned micropatterned beyond seven days may increase velocity. As with contractile strain, mean conduction velocity of hiPS-CMs on elongated scaffolds is dependent on culture time in that velocity increases ten-fold after extending culture time from day 7 (3.7 cm/sec) to day 21 (24.2 cm/sec).[42] This has been verified in additional cardiac patches in which conduction velocities double in speed in between one and three weeks in culture.[40] Directional hiPS-CM voltage or calcium transient propagation on micropatterned leaves would further demonstrate intercellular coupling[44] and synchronized electrophysiology on the leaf.

7.3.3 Leaf Cardiac Patch Application

For its application, we envision that the leaf cardiac patch system could be used as an *in vivo* therapy. As the leaf has an inherent vasculature capable of perfusion, the leaf stem could be anastomosed to a host vessel *in vivo* to perfuse blood through the scaffold to cells on its surface. An initial perfusion study in our laboratory demonstrated that heparinized bovine blood perfuses through the decellularized spinach leaf without clotting. In addition, to assist in anastomosis of the leaf stem, preliminary research in our laboratory has been conducted to design electrospun cuffs to place around the leaf stem. These cuffs for the leaf stem would allow for easier anastomosis of leaf and blood vessels in that suture could anchor to the leaf cuff, rather than the pliable stem. Cuffs could also be composed of medical-grade materials such as Dacron (Medi-Tech, Boston Scientific, Natick, MA), a common polymer vascular graft replacement.[45]

Although we can initiate perfusion of arterial blood through the leaf vasculature to cells with anastomosis, an *in vivo* implanted cardiac patch should also return "venous" blood through its vasculature as a closed loop system. Previous work has demonstrated that leaves can be grafted during propagation to achieve trans-leaf vascular connections with input and output flow.[46] These grafted leaves can then be decellularized and perfused, demonstrating flow from the input petiole and through the second grafted leaf prior to exiting the output petiole. The grafted leaf system may function as an arterial-venous vascular network, capable of venous return within the leaf. Future consideration should be applied to spinach leaf grafting during development to develop such an arterial and venous system within the vascularized leaf patch. A vascular system with venous return would allow for contained perfusion flow in and out of the leaf *in vivo*.

Furthermore, anchoring the patch to the myocardium is an important consideration for *in vivo* implantation. Several implanted cardiac patches in animal models have used ligation sutures for anchoring the patch to the heart. However, these patches are typically composed of biologically derived, and not plant derived, materials. For initial adhesion, spinach leaf scaffolds may require ligation suture anchoring in addition to an intermediate substrate for heart tissue adhesion. An intermediate medium would enhance tissue adhesion from the tissue to the leaf and promote electromechanical propagation from the healthy native heart muscle across the patch. To do this, we envision the use of fibrin glue on the periphery of the leaf to the heart muscle. Fibrin glue is commonly used in clinical surgical procedures to promote adhesion of tissues, vascular grafts,

and wound healing.[11] As cardiomyocytes' action potentials propagate across fibrin microthreads[42] and hydrogels[40], we hypothesize that host CMs' electromechanical behavior should propagate through the fibrin glue and synchronize with hiPS-CMs on the leaf scaffold.

In addition to *in vivo* application, the decellularized spinach leaf scaffold could be potentially used as an *in vitro* model system since we have demonstrated that the leaf's vasculature can perfuse cardioactive drugs to hiPS-CMs on the leaf surface. With further study of fluid and diffusion transport in the leaf vasculature to cells on its surface, drugs in development could be perfused through the leaf to see indirect effects such as cardiotoxicity. For this model to be applied, further study needs to be performed to model and better understand decellularized leaf vasculature transport to the leaf tissue and surface during perfusion.

In conclusion, in this dissertation we developed a contractile, vascularized cardiac patch composed of decellularized spinach leaves and stem cell derived cardiomyocytes. We demonstrated that perfusion of the decellularized spinach leaf's vasculature can affect hiPS-CM function on the leaf surface, hiPS-CMs adhere and function on the leaf surface without protein coatings, and micropatterned leaf surfaces initiate hiPS-CM anisotropy. Although the patch has not yet met all of the benchmarks that we aim to achieve, there is promise for the technology with future development.

7.4 References

1. Yokoo N, Baba S, Kaichi S, et al. The effects of cardioactive drugs on cardiomyocytes derived from human induced pluripotent stem cells. Biochem Biophys Res Commun. 2009;387(3):482-488. doi:10.1016/j.bbrc.2009.07.052
2. Ren J, Prentice H, Ge W, et al. Unraveling the Mystery of Cold Stress-Induced Myocardial Injury. Front Physiol. 2020;11:580811. doi:10.3389/fphys.2020.580811
3. Wang K, Climent A, Gavaghan D, Kohl P, Bollensdorff C. Room Temperature vs Ice Cold - Temperature Effects on Cardiac Cell Action Potential. Biophys J. 2016;110(3):587a. doi:10.1016/j.bpj.2015.11.3134
4. Pittermann J. The evolution of water transport in plants: An integrated approach. Geobiology. 2010;8(2):112-139. doi:10.1111/j.1472-4669.2010.00232.x
5. Sack L, Holbrook NM. Leaf Hydraulics. Annu Rev Plant Biol. 2006;57(1):361-381. doi:10.1146/annurev.arplant.56.032604.144141
6. Entcheva E, Bien H, Yin L, Chung C-Y, Farrell M, Kostov Y. Functional cardiac cell constructs on cellulose-based scaffolding. Biomaterials. 2004;25(26):5753-5762. doi:10.1016/j.biomaterials.2004.01.024

7. Stevens MM, George JH. Exploring and Engineering the Cell Surface Interface. Science (80-). 2005;310:1135-1138. doi:10.1126/science.1106587
8. Wu X, Sun Z, Foskett A, Trzeciakowski JP, Meininger GA, Muthuchamy M. Cardiomyocyte contractile status is associated with differences in fibronectin and integrin interactions. Am J Physiol Circ Physiol. 2010;298(6):H2071-H2081. doi:10.1152/ajpheart.01156.2009
9. Baharvand H, Azarnia M, Parivar K, Ashtiani SK. The effect of extracellular matrix on embryonic stem cell-derived cardiomyocytes. J Mol Cell Cardiol. 2005;38(3):495-503. doi:10.1016/j.yjmcc.2004.12.011
10. Santoro R, Perrucci GL, Gowran A, Pompilio G. Unchain My Heart: Integrins at the Basis of iPSC Cardiomyocyte Differentiation. Stem Cells Int. 2019;2019:8203950. doi:10.1155/2019/8203950
11. Silver FH, Wang M-C, Pins GD. Preparation and use of fibrin glue in surgery. Biomaterials. 1995;16(12):891-903.
12. Tanaka N, Moriguchi H, Sato A, et al. Microcasting with agarose gel via degassed polydimethylsiloxane molds for repellency-guided cell patterning. RSC Adv. 2016;6(60):54754-54762. doi:10.1039/c6ra11563b
13. McDevitt TC, Woodhouse KA, Hauschka SD, Murry CE, Stayton PS. Spatially organized layers of cardiomyocytes on biodegradable polyurethane films for myocardial repair. J Biomed Mater Res - Part A. 2003;66(3):586-595. doi:10.1002/jbm.a.10504
14. Herron TJ, Da Rocha AM, Campbell KF, et al. Extracellular matrix-mediated maturation of human pluripotent stem cell-derived cardiac monolayer structure and electrophysiological function. Circ Arrhythmia Electrophysiol. 2016;9(4):1-12. doi:10.1161/CIRCEP.113.003638
15. Chun YW, Balikov DA, Feaster TK, et al. Combinatorial polymer matrices enhance in vitro maturation of human induced pluripotent stem cell-derived cardiomyocytes. Biomaterials. 2015;67:52-64. doi:10.1016/j.biomaterials.2015.07.004
16. Baudino TA, Carver W, Giles W, Borg TK. Cardiac fibroblasts: Friend or foe? Am J Physiol - Hear Circ Physiol. 2006;291(3). doi:10.1152/ajpheart.00023.2006
17. Souders CA, Bowers SLK, Baudino TA. Cardiac Fibroblast: The Renaissance Cell. Circ Res. 2009;105(12):1164-1176. doi:10.1161/CIRCRESAHA.109.209809
18. Au HTH, Cheng I, Chowdhury MF, Radisic M. Interactive effects of surface topography and pulsatile electrical field stimulation on orientation and elongation of fibroblasts and cardiomyocytes. Biomaterials. 2007;28(29):4277-4293. doi:10.1016/j.biomaterials.2007.06.001
19. Gomez-Garcia MJ, Quesnel E, Al-attar R, Laskary AR, Laflamme MA. Maturation of human pluripotent stem cell derived cardiomyocytes in vitro and in vivo. Semin Cell Dev Biol. Published online May 2021. doi:10.1016/j.semcdb.2021.05.022
20. Liau B, Christoforou N, Leong KW, Bursac N. Pluripotent stem cell-derived cardiac tissue patch with advanced structure and function. Biomaterials. 2011;32(35):9180-9187. doi:10.1016/j.biomaterials.2011.08.050
21. Huebsch N, Loskill P, Deveshwar N, et al. Miniaturized iPS-Cell-Derived Cardiac Muscles for Physiologically Relevant Drug Response Analyses. Sci Rep. 2016;6(November 2015):1-12. doi:10.1038/srep24726
22. Ronaldson-Bouchard K, Yeager K, Teles D, et al. Engineering of human cardiac muscle electromechanically matured to an adult-like phenotype. Nat Protoc. 2019;14:2781-2817. doi:10.1038/s41596-019-0189-8

23. Severs NJ. Gap junction remodeling in heart failure. J Card Fail. 2002;8(6):S293-S299. doi:10.1054/jcaf.2002.129255
24. Goodenough DA, Paul DL. Gap junctions. Cold Spring Harb Perspect Biol. 2009;1(a002576):1-19. doi:10.1101/cshperspect.a002576
25. Lundy SD, Zhu W-Z, Regnier M, Laflamme MA. Structural and Functional Maturation of Cardiomyocytes Derived from Human Pluripotent Stem Cells. Stem Cells Dev. 2013;22(14):1991-2002. doi:10.1089/scd.2012.0490
26. Ahmed TAE, Dare E V., Hincke M. Fibrin: A Versatile Scaffold for Tissue Engineering Applications. Tissue Eng Part B Rev. 2008;14(2):110306231744007. doi:10.1089/teb.2007.0435
27. Caves JM, Kumar VA, Xu W, Naik N, Allen MG, Chaikof EL. Microcrimped Collagen Fiber-Elastin Composites. Adv Mater. 2010;22(18):2041-2044. doi:10.1002/adma.200903612.Microcrimped
28. Ayhan Atmanli, Hu D, Domian IJ. Molecular Etching – A Novel Methodology for the Generation of Complex Micropatterned Growth Surfaces for Human Cellular Assays. Adv Healthc Mater. 2014;3(11):1759-1764. doi:10.1002/adhm.201400010.Molecular
29. Griffiths M, Ojeh N, Livingstone R, Price R, Navsaria H. Survival of Apligraf in Acute Human Wounds. Tissue Eng. 2004;10(7):1180-1195. doi:10.1089/1076327041887835
30. Schmidt C. FDA approves first cell therapy for wrinkle-free visage. Nat Biotechnol. 2011;29(8):674-675. doi:10.1038/nbt0811-674
31. Schmidt C. Gintuit cell therapy approval signals shift at US regulator. Nat Biotechnol. 2012;30(6):479-479. doi:10.1038/nbt0612-479
32. Fischer A. FDA approves first autologous cellularized scaffold for the repair of cartilage defects of the knee. US Food & Drug Administration. Published 2016. https://www.fda.gov/news-events/press-announcements/fda-approves-first-autologous-cellularized-scaffold-repair-cartilage-defects-knee
33. Cheng CW, Solorio LD, Alsberg E. Decellularized tissue and cell-derived extracellular matrices as scaffolds for orthopaedic tissue engineering. Biotechnol Adv. 2014;32(2):462-484. doi:10.1016/j.biotechadv.2013.12.012
34. U.S. Food and Drug Administration (FDA). Regulatory Considerations for Human Cells, Tissues, and Cellular and Tissue-Based Products: Minimal Manipulation and Homologous Use.; 2020. https://www.fda.gov/CombinationProducts/default.htm
35. Gilpin A, Yang Y. Decellularization Strategies for Regenerative Medicine: From Processing Techniques to Applications. Biomed Res Int. 2017;2017:1-13. doi:10.1155/2017/9831534
36. Guyette JP, Gilpin SE, Charest JM, Tapias LF, Ren X, Ott HC. Perfusion decellularization of whole organs. Nat Protoc. 2014;9(6):1451-1468. doi:10.1038/nprot.2014.097
37. Zhang Y, Iwata T, Nam K, Kimura T, Wu P. Water absorption by decellularized dermis. Heliyon. 2018;(February):e00600. doi:10.1016/j.heliyon.2018.e00600
38. Ott HC, Matthiesen TS, Goh S-K, et al. Perfusion-decellularized matrix: using nature's platform to engineer a bioartificial heart. Nat Med. 2008;14(2):213-221. doi:10.1038/nm1684
39. Gershlak JR, Hernandez S, Fontana G, et al. Crossing kingdoms: Using decellularized plants as perfusable tissue engineering scaffolds. Biomaterials. 2017;125:13-22. doi:10.1016/j.biomaterials.2017.02.011
40. Shadrin IY, Allen BW, Qian Y, et al. Cardiopatch platform enables maturation and scale-up of human pluripotent stem cell-derived engineered heart tissues. Nat Commun. 2017;8(1):1825. doi:10.1038/s41467-017-01946-x

41. Wendel JS, Ye L, Tao R, et al. Functional Effects of a Tissue-Engineered Cardiac Patch From Human Induced Pluripotent Stem Cell-Derived Cardiomyocytes in a Rat Infarct Model. Stem Cells Transl Med. 2015;4(11):1324-1332. doi:10.5966/sctm.2015-0044
42. Hansen KJ, Laflamme MA, Gaudette GR. Development of a Contractile Cardiac Fiber From Pluripotent Stem Cell Derived Cardiomyocytes. Front Cardiovasc Med. 2018;5(52):1-11. doi:10.3389/fcvm.2018.00052
43. Querdel E, Reinsch M, Castro L, et al. Human Engineered Heart Tissue Patches Remuscularize the Injured Heart in a Dose-Dependent Manner. Circulation. 2021;143(20):1991-2006. doi:10.1161/CIRCULATIONAHA.120.047904
44. De Boer TP, Van Rijen HVM, Van Der Heyden MAG, De Bakker JMT, Van Veen TAB. Adrenergic regulation of conduction velocity in cultures of immature cardiomyocytes. Netherlands Hear J. 2008;16(3):106-109. doi:10.1007/BF03086127
45. Etz CD, Homann T, Silovitz D, et al. Vascular Graft Replacement of the Ascending and Descending Aorta: Do Dacron Grafts Grow? Ann Thorac Surg. 2007;84(4):1206-1213. doi:10.1016/j.athoracsur.2007.05.034
46. Wang Y, Dominko T, Weathers PJ. Using decellularized grafted leaves as tissue engineering scaffolds for mammalian cells. Vitr Cell Dev Biol - Plant. 2020;56(6):765-774. doi:10.1007/s11627-020-10077-w

8. Appendix

8.1 Reprint Permissions

Reprint permission for work included in Chapter 4, from the publisher:

"If you are the author of a published Wiley article, you have the right to reuse the full text of your published article as part of your thesis or dissertation. In this situation, you do not need to request permission from Wiley for this use."

Reprint permission for work included in Chapter 4:

Robbins, Emily R.

From: no-reply@copyright.com
Sent: Friday, June 11, 2021 1:43 PM
To: Robbins, Emily R.
Subject: [EXT] Thank you for your order with RightsLink / John Wiley and Sons

Thank you for your order!

Dear Emily Robbins,

Thank you for placing your order through Copyright Clearance Center's RightsLink® service.

Order Summary

Licensee:	Worcester Polytechnic Institute
Order Date:	Jun 11, 2021
Order Number:	5086040142444
Publication:	JOURNAL OF BIOMEDICAL MATERIALS RESEARCH PART A
Title:	Creation of a contractile biomaterial from a decellularized spinach leaf without ECM protein coating: An in vitro study
Type of Use:	Dissertation/Thesis
Order Total:	0.00 USD

View or print complete details of your order and the publisher's terms and conditions.

Sincerely,

Copyright Clearance Center

Tel: +1-855-239-3415 / +1-978-646-2777
customercare@copyright.com
https://myaccount.copyright.com

CCC RightsLink®

8.2 **Appendix A: Plant Decellularization and Rehydration**

8.2.1 Plant Decellularization Protocol

Materials:

- 27G Needles
- 0.38 ID 1.09 OD LDPE Medical tubing
- Hexanes
- PBS 1x
- DI H2O
- 1X SDS solution in DI H2O
    - For 2L of solution mix 200 mL of 10x SDS with 1800 mL of DIH20
        - 2L of 10x SDS Solution: Mix 200 g of SDS powder in 2L DIH20 until there are no more visible SDS pellets
- 0.1% Triton-X with 10% bleach in DI H2O
    - 48 mL of concentrated Clorox bleach and 20 mL of TritonX-100 Solution are added to 2L of DiH20 and mixed until in solution
- Tris buffer solution
    - 10 mM Tris Buffer (605.7 mg in 500 mL of DiH2O)
    - Buffered to pH 9.0
    - Gaudette Lab perfusion decellularization apparatus

Decellularization Protocol:

1. Cannulate leaves via the stem, affixing cannulas with suture.
2. Once leaves are cannulated, submerge in hexanes and wash vigorously for 2 minutes. Remove and rinse in 1x PBS for 2 minutes. Repeat 3x times.
3. Affix plant materials to decellularization set up.
4. Attach 4 L of 1x SDS solution to the set up and begin flow. Monitor plant materials to ensure proper flow through the leaf vasculature, modifying flow rate to ensure a slow, steady drip.
    a. Rapid flow rate will deplete SDS too quickly, whereas too little flow runs the risk of dehydrating the plant material and damaging the plant structure.
5. Maintain in SDS for 1 day in order to decellularize plant material, until leaves and stems become more transparent in appearance. Green coloration at this step is normal and not indicative of an unsuccessful decellularization.
6. Remove 1x SDS and add 4L of Triton-X/Bleach solution to set up.
7. Maintain set up in Triton-X/Bleach for 24 hours, can go longer if needed. Watch until leaves and stems have become clear/transparent. This solution should purge any remaining coloration from the plant matter.
8. Remove Triton-X/Bleach solution and attach DI H2O to set up. Perfuse leaves/stems in DI H2O for 24 hours.
9. Wash decellularized leaves on rotator in Tris buffer solution overnight.
10. Remove leaves from solutions, freeze overnight in -20°C freezer
11. Lyophilize leaf/stem for 24 hours
12. Store at lyophilized leaf scaffold at room temperature until needed.

8.2.2 Decellularized Leaf Rehydration, Sterilization, and ECM Coating Protocol

Materials:

- Lyophilized decellularized spinach leaves
- Biosafety cabinet
- Petri dish(es)
- Non-TCP coated 6 well plates (or alternative)
- Orbital or linear shaker plate
- 2 sterile forceps
- Sterile 10mm Pyrex cloning cylinders
- 10mM Tris buffer, pH 9.0
- DI water
- 70% ethanol
- Sterile 1X PBS
- Cell media
- Serological pipette gun and pipettes
- ECM proteins: Human plasma fibronectin (100ug/mL) in sterile 1X PBS; Human collagen IV (10ug/mL) in sterile 1X PBS
- 200uL micropipette and sterile tips

Rehydrating and sterilizing leaves:

1. Put lyophilized leaf pieces in Petri dish(es)
2. Rehydrate leaves in 10mM Tris buffer on shaker plate for 30 minutes
3. Aspirate Tris buffer from dish and rinse with DI water
4. Add new DI water to leaves and keep on shaker plate for 30 minutes (for perfused whole leaves, maintain for 1 hour)
5. Aspirate DI water
6. Add 70% ethanol and wash for 30 minutes on shaker plate (for perfused whole leaves, maintain for 1 hour)
7. Bring closed dish containing ethanol and leaves into the biosafety cabinet
8. Aspirate ethanol from dish and rinse with sterile 1X PBS
9. Move leaf into well plates with sterile forceps (or sterile 150mm Petri dish for whole leaf)
10. Rinse leaves 2X with sterile PBS in plates, 5 minutes each
11. If desired, can UV sterilize at this point in biosafety cabinet (but not necessary)
12. Aspirate remaining PBS and add appropriate cell media to leaf
13. Incubate leaves overnight at 37C

Coating leaves with ECM proteins:

1. Bring leaves into biosafety cabinet after overnight incubation and aspirate off cell media
2. Place cloning cylinders on the leaf surfaces with sterile forceps
    a. Try to place cylinders on flat areas of leaf
    b. If not coating with ECM proteins, seed cells after cloning cylinders are placed
3. Coat leaf with 100uL of protein suspension within the cloning cylinder. If needed, add more suspension.

4. With the culture plate's lid removed, let leaves air-dry in the biosafety cabinet for approximately 45 minutes, or until the protein-coated surface is dry.

8.3 **Appendix B: hiPS-CM Differentiation and Thaw**

8.3.1 Cardiac Differentiation Protocol (Laflamme Lab at McEwen Stem Cell Institute)

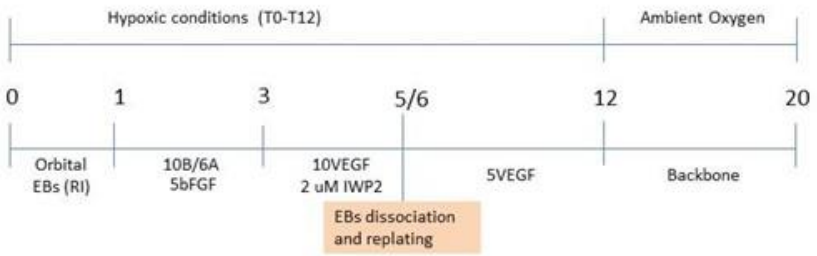

Day 0-1: Generation of embryoid bodies (EBs)

1. Aspirate media and incubate cells in 1ml/well (6w plate) TrypLE for 3 to 5 minutes, monitor cells to avoid over trypsinization and cell loss (Cells should round up).
2. If possible, remove TrypLE and add 1ml of mTESR1 supplemented with 10 ug/ml DNAse and 10 uM Rock inhibitor (Y-27632).
3. Harvest cells after resuspending them into single cells with a p1000 pipetman. Add an additional 1 ml of mTESR1 WASH and filter the cells using a 70 uM filter cap into a 50 ml conical tube.
4. Pellet at 1200 rpm for 4-5 minutes.
5. Re-wash cells with mTESR1 WASH, re-pellet at 1200 rpm for 4-5 minutes
6. Resuspend cells with Aggregation Media. Optimal concentration of cells for aggregration is $5x10^5$-$7.5x10^5$ cells/mL.
7. Incubate cell suspension overnight at a speed of 45 rpm (150mm plates) - 60 rpm (6w plates) (37°C in a 5% CO2, 5% O2 incubator). Rotational speed should be optimized.

Day 1-3: Induction 1 (Stage 1)

1. There will be some debris in the cultures after 24 hours. To separate the aggregates from the debris, filter the EBs through a 100 uM filter into a 50 ml conical tube and allow them to settle for 15-20 min in a 37°C, 5%CO_2, 5%O_2 incubator or spin down at 350-400 rpm for 2-3 min.
2. Once settled, aspirate the Aggregation Medium. Gently resuspend the aggregates in INDUCTION MEDIA 1 and incubate in hypoxic conditions (without shaking) until Day3. (The induction time can vary and must be determined for each line).

Day 3-5/6: Induction 2 (Stage 2)

1. Harvest EBs and allow to settle for 20 minutes in hypoxic conditions (or spin down at 300-400 rpm for 2-3 min).

2. Aspirate supernatant carefully and wash EBs with 10-20 mL IMDM to wash out residual inductive cytokines (especially Activin A which is potent signaling molecule even at very low concentrations).
3. Centrifuge the EBs at 400 rpm for 3 minutes and aspirate supernatant.
4. Resuspend EB-pellet in INDUCTION 2 MEDIA and re-plate intoplates.
5. Incubate in hypoxic conditions until Day 5-6.

Day 5/6-12: Induction 3 (Stage 3) and cells replating

1. Harvest the EBs and allow to settle for 20 minutes in hypoxic conditions (or spin down at 300-400 rpm for 2-3 min).
2. Aspirate media and add warm TrypLE for 3 to 5 minutes at 37C. Monitor cells to avoid over trypsinization.
3. Pipette the cells using 5ml pipette and make sure no aggregates left in cell suspension.
4. Add Stempro WASH media supplemented with 10 ug/ml DNAse.
5. Pellet at 1200 rpm for 4-5 minutes.
6. Re-wash cells with Stempro WASH, re-pellet at 1200 rpm for 4-5 minutes
7. Count the cells and replate on GFR matrigel coated plate in INDUCTION MEDIA 3 containing VEGF **and RI**. Recommended density for replating is 1-1.2x10^5 cells/cm^2. Incubate cells under hypoxic conditions until Day 12, change media every other day.
8. After Day 12, monolayers can be cultured in INDUCTION MEDIA 3 and maintained under ambient oxygen levels for remainder of the experiment (37 °C, 5% CO_2)
9. Re-feed every 2-3 days or as needed, until day 20. Perform cardiac Troponin T staining at Day 20.

Media Formulations:

AGGREGATION MEDIUM (Day 0-1)

	Stock Conc.	Final Conc	per mL	For 50 mL
STEMPRO 34				50mL
Glutamine	100x	1%	10uL	500uL
Transferrin	30mg/mL	150ug/mL	5uL	250uL
Ascorbic Acid	5mg/mL	50ug/mL	10uL	500uL
MTG	26ul/2mL		3uL	150uL
BMP4*	10ug/mL	1ng/mL	0.1uL	5uL
ROCK INHIBITOR	10 mM	10 uM	1 uL	50uL

INDUCTION 1 MEDIUM (Day 1-3)

	Stock Conc.	Final Conc	per mL	For 50 mL
STEMPRO 34				50mL
Glutamine	100x	1%	10uL	500uL
Transferrin	30mg/mL	150ug/mL	5uL	250uL
Ascorbic Acid	5mg/mL	50ug/mL	10uL	500uL
MTG	26ul/2mL		3uL	150uL
BMP4*	10ug/mL	10ng/mL	1uL	50uL
bFGF*	10ug/mL	5ng/mL	0.5uL	25uL
Activin A*	10ug/mL	6ng/mL	0.6 uL	30 uL

INDUCTION 2 MEDIUM (Day 3-5/6)

	Stock Conc.	Final Conc	per mL	For 50 mL
STEMPRO 34				50mL
Glutamine	100x	1%	10uL	500uL
Transferrin	30mg/mL	150ug/mL	5uL	250uL
Ascorbic Acid	5mg/mL	50ug/mL	10uL	500uL
MTG	26ul/2mLs		3uL	150uL
VEGF*	10ug/mL	10ng/mL	1uL	50uL
IWP2	2mM	1-2uM	0.5-1uL	25-50uL

*****cytokine concentrations may vary according to lot# or the hES cell line used

INDUCTION 3 MEDIUM (Day 5/6-12)

	Stock Conc.	Final Conc	per mL	For 50 mL
STEMPRO 34				50mL
Glutamine	100x	1%	10uL	500uL
Transferrin	30mg/mL	150ug/mL	5uL	250uL
Ascorbic Acid	5mg/mL	50ug/mL	10uL	500uL
MTG	26ul/2mLs		3uL	150uL
VEGF*	10ug/mL	5ng/mL	0.5uL	25uL
**ROCK INHIBITOR	10 mM	10 uM	1 uL	50uL

*****cytokine concentrations may vary according to lot# or the hES cell line used and may not be required after Day 12 of differentiation.

** Add RI for replating only

8.3.2 hiPS-CM Thaw and Seeding

Materials:

- RPMI-B27 media + supplements
- 50ug/mL Aprotinin-supplemented RPMI-B27 media (if working with fibrin)
- DNaseI (Invitrogen 18047-019)
- Rock Inhibitor (Y-27632 dihydrochloride, Sigma) – aliquoted to 1mM
- Fetal Bovine Serum (FBS)
- 10ml serological pipettes
- Pipette aid
- 1000ul pipette tips
- 1000ul pipettor
- 50ml conical tube
- Conical tube rack
- Centrifuge
- Pasteur Pipettes

****Note**: If seeding on fibrin microthreads, prior to thawing iPS-CM, hydrate microthreads in the biosafety cabinet with sterile PBS for 20 min. Coat microthreads with 150uL of 10ug/mL Col4 on glass coverslip posts for total of 2 hours before cell seeding. Start cell thaw process after 1 hour of coating. **

Protocol:

1) Place RPMI-B27 media and Aprotinin-supplemented RPMI-B27 media in the water bath at 37C to warm up
2) Place all materials in the biosafety cabinet by spraying with 70% ethanol
3) Place 5ml of RPMI-B27 media into a 50ml conical tube and place in the water bath
4) Put DNase I on ice next to biosafety cabinet
5) Obtain cells from cryotank
6) Place in water bath so that the lid is never submerged. Thaw for 30 seconds, until a small ice chunk remains
7) Remove vial and conical tube from water bath, spray with ethanol and introduce into the hood
8) Add ~1 ml warm RPMI-B27 media dropwise to cryovial
9) Pull up cells from cryovial (1mL at a time) and transfer dropwise to 50ml conical tube with 5ml of media (approx 1 drop/second)
    a. Should have ~6mL cell suspension in conical tube
10) Add 20 ml of fresh/warm media slowly on side of tube
11) Add 14ul of DNase1 – 150U (DNAse is at 267U/ul) into conical, then cap DNaseI and put back on ice
12) Centrifuge conical for 5min at 300g (slow)
13) Aspirate media off pellet
14) Resuspend in 1ml AP-supplemented RPMI-B27 media (for 5mill cell vial, more media if more cells)→ **swirl**, don't pipette more than once
    a. Only use AP if working with fibrin; if not, RPMI-B27 is fine

15) Count cells: 20uL cells, 20uL trypan blue
    a. Perform a viability count (Live cell count/Total cells –trypan blue included) = % viability
16) Add more AP media with FBS and Rock inhibitor to get desired cell suspension
    a. AP-supplemented RPMI-B27 media + 10% FBS + 1% Rock inhibitor (Y-27632 dihydrochloride, Sigma) (for total volume suspension)
17) Use immediately to seed appropriate cells and volume per sample
18) Transfer constructs after **18 hours** into wells containing AP-RPMI-B27 media
19) Change media every other day from there

8.4 Appendix C: High Density Mapping (HDM) for Mechanical Contractile Cell Analysis

1. All raw images should be saved in raw data folder. Create new analyzed folder in different location than raw data. Open this folder in MATLAB directory to save new files into for analysis.
    a. E2= contraction; E1= relaxation
2. Make tiffs into AVIs
    a. Define data set folder; ds='…'

    For batch data set images code:

    tiff2avi_batch ([], record rate, sample rate, output rate, min tiffs)

    eg. tiff2avi_batch ([], 60, 60, 30, 11)

    It will have you self select the folder (in raw images) that contain the tiffs you want to make into AVIs

    This function will create folders and structure data so that you can run hdm code
3. Define your data set (ds) which is whatever the folder name (ie. Video file) is that you are analyzing
4. Run HDM
    a. Define your dataset (ds) you want to analyze
    b. hdm2(ds, frame rate, frames to use, pixel subsize, pixel shift)
        i. Eg. hdm2(ds, 60, 3:500, 32,16)
    c. Select the region of interest; click to close the area. Close out of the image window to continue to run code.
5. To output strain data to excel
    a. hdm2_avgstrain(ds,1)
    b. Excel file contains beat frequency (in Hz)
6. to rezero (calculate cyclic strain)
    a. hdm2_cyclicstrain(ds, 'E2', 'maxfreqmaxs')
        i. this rezeroes it to your E2 strain
7. to quantify strain values
    a. open matlab data folder…drag cyclicstrain.mat into the MATLAB workspace
        i. e2=straindata.E2
        ii. Ic=e2<-0.05; (this is your "noise" threshold value…aka less than 0.5% strain)
        iii. mean(mean(e2(Ic)); this is your avg strain aka Contractile strain
        iv. min(e2(Ic)); this is your maximum contractile strain

8.5 Appendix D: ECM and Cardiac-Specific IF Antibodies

Primary and secondary antibodies used in IF staining in Specific Aims 1, 2, and 3. Table indicates antibody target proteins, host species, vendors, and dilution factors.

Primary Antibodies

Protein	Host Species	Vendor	Product ID	Dilution Factor
Fibronectin	rabbit	Abcam	ab23751	1:100
Collagen IV	mouse	Abcam	ab6311	1:100
Sarcomeric alpha-actinin	mouse	Abcam	ab9465	1:100
Sarcomeric alpha-actinin	rabbit	Abcam	ab137346	1:100
Connexin 43	goat	Abcam	ab87645	1:100

Secondary Antibodies

Product	Antibody	Vendor	Product ID	Dilution Factor
AlexaFluor 488	goat anti-mouse	Invitrogen	A-11029	1:400
AlexaFluor 488	goat anti-rabbit	Invitrogen	A-11034	1:400
Alexa Fluor 488	donkey anti-rabbit	Invitrogen	A-21206	1:400
Alexa Fluor 568	donkey anti-goat	Invitrogen	A-11057	1:400
Alexa Fluor 647	donkey anti-mouse	Invitrogen	A-31571	1:400

8.6 Appendix E: Immunofluorescence (IF) Staining Protocols

8.6.1 Fibronectin or Collagen IV ECM Coating

Materials:

- Phosphate buffered saline (PBS)
- 0.25% Triton-X 100 in DI H2O
- 5% normal goat serum in PBS
- Primary:
  - Rabbit anti-human fibronectin or mouse anti-human collagen IV antibody 1:100
  - In 5% goat serum
- Secondary:
  - Alexa-fluor 488 goat anti-mouse or rabbit 1:400
  - In 5% goat serum

Procedure:

1. Wash 3x in PBS for 5 mins
2. Permeabilize with 0.25% Triton X for 10 mins
3. Wash 3x in PBS for 5 mins
4. Block with 5% goat serum in PBS for 45 mins
5. Incubate in primary antibody for 1 hour at room temperature, or overnight at 4 degrees C
6. Wash 3x in PBS for 5 mins
7. Incubate in secondary antibody for 1 hr at room temperature
8. Wash 3x in PBS for 5 mins
9. Image or store in 1X PBS at 4 degrees C

8.6.2 Sarcomeric α-actinin, Connexin-43, and Hoescht

Materials:

- Phosphate buffered saline (PBS)
- 0.25% Triton-X 100 in DI H2O
- 5% donkey serum in PBS
- Primary:
  - Mouse anti Alpha actinin monoclonal 1:100
  - Goat anti Cnx43 monoclonal 1:100
  - In 5% donkey serum
- Hoechst dye 1:6000 in PBS
- Secondary:
  - Alexa-fluor 568 donkey anti-goat 1:400
  - Alexa-fluor 647 donkey anti-mouse 1:400
  - In 5% donkey serum

Procedure:

1. Wash 3x in PBS for 5 mins
2. Permeabilize with 0.25% Triton X for 10 mins
3. Wash 3x in PBS for 5 mins
4. Block with 5% donkey serum in PBS for 45 mins
5. Incubate in primary antibody for 1 hour at room temperature, or overnight at 4 degrees C
6. Wash 3x in PBS for 5 mins
7. Incubate in secondary antibody for 1 hr at room temperature
8. Wash 3x in PBS for 5 mins
9. Counterstain with Hoechst for 5 minutes
10. Wash 3x in PBS for 5 mins
11. Coverslip with cytoseal if threads; if leaves, store in 1X PBS at 4 degrees C

8.6.3 Sarcomeric α-actinin, Phalloidin, and Hoescht

Materials:

- 0.25% Triton-X V/V Triton-X in PBS
  - Ex. 10 μL Triton-X in 3990 μL PBS
- 5% donkey goat serum in PBS
- Primary antibody – Mouse anti Alpha actinin monoclonal 1:100 (Abcam 9465) in blocking agent
- Secondary antibody – 1:400 donkey anti-mouse Alexa Fluor 647 in your blocking agent
- Phalloidin (AF 488 Phalloidin A12379, Invitrogen)
  - 2.5% V/V Phalloidin in NGS – add to solution with secondary
  - Ex. 50 μL in 1950 μL
- Hoescht

- 0.0167% Hoescht dye in PBS
- 0.5ul in 3000ul PBS

Procedure (for fixed tissue samples)

1. 3 washes in PBS, 5 minutes each
2. 0.25% Triton X-100 – 10 minutes
3. 3 washes in PBS, 5 minutes each
4. Block with 5% donkey serum, 45 minutes
5. Leave goat serum on negatives but aspirate serum off the positives
6. Primary actinin mouse monoclonal anti-alpha -actinin 1:100, overnight in refrigerator or for 1 hour at room temperature
7. 3 washes in PBS, 5 minutes each
8. A. Secondary antibody – 1:400 donkey anti-mouse Alexa Fluor 647, one hour at room temperature in the dark
   B. Phalloidin solution for one hour
9. 3 washes PBS, 5 minutes each
10. Hoescht – 1:6000 in PBS, 5 minutes
11. 3 washes in PBS, 5 minutes each
12. Coverslip and store frozen in -20 degrees C, or if leaves store in 1X PBS at 4 degrees C

8.6.4 Phalloidin and Hoescht

Reagents:

- Phosphate Buffered Saline
- 4% Paraformaldehyde (Only needed for tissues/cells that have not been fixed);
- 0.25% Triton-X
  - 0.25% V/V Triton-X in PBS
  - 10 μL Triton-X in 3990 μL PBS
- 1% BSA
  - 1% V (W)/V BSA in PBS
  - 40 μL in 3960 μL PBS
- Phalloidin (AF 488 Phalloidin A12379 or FITC Phalloidin, Invitrogen)
  - 2.5% V/V Phalloidin in PBS
  - 50 μL in 1950 μL
- Hoechst
  - 0.0167% Hoechst dye in PBS
  - 0.5 μL in 3000 μL PBS

For fixed sections/cells:

1. Rinse with PBS x2
2. Triton-X solution for 10 minutes
3. Rinse with PBS x2
4. Block with BSA solution (or 5% donkey serum) for 30 minutes
5. Phalloidin solution for 30 minutes
6. Rinse with PBS x2
7. Hoechst solution for 3-5 minutes (typically 3)

8. Rinse with PBS x2
9. Cytoseal and coverslip if slides. Store frozen at -20 degrees C.
    a. If leaves, store in 1X PBS at 4 degrees C

8.7 Appendix F: Sarcomere Distance MATLAB Code

```
function [peak_distance]=FFT_sarcomere_distance(ds)
% Fast Fourier transform for positive real portion of the fft
% to transform sarcomere band intensity distances into frequency
% Emily Robbins, Gaudette Lab 2019
% ds='....csv';
data=xlsread(ds);
x=data(:,1);
y=data(:,2);
figure(1);
plot(x,y)
xlabel('Distance')
ylabel('Gray value')
title('Raw data')
y_mean=y-mean(y); %remove mean to reduce noise
y_mean(y_mean<0)=0; %remove negative values
figure(2);
plot(x,y_mean)
xlabel('Distance')
ylabel('Gray value')
title('Positive Raw data')
fs=1/0.24026; %0.2403 sampling from ImageJ analysis
Y=fft(y_mean);
n=length(x);
f=(0:n-1)*(fs/n);
power=abs(Y).^2/n;
figure(3);
plot(f,power)
xlabel('Frequency (Hz)')
ylabel('Power')
figure(4);
plot(1./(f(2:end)),power(2:end))
xlabel('Distance (um)')
ylabel('Power')
[max_power] = max(power(2:end));
A=find(power==max_power);
peak_distance=1/f(A(1)) %calculate most frequent distance between peaks
```

8.8 **Appendix G: Fibrin Microthread Manufacturing and Cell Seeding**

8.8.1 Making Threads

Materials:

- Silver pan
- Syringe pump
- 1 aliquot fibrinogen - 70mg/ml
- 1 aliquot thrombin – 8U/200µl
- 10mM HEPES solution
- 2 - 1mL syringes
- 1 – 3ml syringe
- 1000mL graduated cylinder
- Clear cup of warm water
- Blue foam tube holder
- 40mM $CaCl_2$
- 1000µl Micropipetter
- 2 sets of tweezers
- Drying box
- Latex gloves- wear at all times
- Kimwipes
- Extruding tube
- Syringe connector
- Syringe co-extruder

Preparation:

1. Rinse graduated cylinder with DI water. Pour into 500mL of 10mM HEPES solution the silver pan.
2. Obtain 1 aliquot of Fibrinogen and 1 aliquot of Thrombin from the freezer. Also obtain 40mM $CaCl_2$ from fridge. Thaw at 37 degrees C.
3. Once completely defrosted, Add 850µL of 40mM $CaCl_2$ into the thrombin, mix in vortexer.
4. Label two 1ml syringes, one as T, and one as F. Draw up thrombin and fibrinogen into appropriate syringes. Remove all air bubbles from syringes.
5. Balance the two syringes so that they contain the same amount of liquid. Make sure to tap out any air bubbles.

Setting up Machine:

1. Plug in syringe pump and turn on. Make sure diameter is set to 4.699mm and the rate is set to 0.23 mL/min.
2. Put the two syringes in the white co-extruder. Make sure to use correct side with the matching syringe.
3. Place syringes into syringe pump. Make syringe pump block flush with the syringe connector.
4. Attach extruding tube with a 27G needle to co-extruder.

Making Threads:

1. Press start on the machine.
2. Wait for ALL the air bubbles to pass through the extruding tube. Use a Kimwipe to collect anything that comes out while air bubbles are passing through.
3. Once there is a constant flow, start making the threads. Hold extruding tube ≈ 1 inch from the end. Drag end of tube horizontally along the bottom of the silver pan filled with 10mM HEPES. Move the tube from the left side of the pan to right side at a constant rate. At the end of one thread move quickly bring the end of the tube back to the left side of the pan, move ≈ 1 inch down and begin a new thread. Repeat until you cannot make anymore. *Make sure the end of the tube is clean and free of fibrin debris, wipe clean if needed
4. Do Not Overlap Threads!
5. Turn off machine once you are done.
6. Immediately clean tube. Fill a 3ml syringes with water and flush extruding tube with water. Remove syringe from extruding tube, withdraw syringe with just air and blow air through extruding tube with syringe. Repeat with white co-extruder.

Transferring Threads:

1. After 15 minutes, use two sets of forceps to remove threads from the pan
    a. Grab each end of the thread with the tweezers. Move right hand counterclockwise and left hand clockwise slowly so you can pick up the thread
2. Transfer the threads to the cardboard box. Secure one side to the box and stretch the thread. Secure the middle of the stretched out thread to the box. One extruded thread should produce two threads
3. Repeat this for all threads. Leave threads out to dry.

8.8.2 Seeding Cells on Fibrin Microthreads on Static Seeding Platform

Materials:

- Sterile thread construct (PDMS ring attached with fibrin threads) in 6 well plate (sterilize using ETO)
- 6 well plate with seeding platforms
- Sterile PBS
- Sterile forceps
- Cell Suspension (cells in 150 µL) in 50ug/mL Aprotinin supplemented media

Procedure:

1. Add 2 mL of sterile PBS to each 6 well that had a thread construct. Hydrate for 20 min.
    a. While threads hydrate, prepare collagen IV (10ug/mL) solution (if using, or proceed to step 5)
2. Use sterile forceps to place construct on the coating platform, making sure all threads are draped across the coverslip

3. If coating fibrin threads with collagen, add 150uL of Collagen IV solution onto coverslip ensuring all solution stays on the coverslip
    a. Coat control plate with collagen IV also
4. Incubate at 37 degrees C for 2 hours
5. During the coating period, prepare your cell suspension in 50ug/mL aprotinin supplemented media
6. Move constructs from coating platforms to seeding platforms
7. Add 150uL of cell suspension to each thread construct
8. Place the constructs with cell suspensions into the incubator at 37C with 5% CO2 for 18 hours
9. After 18 hours, carefully remove constructs from seeding platform and place in a new 6 well plate with 1-2mL of Aprotinin supplemented media, enough to cover all the threads
10. Change media every 2-3 days

8.9 **Appendix H: hMSC Thawing, Passaging and Qdot Loading**

8.9.1 hMSC Thaw

Materials:

- MSCGM (Lonza)
- T-75 Sterile Culture flasks
- 5 and 10ml serological pipettes
- Pipette aid
- 200 and 1000ul pipette tips
- 200 and 1000ul pipettor
- 15ml conical tube
- Conical tube rack
- Centrifuge

Procedure:

1. Place media into the 37°C water bath
2. Spray surface of hood with 70% Ethanol, spray exterior of all containers before being placed into the hood, set up the necessary items inside the hood
3. Place 10mL of media into a 15mL conical tube and place into water bath
4. Retrieve cryovials from cyrotanks/dry ice/-80°C freezer
   – optional spray vile with ethanol place under the hood and twist cap quarter turn to relieve pressure then retighten cap
5. Thaw cryovial rapidly by immersing into the water bath, do not completely submerge. Keep the water line below the cap. Gently agitate for approx. 1-2min until all ice crystals are melted
6. Remove cryovial and 15mL conical tube from water bath. Spray both with ethanol and reintroduce into the hood, with the 1mL pipette extract all cell solution from vial and slowly/trip-wise add to the pre-warmed media in the 15mL conical tube. Once all cell solution has been added triturate solution.
7. Place conical into centrifuge and spin @ 1000rpm for 5min

8. Aspirate supinate, suspend in known amount of media (Between 0.5-10mL). Perform cell count to determine cell concentration and cell viability.
9. After determining cell number plate in appropriate tissue flask, for optimum growth plate at a density of ≈7000 cells per cm^2
10. Place cells into incubator for seeding, allow for 24hrs
11. After 24hrs, confirm seeding. Replace media in flask with fresh pre-warmed media.

8.9.2 hMSC Passaging

Materials:

- 0.05% Trypsin/0.53mM EDTA (Corning)
- MSCGM
- T-75 Sterile Culture flasks
- 5 and 10ml serological pipettes
- Pipette aid
- 200 and 1000ul pipette tips
- 200 and 1000ul pipettor
- 15ml conical tube
- Conical tube rack
- Centrifuge

Protocol:

1. Place media, trypsin in water bath at 37C.
2. Remove T-75 flask from incubator and verify cell viability and confluence with scope. Place in bio-safety cabinet.
3. Remove cap and aspirate media off cells with sterile Pasteur pipettes.
4. Add 5ml of trypsin to flask.
5. Put flask back in incubator and let sit for 5 min.
6. Remove flask and confirm cell detachment with scope. (Detached cells will float freely and appear round)
7. Add 5ml of 10% FBS in DMEM (or MSCGM) to T-75 flask. (This deactivates the trypsin)
8. Pipette contents of tube in 10ml pipette and place in a 15ml conical tube.
9. Centrifuge the 15ml conical tube for 5min @ 1000rpm making sure to balance the centrifuge.
10. Being sure to spray down the 15ml conical tube, reintroduce it into the sterile field and aspirate off the supernatant being sure not to disturb the cell pellet.
11. Resuspend the pellet in desired amount of media. (Varies between 0.5ml to 1ml based on pellet size)
12. Triturate the solution with a 1000ul pipette to ensure the solution is homogenous.
13. Remove 30ul of cell suspension and add it to the 30ul of trypan blue stain.
14. Load 10ul of the cell+trypan blue mixture in each side of the hemocytometer.
15. Count enough boxes to achieve a count of 100 cells of greater. Once you begin counting a box you must count the whole box.
16. Use this formula to determine the cell density.

$$\frac{\#\ of\ cells\ counted}{\#\ of\ boxes\ counted} * 2 * 10{,}000 * \#\ of ml = \frac{cell\ count}{1\ ml}$$

17. Either seed 500,000 cells per T-75 flask, with 10-12ml of media, or use cells for other intended purpose. Recommended seeding density of ≈7000 cells per cm^2

8.9.3 hMSC Qdot Loading

Use: Qdot 655 ITK Carboxyl quantum dots (Q21321MP, Invitrogen). Stored in the refrigerator.

1. Culture hMSCS to desired confluency*
2. Prepare 8.2nM solution of Qdots in complete MSCGM
   QD vials contain 250µL of 8µL solution. Use $C_1V_1=C_2V_2$ formula to calculate volume of QDs required for a desired volume of media.

   Example: For 100ml complete MSCGM+QDs

   $8\mu M * V_1 = 8.2nM * 100ml$; $V_1 = 102.5\mu L$

   Need 102.5µL of QD 655 solution to add to 100ml of media.
3. Obtain required volume of QD solution and add directly into the flask containing the hMSCs.
4. Incubate for 24 hours prior to use of hMSCs

Notes:

- *Cells must be less than 80% confluent when QDs are added.
- Cells must be plated at least 24 hours prior to QD loading.
- Cells must be incubated for 24 hours after QD loading, before use.

8.10 **Appendix I: Nuclear Alignment Quantification**

1) Image using 40X objective on confocal microscope (Leica)
2) Open channel image in Image J
3) Threshold the blue (nuclei) channel:
   a) Image-adjust-threshold
   b) Set Parameters-Default-Red Dark background
   c) Apply
4) Set Scale: Analyze-Set Scale
   a) 40X Image Confocal Distance in Pixels = 1024
   b) Known Distance = 387.50 µm
5) Set Measure:
   a) Analyze-Set Measurements
      i) Area
      ii) Fit Ellipse
      iii) All Other uncheck
6) Particles: Analyze-Analyze Particles

a) Size (μm^2) = 20-400
b) Circularity = 0-1
c) Show: Select ellipses
    i) Display Results
    ii) Clear Results
    iii) Exclude on Edges
    iv) Include Holes
7) Save File (will save as a .xls) file name = picture label
8) Open in excel- Adjust A~ 90° = If (Θ>90°, 180- Θ, Θ) → this assumes thread or reference is at 0 degrees
9) Elongation = Major/Minor
10) Measure thread or reference angle using Angle tool
11) Save file as a .xlsx

8.11 **Appendix J: SU8 Microfabrication on Silicon Wafer**

DraftSight software (Dassault Systemes, Waltham, MA, USA) was used to create a high-resolution transparency mask of microchannels with spacing of 10, 15, 25, 50, and 100 μm.

Materials:

- Photoresist Spin Coater (Laurell WS-650MZ-23NPP)
- UV exposure unit (UV-KUB)
- Hot plates (PMC Dataplate 720 and 732)
- DEKTAK 3 Profilometer and computer (DEKTAK3)
- Wafer inspection stereomicroscope (Zeiss Stemi 2000)

Protocol:

1) 15' @ 130C
2) Cool to room temperature
3) Spin coat 4.5 mL SU8 2000 photoresist (MicroChem)
    a. 100 RPM/S to 500 - 10"
    b. 300 RPM/S to 2150- 30"
4) 3' @ 65C
5) Cool to room temperature
6) Spin coat 4.5 mL SU8 2000 photoresist (MicroChem)
    a. 100 RPM/S to 500 - 10"
    b. 300 RPM/S to 2150- 30"
7) 3' @ 65C
8) 5' @ 96C
9) 2' @ 65C
10) Cool to room temperature
11) UV exposure set to 175 mj/cm^2
    a. 15 sec @ 74%
12) 3' @ 65C
13) 8' @ 96C

14) Cool to room temperature
15) 15' developer
16) Hardbake 90' @ 150C

8.12 **Appendix K: Embedding Leaves and Eosin Staining Protocol**

8.12.1 Manual Leaf Processing

(In TissueTek VIP® 6AI tissue processor)

Put leaf samples in cassettes and submerge in:

1. 100% ethanol (20 minutes)
2. 100% ethanol (30 minutes)
3. Xylene 4 (20 minutes)
4. Xylene 5 (20 minutes)
5. Paraffin 1 in VIP (manual) (20 minutes)
6. Paraffin 2 in VIP (manual) (20 minutes)
7. Paraffin 3 in VIP (manual) (10 minutes)
8. Bring cassettes to embed in paraffin at embedding station (Sakura TissueTek® TEC™ 6)

8.12.2 Eosin staining

Submerge cassettes in:

1. Xylene 1 (3 minutes)
2. Xylene 2 (3 minutes)
3. Xylene 3 (3 minutes)
4. 100% ethanol (3 minutes)
5. 100% ethanol (3 minutes)
6. Eosin (1 minute)
7. 100% ethanol (1 minute)
8. Xylene (1 minute)

8.13 **Appendix L: Micropatterning Fibrin Hydrogel on Leaves and Coverslips**

Materials:

- Sterile, media prepped leaves
- 0.67% gelatin coated sterile 22mm coverslips in petri dish
- Sterile 1% Pluronic F-127 solution
- 1 aliquot fibrinogen - 70mg/ml
- 1 aliquot thrombin – 8U/200µl
- RPMI basal media
- Sterile 3mL syringes, 0.2um syringe filters, and 20G needles
- Sterile micropatterned PDMS stamps
- Sterile forceps

- Autoclaved syringe of vacuum grease
- Sterile 0.7mL microcentrifuge tubes

Protocol:

1) Thaw fibrinogen aliquot for at least 1 hour in 37C water bath
   a) After 1 hour, dilute 70 mg/mL aliquoted fibrinogen in HBSS to get 11 mg/mL. Return to 37˚C
   b) ex. 1 mL of 70mg/mL → add 5.364 mL HBSS for 11mg/mL
2) In biosafety cabinet, put micropatterned PDMS stamps face-up in petri dish and coat with sterile 1% Pluronic solution. Leave for 1 hr.
3) Adhere coverslips to bottom of 6-well plate with sterile vacuum grease and maintain in 37˚C until cell seeding.
4) Warm RPMI basal media in 37˚C water bath
5) Thaw thrombin and sterile filter with 0.2 µm sterile filter
6) Sterile filter 11mg/mL fibrinogen with 0.2 µm sterile filter
7) Aspirate off Pluronics from PDMS stamps after 1 hour and air dry
8) Put fibrinogen and thrombin and RPMI on ice before mixing
9) Add volumes of RPMI, Fb, then Th into microcentrifuge tube (see table)
10) Pipette 30uL of 10mg/mL hydrogels on leaf or coverslip surface, then apply micropatterned PDMS face-down with sterile forceps. Tap down lightly on the back of the stamp to apply pattern. Let polymerize for 30 min. Keep exposed to room temperature air flow in biosafety cabinet.
    a) For control fibrin (non-patterned) surfaces, do not place stamp on surface.
11) Remove stamp in direction of channel pattern.
12) Place a cloning cylinder in center of pattern hydrogel for cell seeding.

10 mg/mL hydrogel	**300 µL total**
RPMI (basal media)	16
11 mg/mL Fb	272
40 U/mL Th	12

Cell seeding:

1. Seed cells using hMSC seeding or hiPS-CM cell thaw and seeding protocols with 50 µg/mL aprotinin-supplemented media.
2. Feed cells after 18 hours at 37˚C, 5% CO_2 and change media according to cell type. Remove cloning wells on coverslips only, and on leaves only according to cell type.